IDENTIFICATION OF METABOLIC ALTERATIONS THAT ACTIVATE THE UNFOLDED PROTEIN RESPONSE OF THE ENDOPLAMIC RETICULUM IN *C. ELEGANS*

by

Jiaming Xu

B.Sc., The University of British Columbia, 2018

A THESIS SUBMITTED IN PARTIAL FULFILLMENT OF

THE REQUIREMENTS FOR THE DEGREE OF

MASTER OF SCIENCE

in

THE FACULTY OF GRADUATE AND POSTDOCTORAL STUDIES

(CELL AND DEVELOPMENTAL BIOLOGY)

THE UNIVERSITY OF BRITISH COLUMBIA

(Vancouver)

August 2021

The following individuals certify that they have read, and recommend to the Faculty of Graduate and Postdoctoral Studies for acceptance, a thesis entitled:

Identification of metabolic alterations that activate the unfolded protein response of the endoplasmic reticulum in *C. elegans*

submitted by Jiaming Xu in partial fulfillment of the requirements for

the degree of Master of Science

in Cell and Developmental Biology

Examining Committee:

Dr. Stefan Taubert, Cell and Developmental Biology, UBC
Supervisor

Dr. Donald Moerman, Cell and Developmental Biology, UBC
Supervisory Committee Member

Dr. Chris Loewen, Cell and Developmental Biology, UBC
Supervisory Committee Member

Dr. Peter Stirling, Department of Medical Genetics, UBC
Additional Examiner

Abstract

Endoplasmic reticulum (ER) stress due to protein misfolding or membrane lipid imbalance is observed in many diseases. ER homeostasis can be restored by activation of the unfolded protein response (UPR-ER), which, in higher eukaryotes, consists of three parallel branches: The Inositol-Requiring-Enzyme 1 (IRE-1) branch, the protein kinase RNA-like ER kinase (PEK-1) branch, and the Activating Transcription Factor 6 (ATF-6) branch. These sensors activate downstream effectors to restore cellular homeostasis. However, we lack a global view of genetic perturbations that activate the UPR-ER in metazoans. To identify\metabolic pathways that affect ER homeostasis, I used RNA interference (RNAi) to inactivate 1247 metabolic genes in *Caenorhabditis elegans* using an IRE-1 branch specific transcriptional reporter, *hsp-4p::gfp*. After screening and validation, I obtained 34 high-confidence hits that also activate the PEK-1 branch. Next, using a strain lacking the key IRE-1 pathway effector XBP-1 (*xbp-1; hsp-4p::gfp*), I showed that these gene inactivations induce canonical IRE-1 signaling. Moreover, dietary choline supplementation, which suppresses UPR-ER in worms defective for phosphatidylcholine (PC) synthesis pathway, partially suppresses UPR-ER activation in 3 of the 34 hits, suggesting that most hits do not activate the UPR-ER via defective PC synthesis. Finally, I performed follow-up studies on two of the 34 hits, the primases *pri-1* and *pri-2*, whose inactivation causes DNA damage due to replication fork stalling. These two RNAi clones were selected because both activate *hsp-4p::gfp* in *C. elegans* embryos in a partially *ire-1*-, *xbp-1*-independent manner. I observed that *pri-1* and *pri-2* RNAi specifically induce the UPR-ER, but not the mechanistically distinct cytosolic or mitochondrial UPRs. This suggests that *pri-1* and *pri-2* RNAi do not cause global protein misfolding. Interestingly, genomic instability caused by loss of

DNA repair pathways did not activate the UPR-ER, suggesting that replication stress specifically activates the UPR-ER in the embryo. In sum, by identifying new genes that affect UPR-ER homeostasis in *C. elegans*, my project provides new insights into mechanisms of UPR-ER regulation. Furthermore, as many genes identified here have human homologues, my data may provide a starting point for the discovery of novel drug targets for human diseases featuring ER dysfunction.

Lay Summary

The endoplasmic reticulum (ER), is an important organelle that is prone to disturbances, resulting in a condition known as “ER stress”. To date, the genetic influence on ER stability is less clear, in other words, we do not have a complete list of human genes that are required for maintaining ER homeostasis. To address this gap, I identified 34 genes out of ~1300 metabolic genes that the small animal *Caenorhabditis elegans* naturally use to maintain its ER homeostasis, including genes whose inactivation results in failed DNA replication (one of the essential steps in cell division). Interestingly, defective DNA replication in the nucleus is sensed at the ER in a non-canonical way. Therefore, our findings, highlighting a novel crosstalk mechanism between DNA quality control and ER homeostasis, both key players in cancer progression, may suggest novel drug targets for cancer therapy.

Preface

A version of chapter 1 has been published. [Jiaming Xu], Stefan Taubert. (2021) Beyond Proteostasis: Lipid Metabolism as a New Player in ER Homeostasis. Metabolites. 11 (1):52. Jiaming Xu and Stefan Taubert wrote and edited the manuscript

A version of chapter 2.1 has been published. Nurulain Ho, Wei Sheng Yap, [Jiaming Xu], Haoxi Wu, Jhee Hong Koh, Wilson Wen Bin Goh, Bhawana George, Shu Chen Chong, Stefan Taubert, Guillaume Thibault. (2020) Stress sensor Ire1 deploys a divergent transcriptional program in response to lipid bilayer stress. Journal of Cell Biology. 291 (7). Stefan Taubert designed the *C. elegans* project. Jiaming Xu conducted all the experiments, Jiaming Xu and Stefan Taubert wrote and edited the manuscript section related to the *C. elegans* screen.

The overall research objectives described in this thesis were developed by Dr. Stefan Taubert Experiments were designed and executed by Jiaming Xu in consultation with Dr. Stefan Taubert

Table of Contents

Abstract ..... **iii**

Lay Summary ..... **v**

Preface ..... **vi**

Table of Contents ..... **vii**

List of Tables ..... **xii**

List of Figures ..... **xiii**

List of Supplementary Tables ..... **xv**

List of Abbreviations ..... **xvi**

Acknowledgements ..... **xviii**

Dedication ..... **xix**

Chapter 1: Introduction **1**

1.1 Functions and distributions of lipids in cellular membranes 1

1.2 The UPR-ER consists of three conserved sensory branches 2

1.2.1 Inositol-required enzyme 1 is the most highly conserved UPR-ER transducer 3

1.2.2 The PERK/PEK-1 branch of the UPR-ER reprograms translation 5

1.2.3 ATF-6 Is a parallel sensor that modulates UPR-ER pathways 6

1.3 Bidirectional interplay between lipid metabolism and the UPR-ER 7

1.3.1 Input: Lipid metabolism modulates ER homeostasis 9

1.3.2 Output: UPR-ER restores lipid homeostasis under lipotoxic stress 10

1.4 Differential activation of UPR-ER by lipotoxicity and proteotoxicity 11

1.4.1 Mechanisms of proteotoxicity-induced UPR-ER activation 11

1.4.2 Mechanisms of lipotoxicity-induced UPR-ER activation 13
1.5 Crosstalk between proteotoxicity- and lipotoxicity-Induced UPR-ER 15
1.6 DNA damage responses in *C. elegans* 17
1.6.1 DNA replication stress and the intra-S phase checkpoint response 18
1.6.2 Cell type-specific response to double strand DNA breaks 19
1.7 Crosstalk between DNA damage response and the UPR-ER 22
1.7.1 Input: DNA damage activates UPR-ER 22
1.7.2 Output: UPR-ER promotes DNA damage response in *C. elegans* 23
1.8 Using *Caenorhabditis elegans* as a model 25
1.8.1 *C. elegans* for studying ER unfolded protein response (UPR-ER) 25
1.8.2 *C. elegans* for studying lipid metabolism 26
1.8.3 *C. elegans* for studying DNA damage response 27
1.9 Hypothesis and objectives of the thesis 28
Chapter 2: Results 30
2.1 New cellular functions necessary to maintain ER homeostasis in *C. elegans* 30
2.1.1 A reverse genetic screen identifies 34 RNAi whose inactivation induced IRE-1 and PEK-1 30
2.1.1.1 Construction of a metabolic RNAi sublibrary 30
2.1.1.2 RNAi proof-of-principle 30
2.1.1.3 Identification of 106 UPR-ER-inducing candidate screen hits 35
2.1.1.4 Triplicate validation of candidate hits yields 38 high-confidence hits 36
2.1.1.5 Sanger sequencing validates 35 RNAi clones as hits 37
2.1.2 Confirmation of endogenous UPR-ER induction in 15 select hits 41

2.1.3 All hits require canonical IRE-1–XBP-1 signaling for UPR-ER activation 42
2.1.4 ATF-4 activation is observed in all 34 hits 42
2.1.5 Choline supplementation suppresses UPR-ER activation in 3 of 34 hits 46
2.1.6 Inactivation of yeast SPC2 homolog *spcs-2* activates UPR-ER in *C. elegans* 50
2.1.7 Discussion 51
2.2 Genotoxic stress activates the UPR-ER 52
2.2.1 *pri-1/2* knockdown activates the *ire-1* pathway 52
2.2.2 *pri-1/2* knockdown activates the *pek-1* pathway 56
2.2.3 *pri-1/2* knockdown induces the UPR-ER specifically 58
2.2.4 *pri-1/2* knockdown induces embryonic *hsp-4* partially independently of *xbp-1* and *ire-1* 62
2.2.5 UV-C treatment phenocopies *pri-1* and *pri-2* RNAi 65
2.2.6 ATF-6 is partially required for *hsp-4* induction in *pri-1/2* knockdown embryos . 69
2.2.7 Knocking down components of the polymerase α primase complex phenocopies *pri-1/2* RNAi 72
2.2.8 Knocking down DNA repair pathway components does not activate the UPR-ER in somatic cells 73
2.2.9 IRE-1 is required for germline protection against hydroxyurea (HU)-induced replication stress 80
2.2.10 *ire-1* and *pek-1* are required for somatic protection against hydroxyurea (HU)-induced replication stress. 83
Chapter 3: Discussion and Conclusion 86
3.1 Metabolic alterations that activate the UPR-ER and their potential mechanisms 86

3.1.1 Loss of myristoylation on conserved *nmt-1* protein targets may cause UPR-ER activation……88
3.1.2 Phenylalanine build-up may cause membrane lipid changes and UPR-ER activation……88
3.1.3 Multiple lipid precursors synthesis pathways are disrupted upon loss of *let-767* 89
3.2 DNA damage caused by stalled replication fork is an activator of UPR-ER 90
3.2.1 UPR-ER in such context may be independent of global protein misfolding..... 90
3.2.1.1 Exclusive activation of the UPR-ER reporter..... 91
3.2.2 Replication stress induces non-canonical *ire-1*- and *xbp-1*-independent *hsp-4* expression in embryos..... 91
3.3 IRE-1 and PEK-1 of the UPR-ER are required for resistance to genotoxicity..... 92
3.4 Caveats and considerations..... 93
3.4.1 Use of RNAi 93
3.4.2 Use of transcriptional GFP reporters 93
3.5 Conclusions..... 94
Chapter 4: Materials and Methods 96
4.1 Worm strains..... 96
4.2 Worm growth conditions 96
4.3 Metabolic RNAi sublibrary construction..... 97
4.4 Feeding RNA interference 97
4.5 Sanger Sequencing..... 98
4.6 RNA isolation and real-time quantitative PCR..... 98
4.7 DIC and fluorescence microscopy 99

4.8 Protein extraction and immunoblots 100

4.9 UV-C exposure 100

4.10 Hydroxyurea treatment 100

4.11 Statistics 101

Bibliography 102

List of Supplementary Material 117

List of Tables

Table 1 List of worm strains used in this thesis 96

Table 2. List of primer sequences used for RT-qPCR 99

List of Figures

Figure 1 Overview of the canonical endoplasmic reticulum unfolded protein response (UPR-ER) pathways. 5

Figure 2 Overview of the bidirectional interplay between lipid metabolism and the IRE-1 branch of the UPR-ER in *C. elegans*. 8

Figure 3 Overview of tissue-specific DNA damage response in *C. elegans*. 20

Figure 4. Metabolic RNAi screen design and proof-of-principle. 34

Figure 5. Summary of screen hit identities and intensities of UPR-ER reporter strains. 40

Figure 6. Dot plots indicate the relative mRNA levels 41

Figure 7. Summary of screen hit identities and intensities of the *Patf-4(uORF)::gfp* reporter strain. 45

Figure 8. UPR-ER activation in select hits is rescued by dietary choline supplementation. 49

Figure 9. Inactivation of *spcs-2* activates UPR-ER. 51

Figure 10. *pri-1/2* knockdown induces the IRE-1 branch in *C. elegans* embryos. 56

Figure 11. *pri-1/2* knockdown induces the PEK-1 branch in *C. elegans* embryos. 58

Figure 12. *pri-1/2* knockdown induces the UPR-ER but not the mitochondrial UPR or the cytosolic UPR. 62

Figure 13. *pri-1/2* knockdown activates embryonic *hsp-4* through a partially *ire-1*- and *xbp-1*-independent mechanism. 65

Figure 14. UV-C treatment phenocopies *pri-1* and *pri-2* RNAi 68

Figure 15. Activation of *hsp-4* by *pri-1/2* knockdown is partially independent of *atf-6*. 71

Figure 16. Polymerase α primase complex subunit knockdown phenocopies *pri-1/2* RNAi. 73

Figure 17. Knockdown of DNA repair pathway components failed to activate the UPR-ER..... 80

Figure 18. *ire-1* is required for germline protection against HU-induced replication stress. 82

Figure 19. *ire-1* and *pek-1* are required for germline protection against HU-induced replication stress..... 84

Figure 20. Overview of lipid synthesis pathways in *C. elegans* (adapted with permission from [145])..... 87

List of Supplementary Material

Table S1. RNAi screen for metabolic genes whose inactivation induces the IRE-1 branch of the UPR-ER in *C. elegans* (readout: activation of the *hsp-4p::gfp* reporter) 117

Table S2. RNAi and sequence validation of yeast hit screen orthologues in *C. elegans* 118

Table S3. A summary of yeast and *C. elegans* screen hit orthologues 119

Table S4. A summary of the PEK-1 branch activation by RNAi against the 34 hit metabolic genes in *C. elegans* (readout: activation of the *Patf-4(uORF)::gfp* reporter) 120

List of Abbreviations

4-PBA	4-phenyl butyrate
ATF-6	Activating Transcription Factor 6
ATF4	Activating Transcription Factor 4
BiP	Binding immunoglobulin protein
C. elegans	*Caenorhabditis elegans*
C/EBP	CCAAT/ Enhancer Binding Protein
CHOP	CCAAT/ Enhancer Binding Protein homologous protein
CL	Cardiolipin
DIC	Differential interference contrast
E. coli	*Escherichia coli*
eIF2α	Eukaryotic translation initiation factor-2
ER	Endoplasmic reticulum
ERAD	ER-associated degradation
FA	Fatty acid
gadd34	DNA damage-inducible gene 34
GFP	Green fluorescent protein
HSP-4	Heat shock protein 4
IPTG	Isopropyl β- d-1-thiogalactopyranoside
IRE-1	Inositol-requiring enzyme 1
LB	Lysogeny broth
LBS	Lipid bilayer stress

LD	Luminal domain
MUFA	Mono-unsaturated fatty acids
PC	Phosphatidylcholine
PE	phosphatidylethanolamine
PEK-1	PRKR-like endoplasmic reticulum kinase
PERK	Protein kinase R (PKR)-like endoplasmic reticulum kinase
PI	Phosphatidylinositol
PS	Phosphatidylserine
PT	Proteotoxic stress
RIDD	Regulated IRE1-dependent decay of mRNA
RNAi	RNA interference
SCD	Stearoyl-CoA desaturase
SEM	standard error of the mean
SERCA	sarco-/endoplasmic reticulum calcium ATPase
TG	Triglyceride
UPR-ER	Endoplasmic reticulum unfolded protein response
XBP-1S	X-Box Binding Protein 1 spliced
XBP-1U	X-Box Binding Protein 1 unspliced

Acknowledgements

I am grateful for the past and current Taubert lab members' input throughout this project. I thank my undergraduate student Angel Chu for her help with RNA extraction.

I thank Dr. Guillaume Thibault for the smooth collaboration and co-first authorship.

I thank Dr. Collin Ewald for providing an important worm strain and Dr. Nigel O'Neil for advice on DNA damage gene candidates

I thank Dr. Chris Loewen, Dr. Don Moerman and Dr. Peter Stirling for helpful scientific advice and generous encouragement for this project.

I would like to thank my supervisor Dr. Stefan Taubert.
Thank you for your contagious passion for science and your continued support through continued periods of non-ideal data and frustration. Thank you for being able to keep a delicate balance between intellectual freedom and professional guidance as a supervisor. Thank you for having your students' best interests in mind, and for being a caring team leader and a kind person in general. As a student, I will always feel proud to say that I have been a member of the Taubert lab.

Dedication

This thesis is dedicated to my parents, for always being there for me through the ups and downs of this memorable journey. ❣️👨‍👩‍👧❣️

Chapter 1: Introduction

1.1 Functions and distributions of lipids in cellular membranes

In all species, lipids are essential as they serve as a source of energy, mediate signal transduction, and form cellular and organellular membranes. In addition to the well-known functions of membranes such as providing a physical barrier, membrane lipids and their modifications play an active role in regulating cellular and subcellular trafficking [1]. In mammals, lipids are categorized into six major classes: fatty acyls, glycerolipids, glycerophospholipids, sterol lipids, prenol lipids, and sphingolipids [2,3]. *C. elegans* has similar lipid composition but with some additional lipid sub-classes [4]. Membrane lipids belong to three main categories: phospholipids (PLs), sphingolipids, and sterols (cholesterol in mammals, ergosterol in yeast) [5]. They are diverse in structure and distribution, and this diversity is maintained from the organismal level to subcellular and membrane subdomain levels. For example, lipidomic analysis in mammalian cells revealed that each organelle has a distinct membrane lipid profile [6]. Phosphatidylcholine (PC) is most abundant in the ER membrane (57%) and less abundant in the inner mitochondrial membrane (41%), whereas cardiolipin (CL) is exclusively found in the mitochondrial membranes [6,7]. Maintaining this unique quantitative and qualitative composition is critical for the normal functions of each organelle and therefore the cellular function and overall health of an organism. For example, reducing CL levels by blocking phosphatidic acid transfer causes cytochrome c release and apoptosis [8]. Moreover, *in vivo* studies show that blocking phosphatidylethanolamine (PE) synthesis at the mitochondrial inner membrane causes embryonic lethality in mice [9]. Therefore, functions and compositional balance of individual lipid classes are critical to maintaining cellular and organismal health, in

various *in vivo* models and in humans. Links between different human diseases and different lipid classes has been reviewed in detail elsewhere [10].

1.2 The UPR-ER consists of three conserved sensory branches

Within the eukaryotic cell, the endoplasmic reticulum (ER) is a dynamic membrane network involved in many essential cellular processes. The rough ER has membrane-bound ribosomes and is a site for synthesis, maturation, and modification of more than one third of the human proteome. The smooth ER functions in lipid and steroid hormone biosynthesis and xenobiotic detoxification. Although ER homeostasis is critical, it is prone to various cellular stressors such as intracellular Ca^{2+} imbalance, viral infection, changes in redox environment, and hypoxia, all of which trigger a condition known as ER stress [11]. Moreover, in highly proliferative or secretory cells, the influx of large amounts of nascent proteins into the ER can temporarily overwhelm the folding machinery, leading to endogenous ER stress [12]. Prolonged ER stress can compromise cellular function and viability and lead to or exacerbate many human diseases, including cancer, diabetes, and neurodegenerative conditions [13].

To ensure viability and proper cellular function, cells have evolved a conserved adaptive mechanism to restore ER homeostasis under stress: the ER unfolded protein response (UPR-ER; Figure 1) [14,15]. In higher eukaryotes, the UPR-ER consists of three parallel ER stress sensing and transducing branches: The Inositol-Requiring-Enzyme 1α (IRE-1α, also known as Endoplasmic Reticulum to Nucleus signaling 1 or ERN1 in mammals) branch [12]; the protein kinase RNA-like ER kinase (PERK/PEK-1, also known as Eukaryotic Translation Initiation Factor 2 Alpha Kinase 3 or EIF2AK3) branch [16]; and the Activating Transcription Factor 6

(ATF-6) branch [17] (Figure 1). These three sensors are embedded in the ER membrane with a single-pass transmembrane domain, which connects a luminal sensor domain to a cytosolic effector domain. This modular design enables these sensors to communicate the input stress signal to transcriptional and translational machineries for effector output. Together, they attenuate ER stress by reprograming transcription and translation to promote protein folding, degradation, and transport, as well as lipid synthesis and remodeling [18]. Alternatively, if ER stress is not resolved, the UPR-ER switches from promoting survival and adaptation to triggering apoptosis [18].

1.2.1 Inositol-required enzyme 1 is the most highly conserved UPR-ER transducer

IRE-1 is an ER resident protein evolutionarily conserved from yeast to humans. It was initially identified in *Saccharomyces cerevisiae* as essential for growth in the absence of inositol [19], and emerged as the sole ER stress transducer in yeast [20,21]. Allosteric IRE-1 activation involves the protein chaperone Binding immunoglobulin protein (BiP) (also known as 78-kDa glucose-regulated protein (GRP78) and heat shock protein 5α (HSP5α) and heat shock protein 4 (HSP-4) in *C. elegans*) as misfolded proteins bind to BiP/HSP-4, which leads to its dissociation from IRE-1's luminal domain (LD; Figure 1) [22]. The dissociation of BiP/HSP-4 from the LD triggers the formation of IRE-1 dimers and higher-order oligomers, leading to robust trans-autophosphorylation [22]. Phosphorylated and active IRE-1 then excises a 26 base pair intron in a target mRNA encoding the transcription factor ATF/ CAMP responsive element binding protein 1(CREB1) homolog (Hac1p; in yeast) or X-box binding protein 1 (XBP-1; in metazoans) with its endoribonuclease domain [23]. The excision and re-ligation shifts the open reading frame, leading to the translation of the spliced *xbp-1* mRNA (*xbp-1s*), which is more active and

stable than the *xbp-1* unspliced mRNA (*xbp-1u*) [24,25]. After translation, HAC1/XBP-1s translocated to the nucleus and activates the transcription of cytoprotective genes involved in protein folding, translocation, and glycosylation; redox metabolism; autophagy; cell wall synthesis; vesicular trafficking; ER-associated degradation (ERAD); and lipid/inositol metabolism [18,20,26,27].

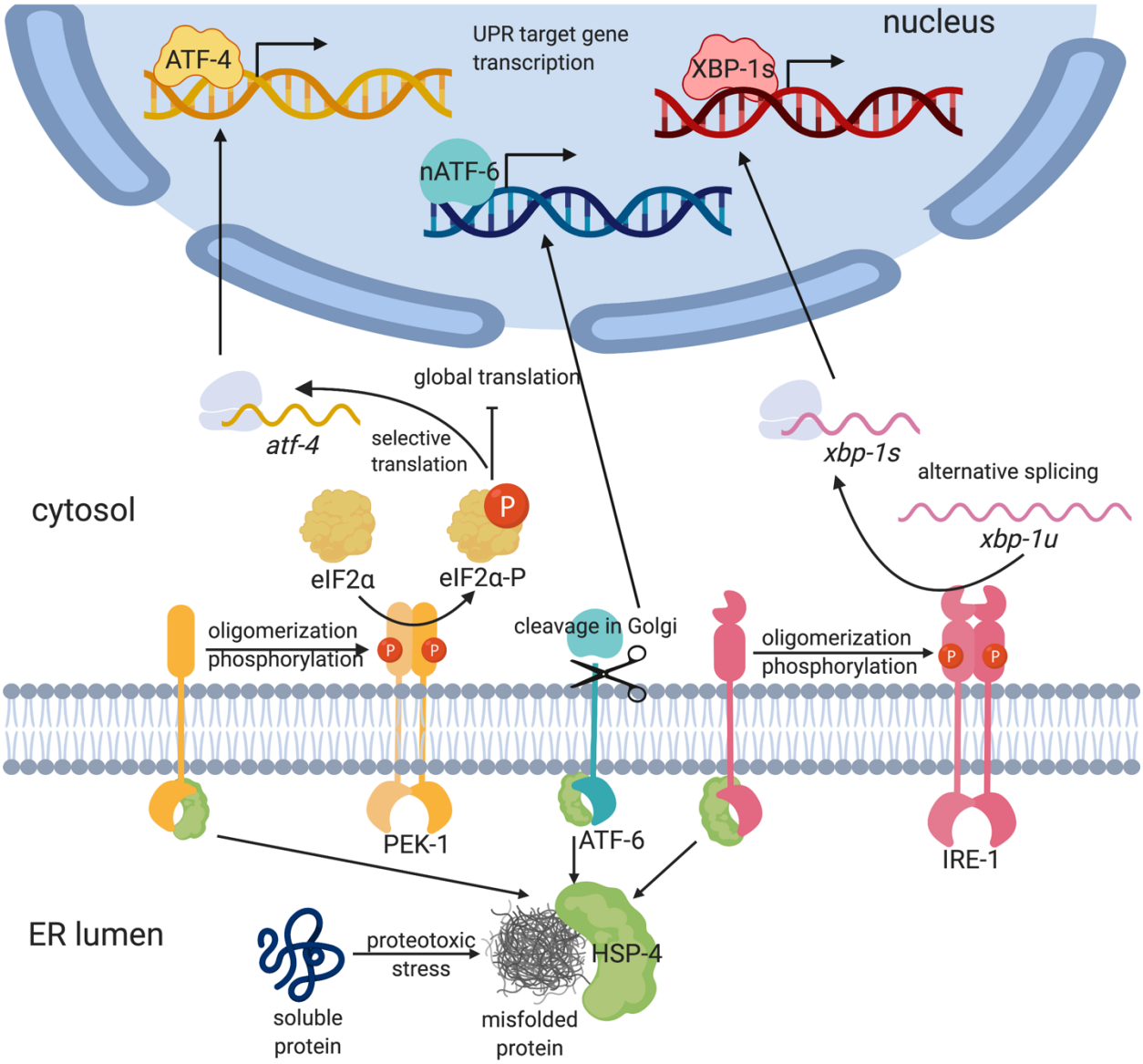

Figure 1 Overview of the canonical endoplasmic reticulum unfolded protein response (UPR-ER) pathways. In higher eukaryotes, upon sensing misfolded proteins by HSP-4/BiP, the three UPR-ER branches—IRE-1α, PEK-1, and ATF-6—are activated to mount distinct downstream transcriptional and translational programs to promote protein folding, processing, and secretion, thereby reducing the load of misfolded proteins in the ER lumen and alleviating ER stress. Abbreviations: ATF-4: Activating Transcription Factor 4; ATF-6: Activating Transcription Factor 6; eIF2α: Eukaryotic Initiation Factor 2α; HSP-4/BiP: heat shock protein 4/ Binding immunoglobulin protein; IRE-1α: Inositol-Requiring-Enzyme 1α; PEK-1: human PERK kinase homolog; UPR: unfolded protein response; xbp-1: X-box Binding Protein homolog 1. (Figure created with Biorender.com, Toronto, ON, Canada).

1.2.2 The PERK/PEK-1 branch of the UPR-ER reprograms translation

In higher eukaryotes including *C. elegans*, the UPR-ER is more complex, as it includes additional ER stress transducers besides IRE-1 (Figure 1). PERK/PEK-1, like IRE1, is a transmembrane kinase whose luminal domain dissociates from BiP upon sensing misfolded proteins, whereupon PERK forms dimers and undergoes auto-phosphorylation [28]. Activated PERK phosphorylates the eukaryotic translation initiation factor-2 (eIF2α), and thus transiently inhibits general protein translation initiation, thereby reducing ER proteostasis stress. However, phosphorylation of eIF2α also allows for the selective translation of activating transcription factor 4 (ATF4), which upregulates a subset of UPR genes, including the apoptosis-inducing CCAAT/ Enhancer Binding Protein (C/EBP) homologous protein (*chop/gadd153*) and the Growth arrest and DNA damage-inducible gene 34 (*gadd34*), restoring balance by dephosphorylating eIF2α [29,30]. Whereas the downstream actions of ATF-4 are not well known in *C. elegans*, worm ATF-4 is similar to human ATF4 in gene structure and regulation by upstream open reading frames [31] and in its response to general translational inhibition [32], implying strong functional similarity.

PERK plays important roles in animal development. Although *C. elegans pek-1* single mutant worms show no noticeable phenotypes, a *pek-1; ire-1* double mutant arrests at the second larval (L2) stage due to intestinal degeneration [33]. Consistent with its function as an important UPR-ER sensor, absence of *pek-1* renders worms hypersensitive to ER stress inducing-toxins such as tunicamycin, and loss of *Perk* in cultured mammalian cells causes similar phenotypes [33,34]. Similarly, *Perk-/-* mice, although viable, develop progressive diabetes mellitus due to the accumulation of misfolded proteins in the highly secretory pancreatic β-cells [35]. In addition, homozygous loss of *Perk* in humans causes onset of type 1 diabetes during infancy [36]. Collectively, these observations highlight the importance of PERK in alleviating exogenous and endogenous ER stress.

1.2.3 ATF-6 Is a parallel sensor that modulates UPR-ER pathways

Animals feature a third UPR-ER pathway consisting of ATF6 (ATF6α and ATF6β in mammals). Like IRE1 and PERK, ATF6α is an ER transmembrane protein (Figure 1). However, ATF6α is different from IRE1 and PERK in its domain architecture and mode of action [12]. In the absence of stress, the luminal domain of ATF6α is bound by the ER resident chaperone BiP, shielding a Golgi localization sequence within ATF6α and thus anchoring it to the ER membrane. Upon ER stress, BiP dissociates from ATF6α, which translocates to the Golgi, where it is proteolytically processed by site 1 and site 2 proteases (S1P and S2P). This releases the cytosolic, N-terminal basic leucine zipper (bZIP) transcription factor domain (ATF6-p50), which translocates to the nucleus and upregulates UPR-ER genes [12]. Specifically, ATF6α is required to express *Xbp1u* mRNA, which is then spliced by activated IRE1 [25,37], leading to synergistic UPR-ER activation by two distinct branches. Moreover, ATF6α can function independently or

heterodimerize with XBP1s to induce the expression of ERAD components, chaperones, and UPR mediators, including BiP and XBP1 in mammals [38,39] and *C. elegans* [40]. Mammalian ATF6α also modulates *XBP1* splicing and promotes the expression of the ATF4 target CHOP in response to chronic ER stress [41], suggesting that ATF6α may function as modulator of the IRE1 and PERK branches. In *C. elegans*, the ATF6α homolog *atf-6* regulates few inducible UPR-ER genes but is required to express many constitutively expressed UPR-ER genes; this distinguishes it from *ire-1* and *pek-1*, which primarily upregulate inducible UPR-ER genes following ER stress, thus highlighting a distinct function for ATF-6 [33]. Consistently, *atf-6* mutant worms do not display overt developmental phenotypes or sensitivity to tunicamycin [42], whereas *ire-1;atf-6* and *xbp-1;atf-6* double mutant worms show synthetic lethality [33,41,42].

Some mammalian species encode two ATF6 isoforms. Atf6α regulates stress recovery *in vitro* [41] and *in vivo* [38], but its target genes vary in different cell types [43]. Under unstressed conditions, the effect of losing either Atf6α or Atf6β is mild [38,44], whereas losing both is embryonically lethal in mice [38]. This is consistent with the finding that *C. elegans* ATF-6 regulates constitutive UPR-ER genes and enables coping with endogenous ER stress during development [42]. Thus, the mammalian Atf6 branch likely possesses both conserved and distinct roles.

1.3 Bidirectional interplay between lipid metabolism and the UPR-ER

It is now clear that the UPR-ER's importance goes beyond proteostasis. In line with the ER's dual function in protein and lipid production, membrane lipid imbalance can directly activate the UPR-ER. In turn, the UPR-ER directly upregulates compensatory pathways to restore lipid

homeostasis. Thus, the UPR-ER is intricately linked to lipid metabolism and homeostasis both upstream and downstream, as outlined in Figure 2.

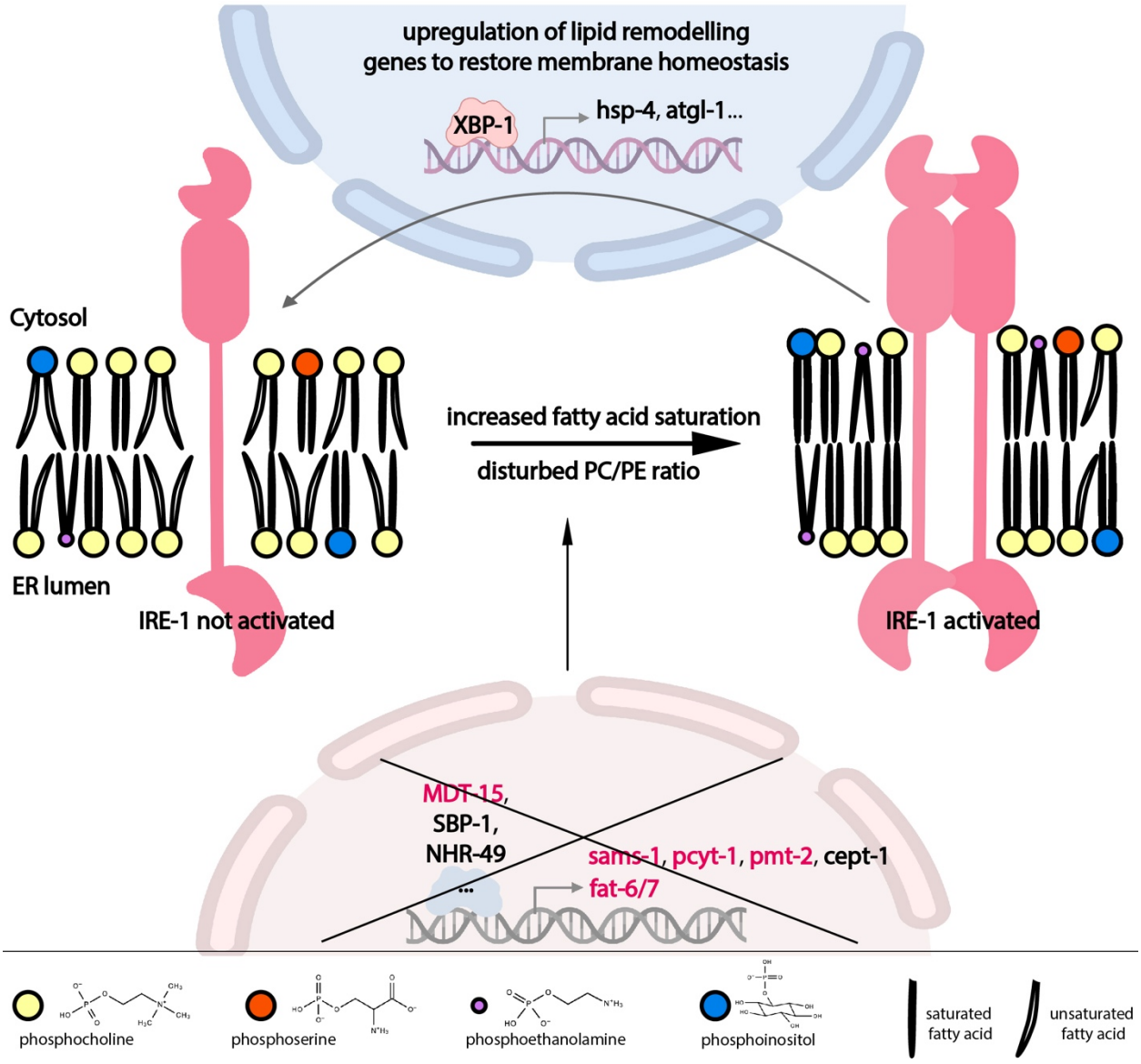

Figure 2 Overview of the bidirectional interplay between lipid metabolism and the IRE-1 branch of the UPR-ER in *C. elegans*.

Disturbed ER membrane lipid composition marked by "X" is caused by the loss of *mdt-15* or *fat-6/7*, which cause increased FA saturation, or by the loss of *mdt-15*, *sams-1*, *pcyt-1*, or *pmt-2*, which cause disturbed PC/PE ratios. All

these disturbances are direct triggers for IRE-1 activation, i.e., independent of protein misfolding. Activated IRE-1 upregulates compensatory genes, which remodel lipid metabolism and restore a proper lipid environment in the ER. Genes colored in red have been experimentally shown to cause IRE-1 activation in *C. elegans* when inactivated. Abbreviations: *atgl-1*: adipose triglyceride lipase; *cept-1*: choline/ethanolaminephosphotransferase; FA: fatty acid; *fat-6/-7*: fatty acid desaturase 6/7; *hsp-4*: heat shock protein 4; IRE-1: IRE1 kinase related; MDT-15: mediator 15; NHR-49: nuclear hormone receptor 49; PC: phosphatidylcholine; *pcyt-1*: phosphocholine cytidylyltransferase; PE: phosphatidylethanolamine; PI: phosphatidylinositol; *pmt-2*: phosphoethanolamine methyltransferase; PS: phosphatidylserine; *sams-1*: S-adenosyl methionine synthetase; SBP-1: sterol regulatory element binding protein; XBP-1: X-box binding protein homolog. (Some parts of the image were created with BioRender.com, Toronto, ON, Canada).

1.3.1 Input: Lipid metabolism modulates ER homeostasis

Feedback from different lipid metabolic pathways modulates ER homeostasis through the UPR-ER sensors (Figure 2), including inputs from fatty acid (FA) tails and from PL head groups; this type of ER stress is also known as lipid bilayer stress (LBS). Diets enriched for long-chain saturated FAs induce the UPR-ER [45,46], as does the inactivation of the FA desaturation machinery, which produces unsaturated FAs in yeast, worms, and human cells [47–49]. In *C. elegans*, RNAi knockdown of the stearoyl-CoA desaturases (SCDs) *fat-6* and *fat-7* activates the transcription of an IRE-1 branch specific *hsp-4*/BiP reporter. Dietary supplementation with oleate, a mono-unsaturated FA (MUFA), is sufficient to suppress the activation of *hsp-4* from SCD knockdown [50], indicating that adequate membrane lipid unsaturation is required to prevent ER stress and concomitant UPR-ER activation in *C. elegans.*

Similarly, the nature of a PL's head group is also important for ER homeostasis (Figure 2). RNAi knockdown of Mediator subunit 15 (*mdt-15*), a conserved transcriptional co-regulator

regulator, leads to significant reduction in PC levels and activates the IRE-1 and PERK branches strongly [50]. This activation is partially suppressed by choline supplementation in *mdt-15*(RNAi) worms [51]; choline supplementation restores PC levels, thus indicating that appropriate PC levels are required for ER homeostasis. Indeed, abnormal PC/PE ratios caused by deleting or inactivating the PC synthesis genes encoding S-adenosyl methionine synthetase (*sams-1*), phosphocholine cytidylyltransferase (*pcyt-1*), and phosphoethanolamine methyltransferase (*pmt-2*) also cause UPR-ER activation in *C. elegans* [50–52], in yeast [53], and in mice [54]. These studies suggest that UPR-ER sensors can sense different types of LBS, i.e. inputs, across species.

1.3.2 Output: UPR-ER restores lipid homeostasis under lipotoxic stress

In terms of output, UPR-ER sensors are critical for maintaining lipid homeostasis following the lipotoxic stresses described above. Recent work has provided molecular evidence for the regulatory role of UPR-ER branches in lipid metabolism (Figure 2). In *C. elegans*, IRE-1 and its downstream target HSP-4 are required for fasting-induced fat granule hydrolysis through the actions of fasting-dependent lipases [55]. Additionally, in a *pmt-2* mutant with defective PC synthesis, IRE-1 is required for the activation of lipid metabolism genes such as lipid droplet-associated lipase *atgl-1* [56], which is necessary for TG hydrolysis. In contrast, this activation is absent in tunicamycin-induced proteotoxic stress [57]. Interestingly, intestinal remodeling of the lipidome can be achieved by neuron-specific *xbp-1s* over-expression in *C. elegans*, through the action of tyramine as an inter-tissue signaling molecule, contributing to proteostasis and increased life span [58,59]. Lastly, several transcriptome studies show that *C. elegans ire-1, pek-1*, and *atf-6* differentially upregulate specific sets of genes in a *pmt-2* deletion mutant, with about

half of the 1069 lipid stress-specific genes being controlled by at least two or more branches, suggesting combinatorial roles of UPR-ER sensors during PC depletion [52]. Overall, these results show that the UPR-ER is an adaptive stress response that is a central lipid metabolism regulator in worms.

1.4 Differential activation of UPR-ER by lipotoxicity and proteotoxicity

1.4.1 Mechanisms of proteotoxicity-induced UPR-ER activation

Two different models have been proposed to explain how misfolded proteins in the ER lumen could activate IRE1. However, whether the activation occurs directly via binding of misfolded proteins to the luminal domain of IRE1 and/or indirectly via the dissociation of the chaperone BiP remains unclear.

The direct association model proposes that misfolded proteins directly bind to the luminal domain (LD) of IRE1, triggering a conformational change in IRE1 which promotes subsequent dimerization and activation [12]. This model is based on thermodynamic evidence of the IRE1 LD having an affinity for hydrophobic peptide ligands *in vitro* and structural evidence of *S. cerevisiae* IRE1 LD dimers, whose interfaces form a putative peptide-binding major histocompatibility complex (MHC)-like groove functionally important for IRE1 signaling [60–62]. Recently, NMR experiments provided putative mechanistic insights into how the human IRE1 LD is able to bind misfolded proteins reversibly via “open” and “closed” conformations and trigger oligomerization [63]. Moreover, the misfolded protein-driven activation model has been proposed for PERK as well, based on a crystal structure of a hydrophobic peptide bound to the conserved hydrophobic groove in PERK’s luminal domain, but away from the dimerization

MHC-like groove [64], raising questions about the site-specificity of these peptide ligand-binding experiments [12,65].

Another model of IRE1 activation is the chaperone inhibition model. In this model, BiP binds to the LD of IRE1, therefore repressing IRE1's activity under unstressed conditions [65–67]. When challenged with unfolded protein accumulation, the inhibitory IRE1-BiP complex is disrupted, favoring IRE1 oligomerization. The original rationale for this model came from the inverse correlation between IRE1 activity and the amount of IRE1-BiP complex recovered [28,68,69], which was recently proved to be causally related *in vivo* [70]. Further, this model is supported by insights about the co-chaperones that are required for trapping misfolded proteins inside BiP, such as the ER-localized J-domain protein ERdj4 and nucleotide exchange factors [12].

However, the mode of IRE-1 activation in *C. elegans* remains unknown. *C. elegans* has two BiP homologs, *hsp-3* and *hsp-4*, both containing an ER-localization signal sequence and potential upstream UPR regulatory elements within their promoter sequences [33,71]. Although both genes are responsive to DTT-induced ER stress, *hsp-3* is constitutively expressed and not induced by heat stress, unlike *hsp-4* [33,71]. Moreover, the two BiP homologs interact through compensatory regulation where *hsp-3* knockdown induces *hsp-4* expression [72]. Therefore, different stress response patterns and regulations for the two BiP homologs suggest that the proteotoxicity-induced activation mechanism of IRE-1 in *C. elegans* is not completely understood, and the exact mechanism will require further investigation.

1.4.2 Mechanisms of lipotoxicity-induced UPR-ER activation

The mechanistic details of how membrane lipid perturbation is sensed by the UPR-ER have begun to emerge over the last few years. Earlier studies showed that UPR-ER induction by saturated FA in yeast [47] can be suppressed by chemical chaperones such as 4-phenyl butyrate (4-PBA) that promote protein folding. Similarly, in studies with obese mouse models with steatotic livers, chemical chaperones such as 4-BPA and tauro-ursodeoxycholic acid (TUDCA) also resolved obesity-induced hepatic lipid accumulation [73]. These observations favor a model of membrane lipid disturbances as an indirect activator of UPR-ER, upstream of proteotoxicity, in other words, through protein misfolding [29].

However, the involvement of chemical chaperones is more complex than facilitating protein folding. 4-PBA reduces Ire1 levels instead of unfolded protein load, providing an alternative interpretation of the above results [74]. Furthermore, 4-PBA and TUDCA have functions beyond protein refolding, such as reducing lipid accumulation [75] and membrane cholesterol levels [76], as well as restoring ER lipid fluidity and calcium permeability [77]. Therefore, interpreting results from experiments with chemical chaperones is challenging.

Indeed, later work from several groups offers an alternative view on the mechanisms underlying lipotoxicity-induced UPR-ER. Long-chain saturated fatty acid reduced Ca^{2+} in the ER of hepatic cells [78]. Consistently, LBS due to altered lipid saturation or PL head group composition in the liver of obese mice inhibits the sarco-/endoplasmic reticulum calcium ATPase (SERCA), thus reducing Ca^{2+} in the ER [54]. However, the effect of Ca^{2+} level changes in the ER is not limited to protein folding capacity changes, as ER Ca^{2+} homeostasis is also implicated in lipid storage in cultured cells and flies [79]. Moreover, comparative proteomics of ER from the liver of obese mice that experience LBS did not show significant alterations in the chaperone

content compared to the lean mouse control, whereas an enrichment in lipid metabolism enzymes was observed [54]. This suggests that, in addition to the idea that Ca^{2+} changes activate the UPR-ER only through the load of misfolded proteins, lipotoxicity-induced changes in ER Ca^{2+} content may also activate the UPR-ER via concurrent lipid alterations.

Furthermore, several lines of evidence indicate that, parallel to proteotoxicity-induced UPR-ER (aka UPR-ER^{PT}), disturbances to lipid composition also directly activate the UPR-ER; this is termed lipid bilayer stress induced UPR-ER or UPR-ER^{LBS}. First, different IRE-1 cluster formation in cells experiencing proteotoxic and lipotoxic stress provides indirect evidence that LBS activates UPR-ER through a mechanism different from protein misfolding. Specifically, in HeLa cells transfected with a IRE1-GFP fusion reporter, tunicamycin-induced ER stress caused IRE1 to form distinctive puncta, whereas palmitate-induced ER stress caused diffuse IRE-1 distribution throughout the ER membrane [80]. Similar findings were reported in yeast where IRE1 forms clustered puncta in response to DTT-induced proteotoxic ER stress, whereas such puncta were absent during UPR-ER^{LBS} in opi3Δ mutants that fail to synthesize PC [51]. Furthermore, 4-PBA was able to attenuate tunicamycin-induced UPR-ER^{PT} but not opi3 deletion-induced UPR-ER^{LBS} [51]. Second, additional evidence confirmed that LBS directly activates the UPR-ER through a novel, membrane-based mechanism that is independent of protein misfolding. In C. elegans, increased lipid saturation or decreased PC content activates the UPR-ER via the IRE-1 branch (Figure 2). Critically, this is independent of protein misfolding as shown by the lack of aggregates of a misfolding-prone protein reporter [50]. Third, the UPR-ER is activated in yeast by reduced PC and PI content [81] and in cell lines by increased lipid saturation [48] even when the luminal misfolded protein sensing domain of IRE1 or PERK is deleted. Thus, the UPR-ER^{LBS} is molecularly separable from protein misfolding induced UPR-

ER. Fourth, there are important mechanistic differences in how proteotoxicity and lipotoxicity activate IRE1 in yeast. Overexpressing the luminal domain of IRE1 ($IRE1^{LD}$) completely attenuated proteotoxicity (tunicamycin) induced UPR-ER, whereas lipotoxicity (opi3Δ) induced $UPR\text{-}ER^{LBS}$ was only partially attenuated by over-expressing either $IRE1^{LD}$ or IRE1ΔLD; this suggests that lipotoxicity requires a novel activation mechanism of IRE1 [51]. This study pinpointed Arginine 537 at the interface of the amphipathic and transmembrane helices in IRE1 as required for $UPR\text{-}ER^{LBS}$ but not $UPR\text{-}ER^{PT}$. Additionally, in yeast, transcriptomic analysis identified a novel subset of genes only induced by lipotoxicity in opi3Δ mutants to further differentiate $UPR\text{-}ER^{PT}$ and $UPR\text{-}ER^{LBS}$ [51]. Similarly, in *C. elegans*, activation of lipophagy by the UPR-ER is sufficient to drive lipid depletion and restructure ER morphology, thus promoting life-span extension. This occurs independently of chaperone induction [82], providing further evidence that proteostasis and lipid homeostasis are separate UPR-ER dependent processes. Collectively, these studies demonstrate that the UPR-ER can be activated directly by two parallel mechanisms: (i) by sensing aberrant protein folding and processing; or (ii) via altered membrane lipid composition, with modest activation in both parallel pathways leading to higher synergistic IRE1 activation. Such a dual sensing and response mechanism is consistent with ER's dual function in protein and lipid synthesis and processing.

1.5 Crosstalk between proteotoxicity- and lipotoxicity-Induced UPR-ER

Intriguingly, despite clear differences, the separation between proteotoxicity and lipotoxicity activated UPR is not absolute. In *S. cerevisiae*, lipid imbalance can be observed concomitantly with disturbed ER proteostasis [29,83,84]. Similarly, chronic palmitate exposure results in disrupted ER lipid rafts and causes protein overload in mouse β-cell lines [85],

providing a mechanistic framework to explain how lipotoxicity leads to proteotoxicity. Indeed, membrane lipid composition affects the sorting of many proteins to different organelles in yeast and mammalian cells, as the properties of protein transmembrane domains interact differentially with the properties of the target membrane bilayer, e.g. the thickness and chemical properties [86]. On the other hand, supplementation of oleic acid reduced disease phenotypes associated with the expression of exogenous poly-Q40, an aggregating polyglutamine peptide, in *C. elegans* [87]. This suggests that changes in the lipidome are sufficient to improve protein homeostasis through mechanisms other than chaperone induction. Molecular evidence also supports the importance of lipid homeostasis in directly maintaining proteostasis. *In vitro* biophysical assays have established the role of different classes of lipids as catalysts or inhibitors for protein folding. Anionic phosphatidylserine accelerates human amylin protein aggregation whereas cholesterol attenuates it [88]. In addition, membrane-vesicle based studies show that PE functions as a lipid chaperone for the folding of the *Escherichia coli* membrane protein lactose permease [89]. These studies suggest that rather than a downstream response, lipotoxicity can induce or exacerbate proteotoxicity directly, determined by the inherent chemical properties of lipids.

Vice versa, proteotoxicity-inducing agents can induce lipid accumulation and changes in lipid droplet size in various models, including UPR-ER deficient, aged *C. elegans* [57], human hepatoma cell lines [90], and mice [91]. However, these studies employed gene expression and visible lipid-related morphological differences to study the effects of proteotoxicity. Attempts to study changes in lipid composition more directly have been made recently. Lipid profiling using ^{1}H Nuclear Magnetic Resonance (NMR) showed protein misfolding caused by acyclic retinoid significantly reduced unsaturated fatty acid content in a human cancer cell line [92]. Raman

spectroscopy and scanning electron microscopy imaging of individual endothelial cells treated with tunicamycin showed a decrease in ER PL content [93]. Further, mass spectrometry-based lipid analysis showed that a short cultivation of *S. cerevisiae* in DTT is sufficient to induce substantial lipidomic changes, including a significant increase in PA and a shift in the profile of PA lipids toward a higher average acyl chain length and more unsaturation [94]. This occurred in an Ire1-independent manner, reinforcing the idea of a direct link between two types of parallel stresses rather than one being a downstream response of the other.

1.6 DNA damage responses in *C. elegans*

Genome integrity is important for the health and reproduction of an individual organism and its cells. Yet, environmental or endogenous genotoxic insults such as ionizing radiation, by-products of cellular metabolism, and DNA damaging agents including monofunctional alkylating agents can induce different types of DNA lesions that compromises genomic integrity. The resulting damage needs to be overcome by specialized cellular events including activation of DNA repair pathways, and cell cycle arrest and/or apoptosis programs, collectively known as the DNA damage response (DDR) [95–97]. The DDR was initially characterized in bacteria, and much of our understanding comes from genetic experiments done in yeast. *C. elegans* has also been proven to be a valuable model system as many of the *C. elegans* DDR genes, such as DNA damage sensors and signaling kinases, have conserved human disease-relevant orthologs [98–100].

1.6.1 DNA replication stress and the intra-S phase checkpoint response

Correct DNA replication and repair are key to the faithfulness of hereditary information flow. Various types of DNA lesions interfere with DNA replication and hamper replication fork progression. This phenomenon, known as replication stress, can cause genomic instability and reduce cell survival. Therefore, DNA replication needs to be an accurately regulated process. Indeed, the accuracy of DNA replication is ensured by the precise control of replication licensing, presence of cell cycle checkpoints, and specialized repair pathways for each type of lesion caused by faulty DNA replication process, such as chromosomal breakage, rearrangement and mis-segregation.

Depending on genome size, DNA replication in eukaryotes originates at hundreds to tens of thousands of replication origins along each linear chromosome, forming bidirectional replication forks during the S phase. Replication is mainly controlled at the origin licensing step during the G1 phase and the origin firing step upon entry into S phase. During licensing, origins are loaded by a conserved combination of licensing proteins [101]. Origin firing is triggered by the binding and phosphorylation of initiation factors, whose amount is limited within the cell. Therefore, different origins fire at different times, including in *C. elegans* embryos [102–104]. The timing of firing is correlated with transcriptional activities and thought to be an optimal solution to complete replication in an efficient and accurate manner [104].

However, replication is subject to many intracellular and extracellular insults, which slow down replication fork progression. Well-established stressors, including interstrand crosslinks and G-rich secondary structures, cause the replication fork to stall, activating the conserved S phase checkpoint pathway, delaying cell cycle progression into mitosis until the lesions are repaired [105].

In the case of a replication block, replication protein A (RPA, RPA-1 in *C. elegans*) binds to single stranded DNA at the replication fork, generating a structure known as primer-template junction. This structure serves as a platform to initiate a highly conserved signaling cascade, including the protein kinase ataxia-telangiectasis mutated (ATM)- and Rad3-related (ATR, ATL-1 in *C. elegans*). ATR is a phosphatidylinositol 3-kinase related kinase (PIKK), which activates the protein kinase CHK-1, slowing or arresting cell cycle progression [105,106]. At the same time, it activates the Fanconi Anemia pathway involved in replication blocks identification and subsequent homologous recombination (HR) repair [105,106]. In *C. elegans*, another member of the PIKK family is ATM-1. ATM-1 and ATL-1 may have independent functions with ATL-1 recognizing replication blocks while ATM-1 recognizes double strand breaks (DSBs) and amplifies the signal to effector molecules like p53 (CEP-1 in *C. elegans*), resolving replication stress [105,106]. However, if a lesion is not repaired, persisting stalled replication forks can lead to double strand DNA breaks [107].

1.6.2 Cell type-specific response to double strand DNA breaks

In adult *C. elegans,* the body consists of 959 post-mitotic somatic cells and a reproductive gonad system made of two U-shaped arms connected to a common uterus. In this model, tissue- and developmental stage-specific DDR mechanisms differ from somatic cells to germline cells or to dividing embryonic cells (see a detailed review [108]) (Figure 3). For example, in germ line cells or during early embryogenesis, global genome repair is the main protective pathway after UV irradiation, whereas as development proceeds, transcription coupled repair becomes more important [109]. Even within the germline, different DDRs are spatially separated in mitotic cells at the distal end of each of the gonad and in meiotic germ cells in the pachytene subphase of the

germline. In response to DSBs induced by ionizing radiation or UV-C, germline cells in mitotic zone undergoes cell cycle arrest whereas the meiotic cells undergo apoptosis [105,108,110].

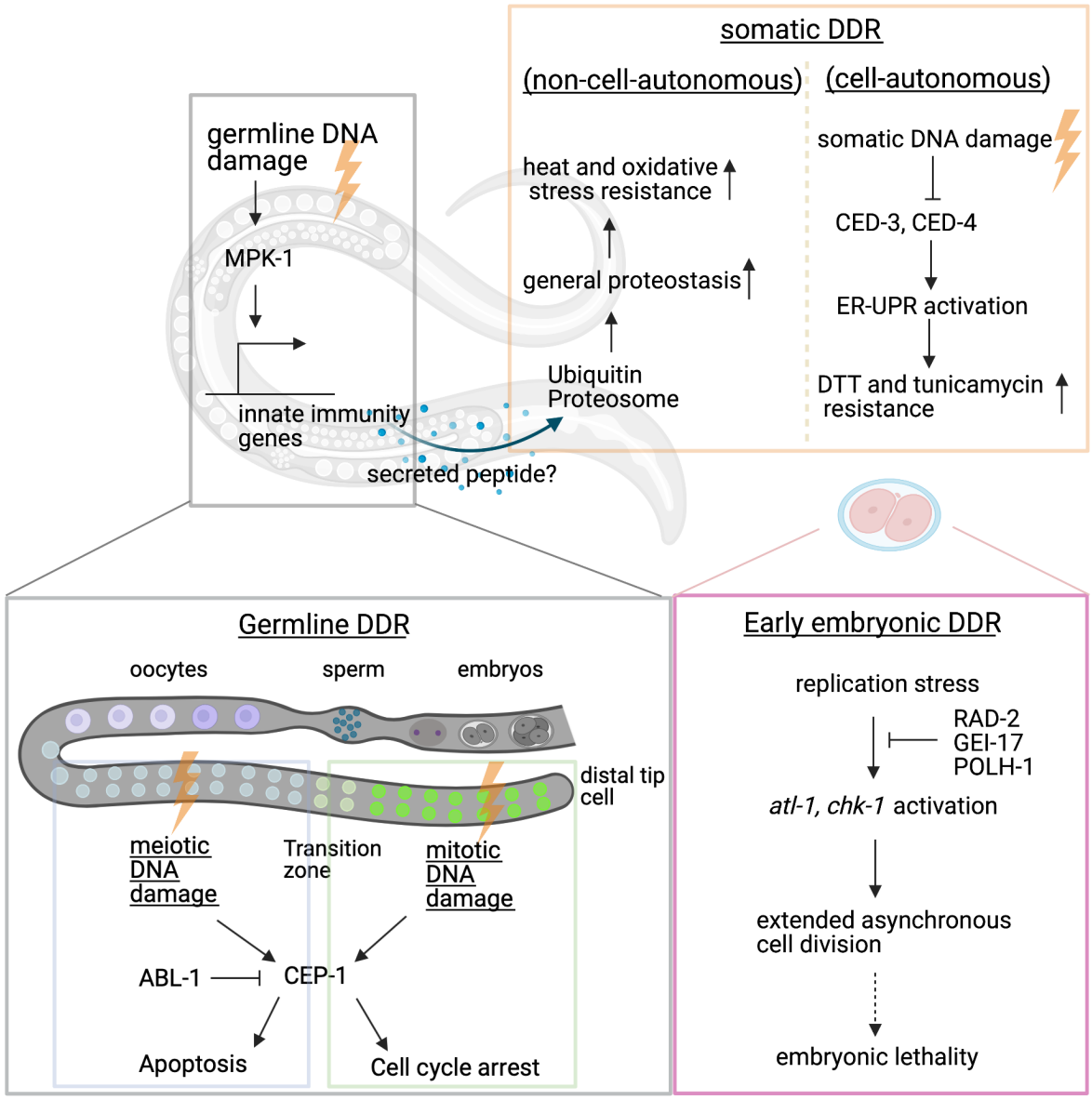

Figure 3 Overview of tissue-specific DNA damage response in *C. elegans*.

Within the germline of adult *C. elegans,* mitotic cells respond to DNA damage by cell cycle arrest whereas meiotic cells undergo apoptosis. Somatic cells are highly resistant to DNA damage-induced apoptosis, and they reprogram stress resistance pathways in a non-cell-autonomous (through germline MPK-1 signaling) and a cell-autonomous

manner (through somatic apoptosis inhibition). In early embryos, the ALT-1/CHK-1 checkpoint response is used as a developmental program to facilitate asynchronous cell division and thus establish developmental patterning. The DDR aspect of ATL-1/CHK-1 checkpoint function is actively silenced in by *rad-2*, *gei-17* and *polh-1*, while DNA damage disrupts the developmental regulation of ALT-1/CHK-1 pathway and results in embryonic lethality. (Figure created with Biorender.com, Toronto, ON, Canada).

In contrast, post-mitotic somatic cells are highly resistant to apoptosis even if similar levels of DNA damage are inflicted [100]. This is likely due to the repression of checkpoint proteins including ATM-1, ATL-1 and their downstream kinases [100]. In addition, *C. elegans* seems to allocate its energy reserves frugally between somatic maintenance and reproduction to optimize offspring fitness and its own survival [111]. DNA repair capability declines with age in post-mitotic somatic cells [108,109], suggesting that mostly-used genes are given priority in DNA repair and that somatic cells exist for a practical reproductive purpose.

In early embryos, the cell cycle alternates between S and M phases rapidly without clear gap phases. Like in somatic cells, high UV doses fail to activate checkpoint responses in rapidly dividing early embryos, because ALT-1/CHK-1 checkpoint response is regulated as a developmental program instead of solely as a DNA damage response [98,112,113]. Indeed, ATL-1/CHK-1 checkpoint controls asymmetric cell division during early embryonic development [112,113]. Therefore, DNA damage-induced ATL-1/CHK-1 checkpoint response is actively silenced in embryos by *rad-2*, *gei-17*, and the *polh-1* trans-lesion DNA polymerase, allowing replication to proceed in the presence of DNA damage [112,113]. Not surprisingly, unscheduled cell cycle arrest due to excessive DNA damage or defective replication machinery subunits like *div-1* loss of function disrupts the regulation of this ALT-1/CHK-1 developmental program and causes embryonic lethality [108,113]. Moreover, chromosome segregation defects

seen in *div-1* RNAi embryos appear to be worsened by the simultaneous knockdown of *chk-1* or *atl-1*, suggesting that the checkpoint response in *C. elegans* early embryos may also have a DDR aspect to their functions [113].

1.7 Crosstalk between DNA damage response and the UPR-ER

Sustaining genomic and proteomic integrity are top priorities for survival and reproduction. Therefore, cells integrate the DDR and UPR-ER for a coordinated stress response. Disruptions to either stress response or their cross-talk can lead to aging and serious human pathologies including cancer and neurodegeneration [114].

1.7.1 Input: DNA damage activates UPR-ER

Numerous lines of evidence indicate a link between DNA damage and UPR-ER activation in several models. For example, yeast Xbp1 protein level is upregulated via the Mec1-Rad9-Rad53 checkpoint pathway (animal ATR pathway equivalent) in response to DNA damage [115]. In addition, in a human cell line model, p53 mediates the remodeling of ER structure in chemically induced genotoxicity [116]. Moreover, DDR kinase ATM facilitates arsenite (ROS inducer)-induced checkpoint activation and clearance of protein aggregates [117]. Further, camptothecin and ionizing radiation-both genotoxic stressors, trigger UPR-ER activation through ATM and the downstream GSK3β-αNAC/γTX axis, leading to apoptosis in HeLa cell model [118].

In *C. elegans*, genome instability in germ cells increases heat and oxidative stress resistance in somatic cells, mediated by the germ line ERK MAP kinase MPK-1 innate immunity response, enhancing overall proteostasis through the ubiquitin-proteasome system (UPS) in

somatic tissues [119] (Figure 3). Because the post-mitotic somatic tissue itself is not able to elevate heat stress resistance upon genotoxicity without germ line signals, it implies that post-mitotic somatic tissue does not have an intrinsic proteostatic response inducible by genotoxicity [119]. However, a recent study showed the germline-deficient *glp-1* strain retains increased resistance to ER stress-inducing agents like DTT and tunicamycin after UV exposure [120]. This suggests that UV is able to induce specific intrinsic stress resistance programs in *C. elegans* somatic tissues, potentially independently of large-scale DNA damage repair, but through the suppression of apoptosis genes [120] (Figure 3).

1.7.2 Output: UPR-ER promotes DNA damage response in *C. elegans*

Evidence from various models has shown that UPR-ER, especially the IRE1 branch, promotes DDR, including several DNA repair pathways. IRE1 is the most conserved UPR-ER sensor and plays an important role in DDR signaling upon DNA damage [114]. Results from yeast and several cell lines show that the IRE1 and XBP1 branch is involved in the DDR [114,121]. Deletion of IRE1 sensitizes yeast to genotoxic stress and results in a ten-fold increase in chromosome loss even under unstressed conditions, and the rate of loss was enhanced upon genotoxic stress [122]. Further, dephosphorylated Xbp1 protein is recruitment to DSB sites where it regulates nucleosome positioning to stabilize the broken ends and promote non-homologous end joining (NHEJ) [115]. Immunoprecipitation of XBP1s in multiple cell lines suggested XBP1s directly regulates DDR including base excision repair (BER), mismatch repair (MMR), and nucleotide excision repair (NER) genes at transcriptional levels under ER stress and UV exposure conditions, whereas loss of XBP1s is correlated with a higher level of DNA

damage [114,123–125]. Similarly, in *C. elegans*, XBP-1s is required for the expression of DNA repair genes [42].

Another aspect of IRE1 involvement in DDR is its regulated IRE1-dependent decay of mRNA (RIDD) activity. In mouse embryonic fibroblasts (MEFs) treated with genotoxic chemicals, IRE1α promotes cell survival by controlling the stability of mRNAs involved in DDR including DNA repair, cell cycle arrest, and apoptosis [126]. Specifically, DNA damage activates the RIDD branch of IRE1α but not the XBP1 branch, through the activation of the c-Abl kinase [126], whose *C. elegans* homolog *abl-1* antagonizes *cep-1*-mediated germline apoptosis (Figure 3) [127]. Moreover, the protective role of IRE1α in DDR is conserved in fly and mouse [126]. Together, evidence collectively suggests that although the activation mechanism of IRE1α may differ among models and genotoxic stressors, IRE1α is a functionally important sensor in promoting DDR during genotoxic stress.

C. elegans relies on different repair pathways to cope with different genotoxic stressors such as ionizing radiation, cisplatin, and methyl methanesulfonate (MMS) [128,129]. While *ire-1* does not appear to be required for protecting the worm germline against ionizing radiation [128], *ire-1* loss of function renders worms more sensitive to cisplatin, which results in DNA intra-strand crosslink [130]. Yet, a whole worm proteomic study of DDR in NER deficient *C. elegans* showed a decrease in ER protein chaperone levels including HSP-3 [131], leaving open questions about the types of DNA damage in which UPR-ER plays a role, the spatial-temporal regulation of IRE-1 activation and its downstream mechanism in promoting DDR.

Less is known about PERK/PEK-1 and ATF-6's roles in DDR. In a cell line model, PERK is required for protection against oxidative DNA damage and subsequent cell cycle arrest

[132]. Similarly, ATF6 was found to have a protective role in radiation treatment, where its activation contributes to radiation-induced upregulation of GRP78/BiP [133].

1.8 Using *Caenorhabditis elegans* as a model

The nematode roundworm *Caenorhabditis elegans* (*C. elegans*) has emerged as a useful model to study a large variety of cellular processes. Genome sequencing and comparative proteomics studies have revealed 41.7% of the *C. elegans* genes has human homologs [134]. Moreover, many genetic pathways that were initially discovered in worms also exist in other species [135], including those involved in the UPR-ER, lipid metabolism, and DNA damage response.

1.8.1 *C. elegans* for studying ER unfolded protein response (UPR-ER)

The three core UPR-ER signal transducers display high levels of conservation between *C. elegans* and mammals, including humans. For example, *C. elegans* IRE-1 shares an overall 36% sequence identity with human IRE1, with the protein kinase domain and KEN (Kinase Extension Nuclease) domain 56% identical. Moreover, key residues of these structural domains are conserved in many species, including in *C. elegans*, suggesting functional conservation of IRE-1 [136]. Similarly, the *C. elegans* IRE-1-XBP-1-HSP-4 pathway (see section 1.2.1) resembles its human counterpart IRE1-XBP-1-BiP/GRP78, not only based on sequence homology, but also functional dependence (i.e. both HSP-4 and GRP78 require IRE1 for induction [137]). Including this reason, the *hsp-4p::gfp* transcriptional reporter in *C. elegans* has been widely used to monitor the IRE-1 branch activity.

PEK-1 shares an overall homology of 22% with its human homolog PERK, with the kinase domain being 41% identical. Moreover, like in mammalian cells, eIF2α phosphorylation and ATF-4 translation through upstream ORFs can be detected in *C. elegans* under ER stress-inducing conditions, suggesting the pathway in humans is functionally conserved in *C. elegans* [138,139].

The ATF-6 branch remains comparably unexplored in *C. elegans*, possibly due to the technical difficulties in monitoring its activation in a multi-cellular animal. Even though *C. elegans* ATF-6 is predicted to have a bZIP DNA binding domain, the sequence identity to its predicted human homolog is only 17%. Moreover, its sequence lacks the RXXL motif required for site 1 protease (S1P) cleavage, the inhibition of which was shown to partially block ATF6*α* processing in human cells [140], suggesting a potentially differential activation mechanism.

Despite the conservation of the mechanisms described above, there are limitations to the use of *C. elegans* to study the UPR-ER, including: (i) a relative lack of accessibility to manipulation with drugs, which sometimes fail or work only at extremely high doses (e.g. chemical chaperones, see below); and (ii) mechanistic differences concerning nuanced roles of the UPR-ER, such as RIDD (see section 1.2.1) and the unexplored roles of ATF-6.

1.8.2 *C. elegans* for studying lipid metabolism

Lipids are biochemically and functionally diverse, affecting nearly every aspect of organismal biology. With over 130 lipid metabolism genes implicated in human genetic diseases, lipid homeostasis plays a pivotal role in human health [141,142]. *C. elegans* emerged as a useful model in studying lipid metabolism because many aspects of lipid biology are conserved from mammals to *C. elegans*, including lipid synthesis, catabolism, transport, and regulatory pathways

[143]. Indeed, 237 of the 471 curated *C. elegans* lipid metabolism genes are conserved in humans and/or other model organisms, and 71 of these are implicated in human metabolic diseases [4,144]. However, there are differences in membrane lipid composition between human cells and worms, as *C. elegans* features very low to no cholesterol in its cellular and subcellular membranes. Further, unlike mammals that require dietary essential PUFA intake, homologs of plant and animal desaturase and PUFA elongases are found in *C. elegans*, enabling endogenous PUFA production [145]. Nevertheless, because of the high levels of conservation of (lipid) metabolism pathways, and because of the powerful genetic and genomic tools including forward and reverse genome-wide screens, *C. elegans* is an excellent model that has provided important new insights into the mechanistic basis of UPR-ER regulation under different stress conditions, including lipotoxicity [42,51,52,58,59,82,87,138,146,147]

1.8.3 *C. elegans* for studying DNA damage response

As a multicellular animal, *C. elegans* employs a tissue-specific DDR to optimize organismal fitness. The germ cells display an evolutionarily conserved response to DNA damage, in contrast, post-mitotic adult somatic cells display a different DDR, as they are extremely resistant to DNA damage induced apoptosis (see section 1.6.2). For this reason, *C. elegans* germ line cells are widely used to study DDR mechanisms. In addition to the general advantages such as short life cycle and invariant developmental cell lineage, tissue-specific susceptibility to DNA damaging agents and the availability of damage scoring methods also contribute to the popularity of nematode in the DDR field (for review, see [148]).

1.9 Hypothesis and objectives of the thesis

The relationship between protein synthesis, modification, and folding and the UPR-ER is well-understood; specifically, the accumulation of misfolded, unfolded, or aggregating proteins triggers UPR-ER activation. However, recently, disturbed lipid metabolism emerged as an alternate activator the UPR-ER in yeast, worms, mice, and mammalian cells) [46,78,80,149]. Results from different models have linked UPR-ER activation to different types of lipid disturbance, such as reduced PC and PI levels, increased sterol and saturated FA content, and dysregulated sphingolipid synthesis [47,48,50,150]. In yeast, gene inactivations that cause UPR-ER induction has been identified on a genome-wide basis [151], but we do not have such a comprehensive list in metazoans. However, yeast and metazoans have different membrane compositions (yeast uses ergosterol whereas mammals use cholesterol as a key membrane component). Moreover, it is possible that the yeast UPR-ER, which has IRE-1 as only sensor branch, is functionally different from that in *C. elegans* and humans, whose UPR-ER consists of IRE-1, PERK, and ATF-6 branches [18,152,153]. Finally, yeast is more evolutionarily distant from humans than *C. elegans*: 31% of yeast genes have a mammalian homolog [154], whereas over 70% of *C. elegans* lipid metabolism genes have human orthologs [144].

Hypothesis: I hypothesize that the IRE-1 branch of the UPR-ER is a sensor of the (lipid) metabolic status with incompletely mapped inputs.

Objective: to identify metabolic genes and pathways that are required for ER homeostasis using *C. elegans* as a model.

This question is important because lipid metabolism pathways regulating ER homeostasis is a theme of broad disease relevance as it offers a common mechanistic link for many currently incurable diseases such as type 2 diabetes, obesity, and cancer [155–157]. By studying these

conserved processes in *C. elegans*, I hope to identify novel (lipid) metabolic pathways that affects ER integrity. Understanding these physiological pathways may suggest new drug targets for metabolic diseases caused by ER stress.

Chapter 2: Results

2.1 New cellular functions necessary to maintain ER homeostasis in *C. elegans*

Membrane lipid composition in the ER is tightly regulated, and its disturbance is implicated in metabolic diseases. To characterize genetic pathways that link membrane lipid composition and ER homeostasis, we performed a reverse genetic screen in duplicate against a core set of 1273 metabolic genes [158] including 471 lipid metabolism genes [144] in live *C. elegans*. The screen was conducted with the ER stress-specific sensor strain *hsp-4p::gfp* that report on IRE-1 branch activity induced when membrane composition or ER proteostasis is compromised.

2.1.1 A reverse genetic screen identifies 34 RNAi whose inactivation induced IRE-1 and PEK-1

2.1.1.1 Construction of a metabolic RNAi sublibrary

We compiled a core set of 1273 metabolic genes with 471 lipid metabolism genes from two published datasets [144,158]. 1247 clones of this set are available in the Ahringer RNAi library (Table S1 tab “Sublibrary”).

2.1.1.2 RNAi proof-of-principle

To identify genes whose inactivation induces the UPR-ER in *C. elegans*, we used a stably integrated transcriptional *hsp-4p::gfp* reporter, which directly reflects the activity of IRE-1 branch of the UPR-ER. Before initiating the screen, I performed a validation experiment with

this reporter. As proof of principle, to test if knockdown approach by feeding RNAi is feasible and if the reporter reflects UPR-ER activation during proteotoxic disturbances, we subjected the reporter strain to *enpl-1* feeding RNAi, which encodes the *C. elegans* ortholog of the ER chaperone GRP94/GP96, whose disruption leads to protein misfolding [50] Indeed, *enpl-1* RNAi caused substantial induction of the hsp-4 reporter after feeding for 40hr (Figure 4A). Moreover, as reported previously, through *SCD* and *sams-1* feeding RNAi treatment, we are able to reproduce *hsp-4p::gfp* activation that reflects membrane lipid disturbance-induced UPR-ER (Figure 4A) [50].

A

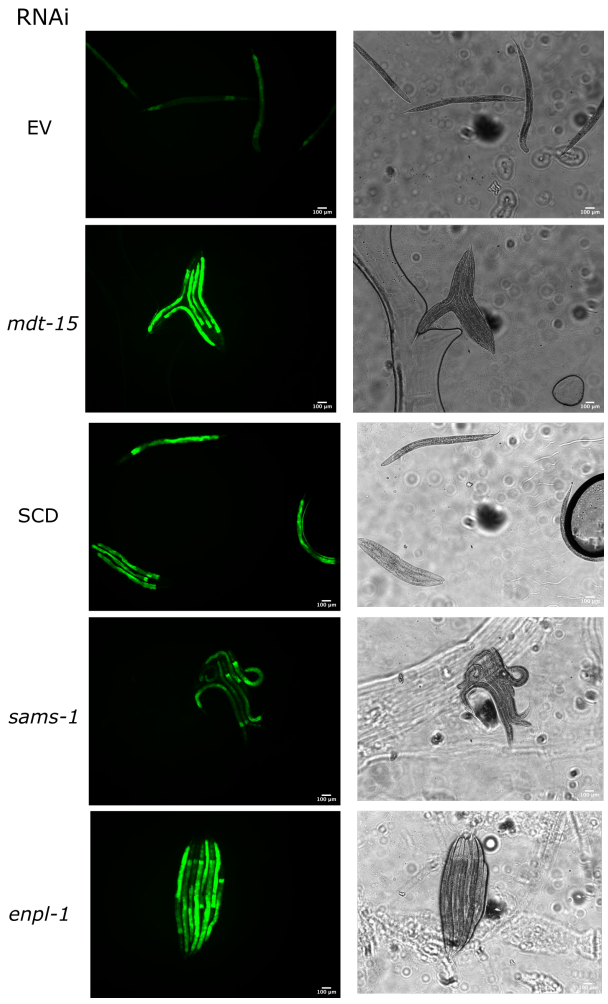

B

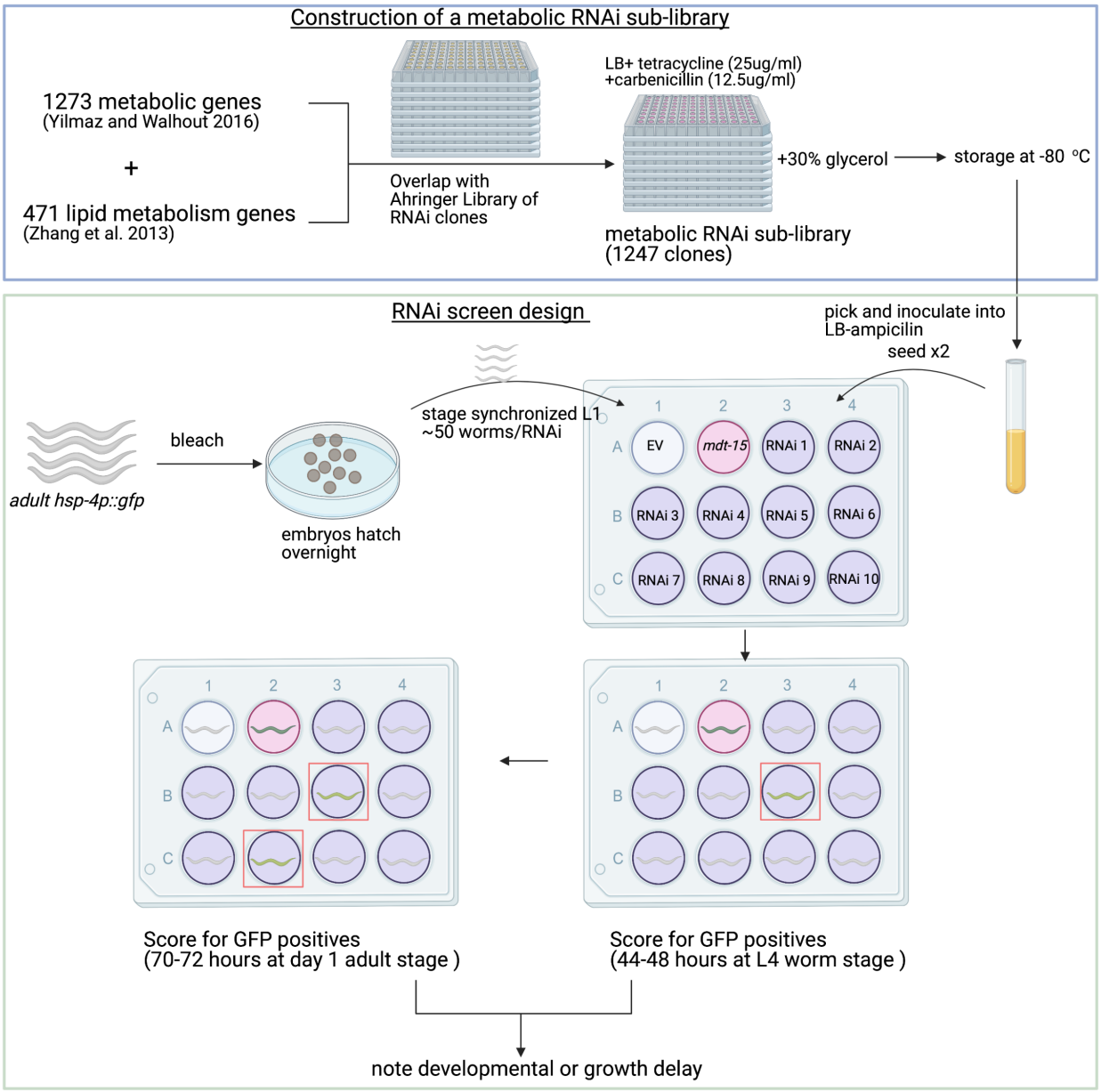
Construction of a metabolic RNAi sub-library
1273 metabolic genes
(Yilmaz and Walhout 2016)
+
471 lipid metabolism genes
(Zhang et al. 2013)
Overlap with
Ahringer Library of
RNAi clones
LB+ tetracycline (25ug/ml)
+carbenicillin (12.5ug/ml)
+30% glycerol
storage at -80 °C
metabolic RNAi sub-library
(1247 clones)
RNAi screen design
pick and inoculate into
LB-ampicilin
seed x2
adult hsp-4p::gfp
bleach
embryos hatch
overnight
stage synchronized L1
~50 worms/RNAi
EV
mdt-15
RNAi 1
RNAi 2
RNAi 3
RNAi 4
RNAi 5
RNAi 6
RNAi 7
RNAi 8
RNAi 9
RNAi 10
Score for GFP positives
(70-72 hours at day 1 adult stage)
Score for GFP positives
(44-48 hours at L4 worm stage)
note developmental or growth delay

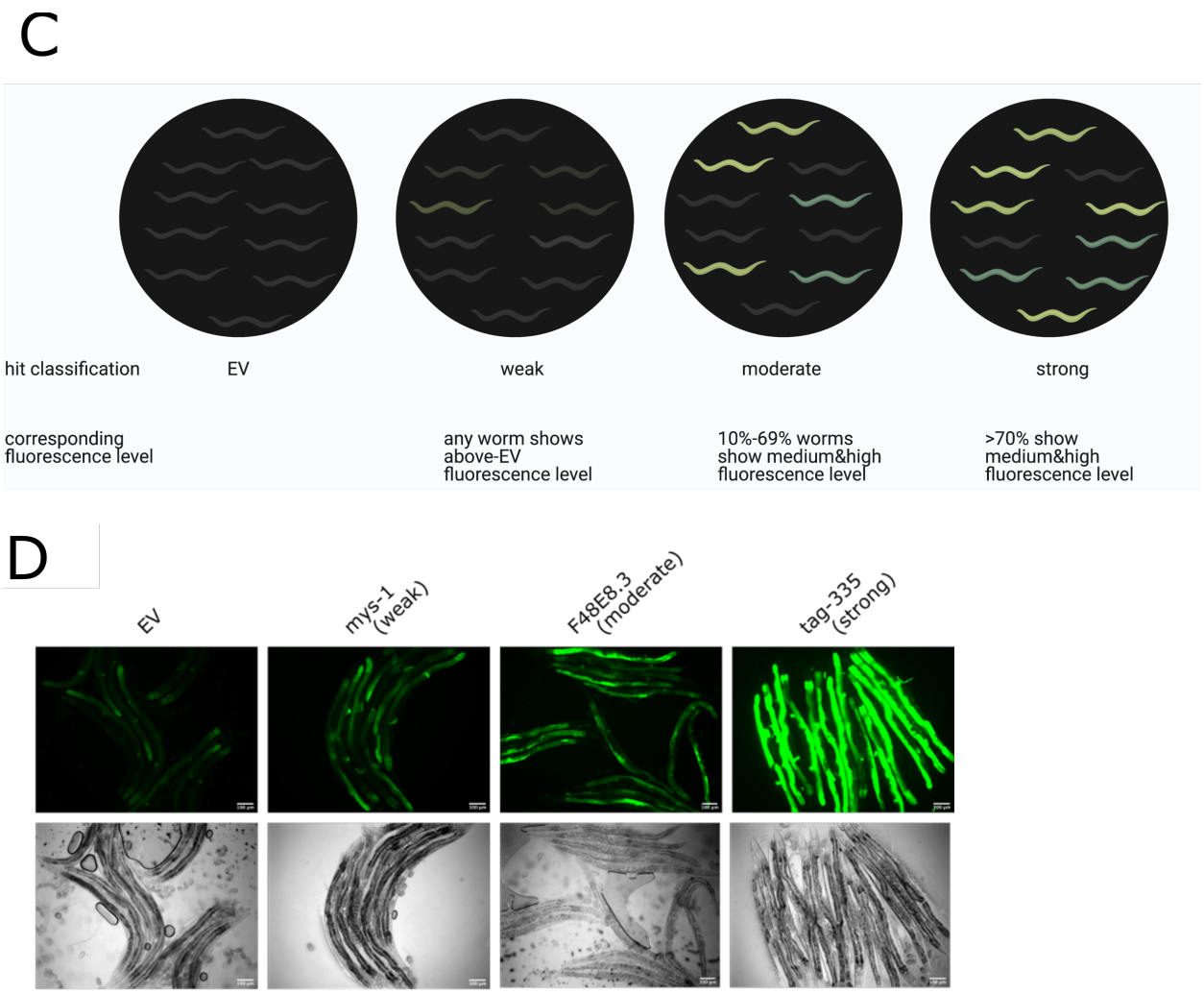

Figure 4. Metabolic RNAi screen design and proof-of-principle.

(A) Proof of principle: Micrographs show control worms expressing the *hsp-4p::gfp* transcriptional reporter grown on empty vector (EV) RNAi, *mdt-15* RNAi*, SCD* RNAi*, sams-1* RNAi, and *enpl-1* RNAi for 44 hours. Fluorescence micrographs depict activation of the *hsp-4* reporter, whereas the DIC micrographs reveal morphological phenotypes at 40hr. The images were taken at 5x magnification and the scale bars indicate 100µm. (B) Schematics of the *C. elegans* screen using the *hsp-4p::gfp* reporter strain. The metabolic sublibrary was constructed by overlapping 1273 metabolism genes and 471 lipid metabolism genes with the Ahringer RNAi library. Hits were scored as positive when above-background fluorescence was detected at either 44-48hr or 70-72hr. (Figure created with Biorender.com, Toronto, ON, Canada). (C) Schematics of hits fluorescence classification rubric: “strong” hit: >70% high and medium fluorescence worms, “moderate” hit: 10-69% strong and moderate fluorescence worms, “weak”

hit: any worms displayed fluorescence above the negative control. (Figure created with Biorender.com, Toronto, ON, Canada) (D) Micrographs show representative images of GFP intensities at 72hr that were classified as "weak", "moderate", and "strong" hits based on the categorization rubric. The scale bars indicate 100μm.

2.1.1.3 Identification of 106 UPR-ER-inducing candidate screen hits

Following validation of the approach, we performed the screen in duplicate. The screen was conducted as follows (Figure 4B): each well in a 12-well plate was seeded twice with appropriate RNAi clone bacteria targeting genes of interest. Each experiment was tested in a batch of 30-40 RNAi clones including a positive control (*mdt-15* RNAi clone) [50] and a negative control (empty vector RNAi clone). Around 50 L1 stage-synchronized worms were placed into each RNAi well, and the GFP fluorescence was scored with a Leica M205FA upright fluorescent microscope at 44-48 hours at L4 worm stage and again at 70-72 hours at day-1 young adult stage. Additionally, knocking down metabolic enzymes can potentially affect worm growth and development. Therefore, along with GFP fluorescence scoring at both time points, developmental or growth delay was noted if any ("comments" section in Table S1 tabs "Screen #1" and "Screen #2"). GFP fluorescence was visually scored into three categories (low, medium, and high), and the number of worms in each category was counted. Then a hit classification was assigned based on a semi-quantitative rubric (Figure 4C): if more than 70% of worms displayed high and medium fluorescence, the RNAi clone was classified as a "strong" hit and assigned an GFP intensity number "5". If 10-69% displaced strong and moderate fluorescence, the clone was classified as a "moderate" hit and assigned an GFP intensity number "3". If any worms displayed fluorescence above what was seen in the negative control, it was classified as a "weak" hit and assigned an GFP intensity number "1". Note in the first round of screening, fluorescence at 72

hours was only scored for 398 clones, and only on a qualitative basis. Based on this rubric, we identified 107 candidate RNAi hits that appeared at least once as a weak hit at either time point in either screen (Table S1, tabs “Screen #1” and “Screen #2”). Note that the C10C5.3 RNAi clone failed to grow in subsequent experiments, thus yielding 106 initial candidate hits. Representative GFP images of hits of “strong”, “moderate”, and “weak” GFP intensities are shown with *tag-335,* F48E8.3, and *mys-1* RNAi treatments (Figure 4D).

2.1.1.4 Triplicate validation of candidate hits yields 38 high-confidence hits

Next, for validation, three independent experimental repeats of RNAi against these 106 initial candidate hits were performed. Briefly, the same screen design and scoring rubric were applied as in the two initial screens. Each repeat was performed in 12 well format, with around 50 worms per well, and the positive *mdt-15* RNAi control and negative EV control. GFP intensity of *hsp-4p::gfp* worm population grown on each of the 106 RNAi was scored at 46-50hr and 70-72hr (Table S1 tabs “Valid. #1” “Valid. #2” “Valid. #3” “Valid. summary”). The same hits classification rubric from the initial 2 screens (section 2.1.1.3) was applied to the three biological repeats of the 106 candidate hits.

Then, the GFP intensities from these five screens (two initial, three validation) were aggregated to generate a summative score. For this purpose, we assigned values of 5, 3, and 1 in each individual experiments to the rubrics “strong,” “moderate,” and “weak,”). A hit was considered validated if it obtained summative score of at least 3 (i. e. being at least a moderate hit once or a weak hit three times at one time point in one of the 5 repeats). As a result, 38 high confidence hits passed the cutoff threshold, the remaining 68 initial hits that failed to reach the threshold were dropped from further testing.

2.1.1.5 Sanger sequencing validates 35 RNAi clones as hits

To ensure that the validated candidate hits are of expected sequence and to eliminate non-specific UPR-ER activation, we confirmed the sequence of the 38 high confidence RNAi hits by sending them for Sanger sequencing (DNA Sequencing and BioAnalyzer Core Facilities, Centre for Molecular Medicine and Therapeutics). This revealed that three of 38 RNAi clones harbored the wrong insert (Table S1, tab "Sequencing"). "*hach-1"* sequencing yielded *let-767* sequence, which we independently identified as a high-confidence weak hit. Similarly, the "*algn-11*" clone revealed *ykt-6* sequence (which is a *C. elegans* homolog of yeast v-SNARE protein), which is required for membrane fusion in vesicle trafficking among numerous cellular compartments [159]. It is possible that reduced YKT-6 levels hamper proper cargo transport from and to the ER, disturbing ER homeostasis and activating the UPR-ER. Lastly, the *fat-2* clone did not appear to have an insert sequence. In addition, although it passed the validation and sequencing step, one weak hit, *ahcy-1*, subsequently consistently failed to induce *hsp-4p::gfp* expression above background level reproducibly and was thus eliminated going forward. Therefore, after vigorous validation of hits, we obtained 34 "true" hits that reproducibly induced *hsp-4p::gfp* expression above background in *C. elegans* at late L4 and/or day 1 adult stages. Importantly, this list includes several genes whose inactivation is known to cause UPR-ER activation, including the fatty acid desaturation enzyme *fat-6*, the PC synthesis enzymes (*pcyt-1*, *sams-1*), the 3-hydroxy-3-methylglutaryl CoA synthase *hmgs-1*, and the sarco-endoplasmic reticulum calcium ATPase *sca-1*, validating our screen [50,52,160].

For direct visualization and comparison of GFP intensity among the 34 true hits, we calculated the average GFP intensity for each RNAi clone (scale 1-5), at each time point, from

the two initial screens and the three biological repeats. The resulting average GFP intensity values were plotted as a heatmap (Figure 5A). Further, we picked 18 of 34 RNAi whose link to UPR-ER activation has not been previously explored and cannot be rationalized by a straight-forward explanation of disturbed proteostasis, unlike for example for protein disulfide isomerase family members [161]. GFP fluorescence was also quantified in a scatter plot with each dot representing GFP intensity in individual worms grown on EV, *mdt-15* and the 18 RNAi hits (Figure 5B).

A

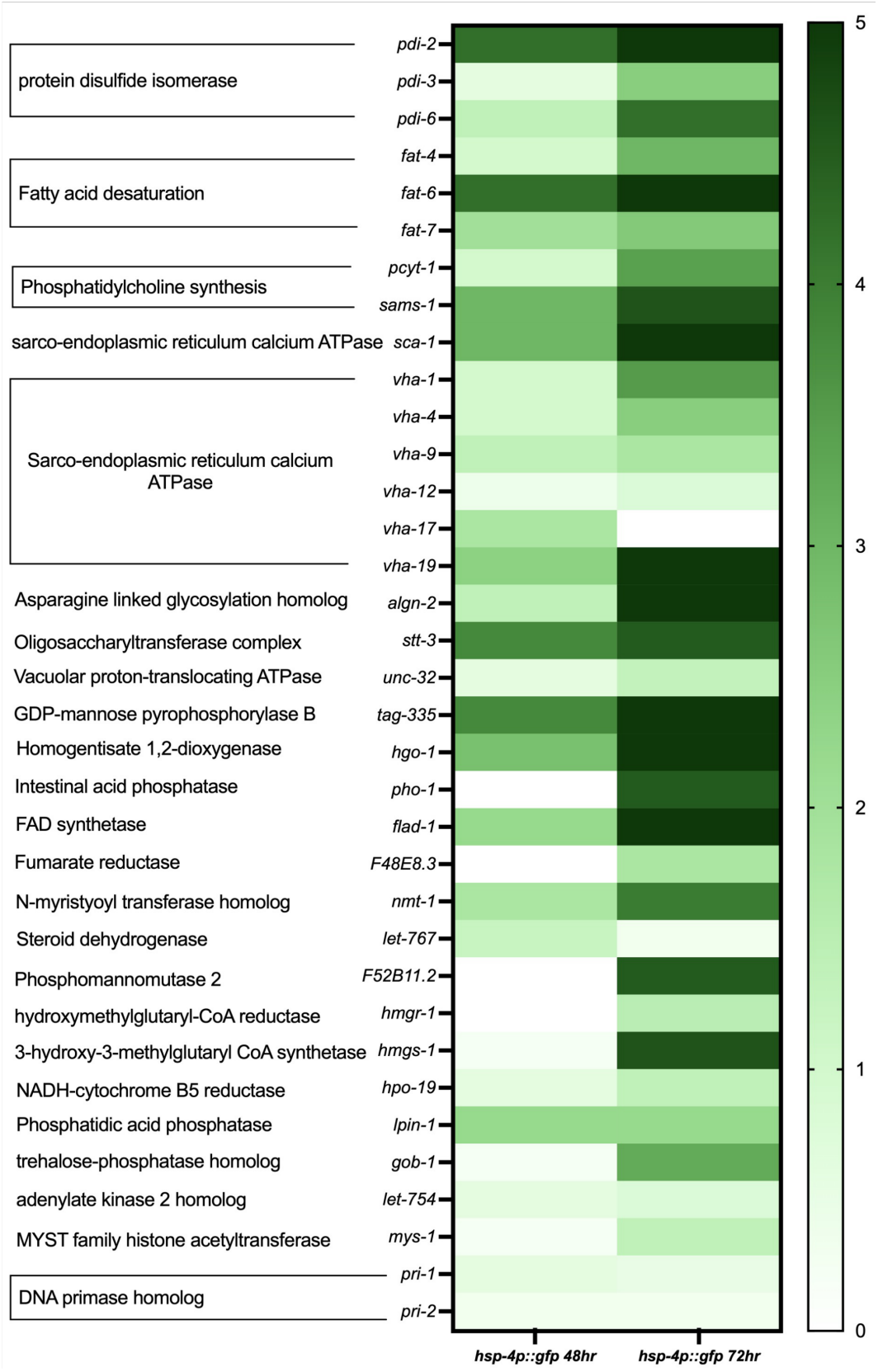
protein disulfide isomerase
pdi-2
pdi-3
pdi-6
Fatty acid desaturation
fat-4
fat-6
fat-7
Phosphatidylcholine synthesis
pcyt-1
sams-1
sarco-endoplasmic reticulum calcium ATPase
sca-1
Sarco-endoplasmic reticulum calcium ATPase
vha-1
vha-4
vha-9
vha-12
vha-17
vha-19
Asparagine linked glycosylation homolog
algn-2
Oligosaccharyltransferase complex
stt-3
Vacuolar proton-translocating ATPase
unc-32
GDP-mannose pyrophosphorylase B
tag-335
Homogentisate 1,2-dioxygenase
hgo-1
Intestinal acid phosphatase
pho-1
FAD synthetase
flad-1
Fumarate reductase
F48E8.3
N-myristoyl transferase homolog
nmt-1
Steroid dehydrogenase
let-767
Phosphomannomutase 2
F52B11.2
hydroxymethylglutaryl-CoA reductase
hmgr-1
3-hydroxy-3-methylglutaryl CoA synthetase
hmgs-1
NADH-cytochrome B5 reductase
hpo-19
Phosphatidic acid phosphatase
lpin-1
trehalose-phosphatase homolog
gob-1
adenylate kinase 2 homolog
let-754
MYST family histone acetyltransferase
mys-1
DNA primase homolog
pri-1
pri-2
5
4
3
2
1
0
hsp-4p::gfp 48hr
hsp-4p::gfp 72hr

B

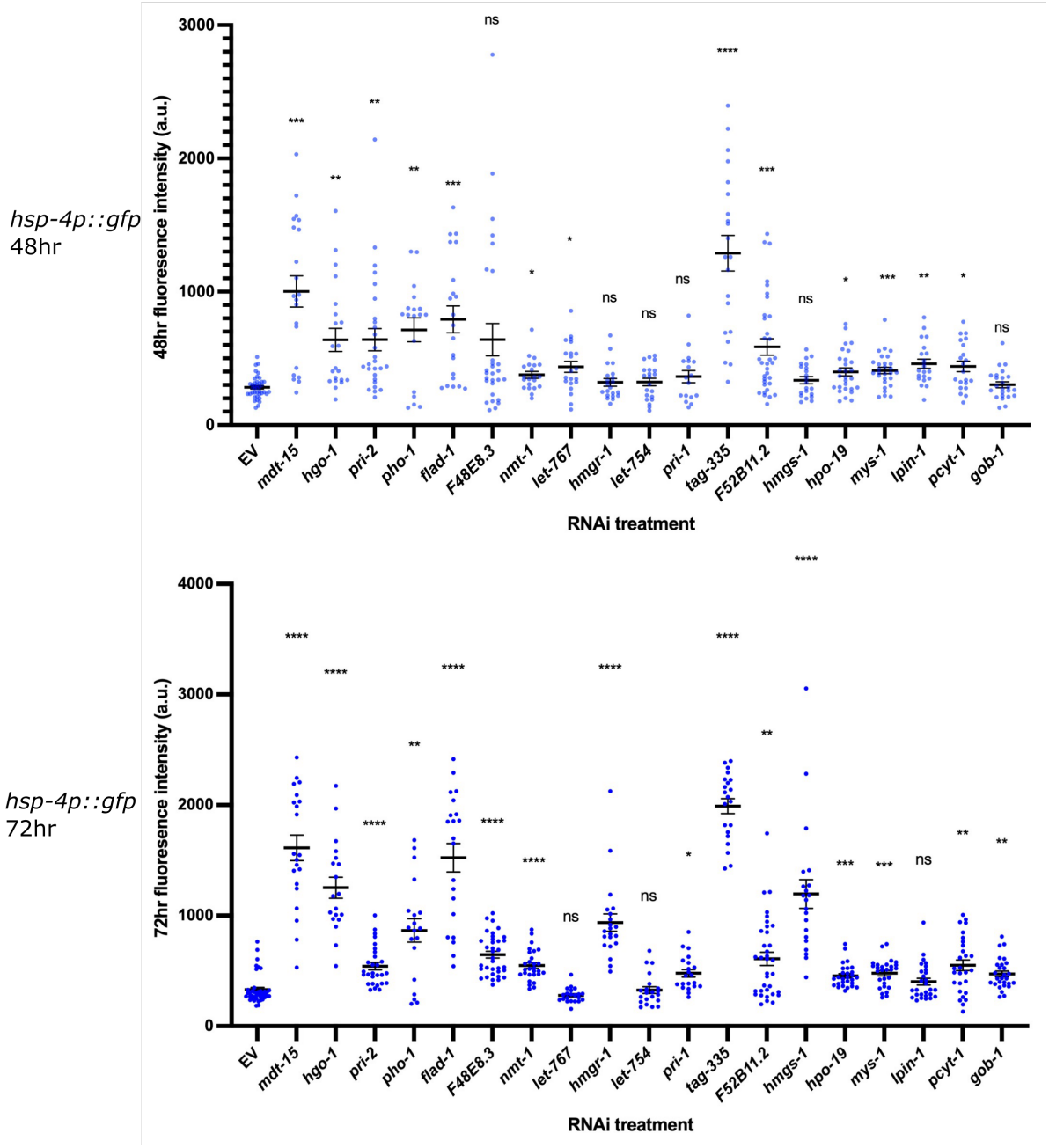

Figure 5. Summary of screen hit identities and intensities of UPR-ER reporter strains.

(A) Heat map of average scores reflecting *hsp-4p::gfp* fluorescence intensity. Average score is aggregated from two screen and three validation experiments (Table S1). (B) GFP signal quantification of *hsp-4p::gfp* on EV, *mdt-15* RNAi, and 18 select hit RNAi at 44-48hr and 70-72hr from ≥ 20 individual worms (n=3 per RNAi treatment). Statistical analysis: Dunnett's T3 multiple comparisons test; all comparisons are to vector RNAi (negative control).

2.1.2 Confirmation of endogenous UPR-ER induction in 15 select hits

To show that our observation of *hsp-4p::gfp* induction is also reflected in the endogenous mRNA levels, we aimed to confirm the induction of the endogenous UPR-ER in WT worms using real-time PCR. We quantified the mRNA levels of *hsp-4* and Y41C4A.11 (a coatomer protein complex subunit), both targets of the IRE-1 branch (Figure 6). *hsp-4* is widely used to monitor the response of the *ire-1* branch of proteotoxic stress and lipotoxic stress [50]. Y41C4A.11 was chosen because its induction is *xbp-1*-dependent upon tunicamycin treatment and exposure to pathogenic strains of bacteria [162,163]. Testing 15 of 34 RNAi clones whose link to UPR-ER activation is unclear, we found that 5 of 15 activate both genes (RNAi against *flad-1*, *let-767*, *lpin-1*, *nmt-1*, and *tag-335*) and 11 induced at least one gene at 44hr post-RNAi treatment. Note that the other four RNAi clones, which failed to induce either gene at 44hr, were classified as non-hits in our initial and validation screens at that timepoint (RNAi against F48E8.3, F52B11.2, *gob-1*, and *mys-1*) (Table S1 tab "Hits Summary"). These results collectively suggest that the *hsp-4p::gfp* transcriptional reporter is able to accurate reflect endogenous UPR-ER activation.

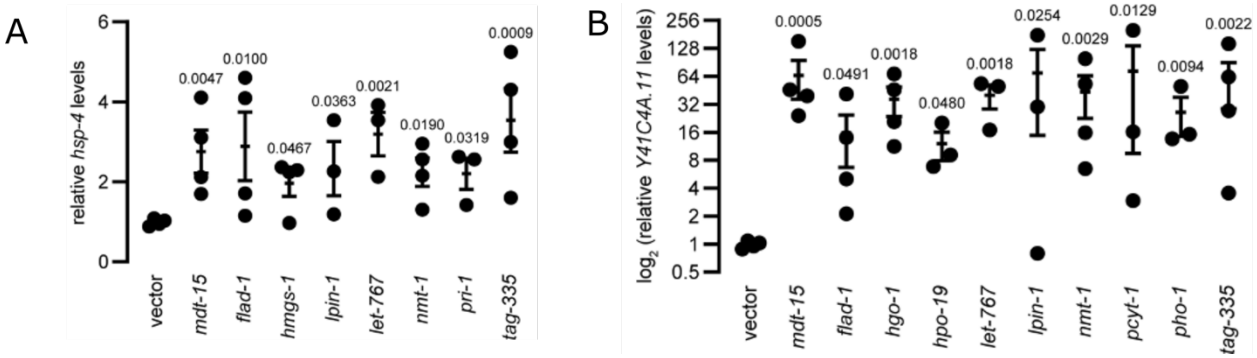

Figure 6. Dot plots indicate the relative mRNA levels

Relative mRNA levels (A) of *hsp-4* and (B) of Y41C4A.11 at the larval 4 stage (i.e., after 44hr; n = 3 or 4 per RNAi treatment). Error bars represent SEM. Statistical analysis: Kruskal–Wallis test; all comparisons are to vector RNAi (negative control). Note, only the RNAi clones that evoked significant changes in *hsp-4* or Y41C4A.11 are shown, out of 15 total tested clones.

2.1.3 All hits require canonical IRE-1–XBP-1 signaling for UPR-ER activation

Next, we wished to test whether the RNAi clones we identified result in canonical, i.e., *xbp-1* dependent, *hsp-4* activation. We confirmed reliance on canonical IRE-1 signaling by monitoring fluorescence after RNAi in a strain lacking XBP-1 (*xbp-1; hsp-4p::gfp*) at 48hr and 72hr. We found that. at least at these two time points, no above-background GFP fluorescence is observable in samples grown on all 34 clones, suggesting all hits required *xbp-1* for induction (Table S1, tab "*xbp-1* dep.").

2.1.4 ATF-4 activation is observed in all 34 hits

Next, we asked whether the *pek-1* branch of the UPR-ER is activated by any of the 34 RNAi clones. The PERK/eIF2α/ATF-4 axis is well established in mammals and upregulated in response to numerous types of stresses including hypoxia, nutritional deprivation and genotoxicity [164]. In *C. elegans*, the *atf-4* transcript contains upstream ORFs that prevents translation of the full-length product under unstressed conditions. However, PEK-1 activation-induced general translation inhibition in turn promotes translation of the full-length *atf-4* transcript [139]. To monitor *pek-1* branch activity in *C. elegans*, we used the *pek-1*-specific reporter *atf-4(uORF)::gfp*, which contains GFP fused to the *atf-4* upstream region, including the uORFs [138]. Using this reporter strain, we performed feeding RNAi experiments for all 34 identified hits and applied the same screening rubric as used in the *hsp-4p::gfp* screens to

generate semi-quantitative values of GFP intensity (Table S4). We found that all 34 hits caused increased *atf-4(uORF)::gfp* fluorescence at either one or both time points (Figure 7A). GFP intensity in 18 of the 34 hits was quantified in a scatter plot with each dot representing GFP intensity in individual worms grown on 18 of the 34 RNAi hits (Figure 7B).

A

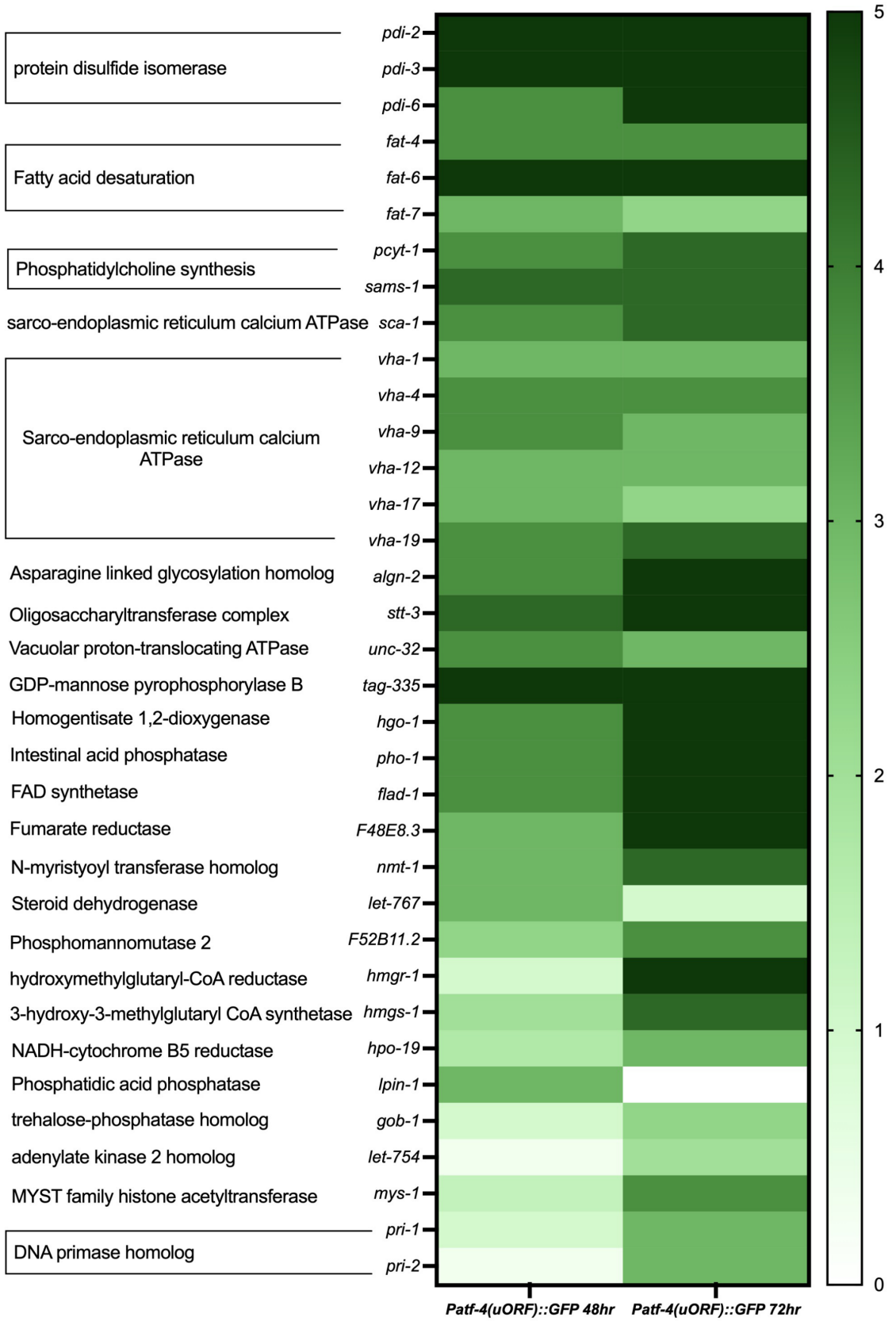
protein disulfide isomerase
pdi-2
pdi-3
pdi-6
Fatty acid desaturation
fat-4
fat-6
fat-7
Phosphatidylcholine synthesis
pcyt-1
sams-1
sarco-endoplasmic reticulum calcium ATPase
sca-1
Sarco-endoplasmic reticulum calcium ATPase
vha-1
vha-4
vha-9
vha-12
vha-17
vha-19
Asparagine linked glycosylation homolog
algn-2
Oligosaccharyltransferase complex
stt-3
Vacuolar proton-translocating ATPase
unc-32
GDP-mannose pyrophosphorylase B
tag-335
Homogentisate 1,2-dioxygenase
hgo-1
Intestinal acid phosphatase
pho-1
FAD synthetase
flad-1
Fumarate reductase
F48E8.3
N-myristyoyl transferase homolog
nmt-1
Steroid dehydrogenase
let-767
Phosphomannomutase 2
F52B11.2
hydroxymethylglutaryl-CoA reductase
hmgr-1
3-hydroxy-3-methylglutaryl CoA synthetase
hmgs-1
NADH-cytochrome B5 reductase
hpo-19
Phosphatidic acid phosphatase
lpin-1
trehalose-phosphatase homolog
gob-1
adenylate kinase 2 homolog
let-754
MYST family histone acetyltransferase
mys-1
DNA primase homolog
pri-1
pri-2
5
4
3
2
1
0
Patf-4(uORF)::GFP 48hr
Patf-4(uORF)::GFP 72hr

B

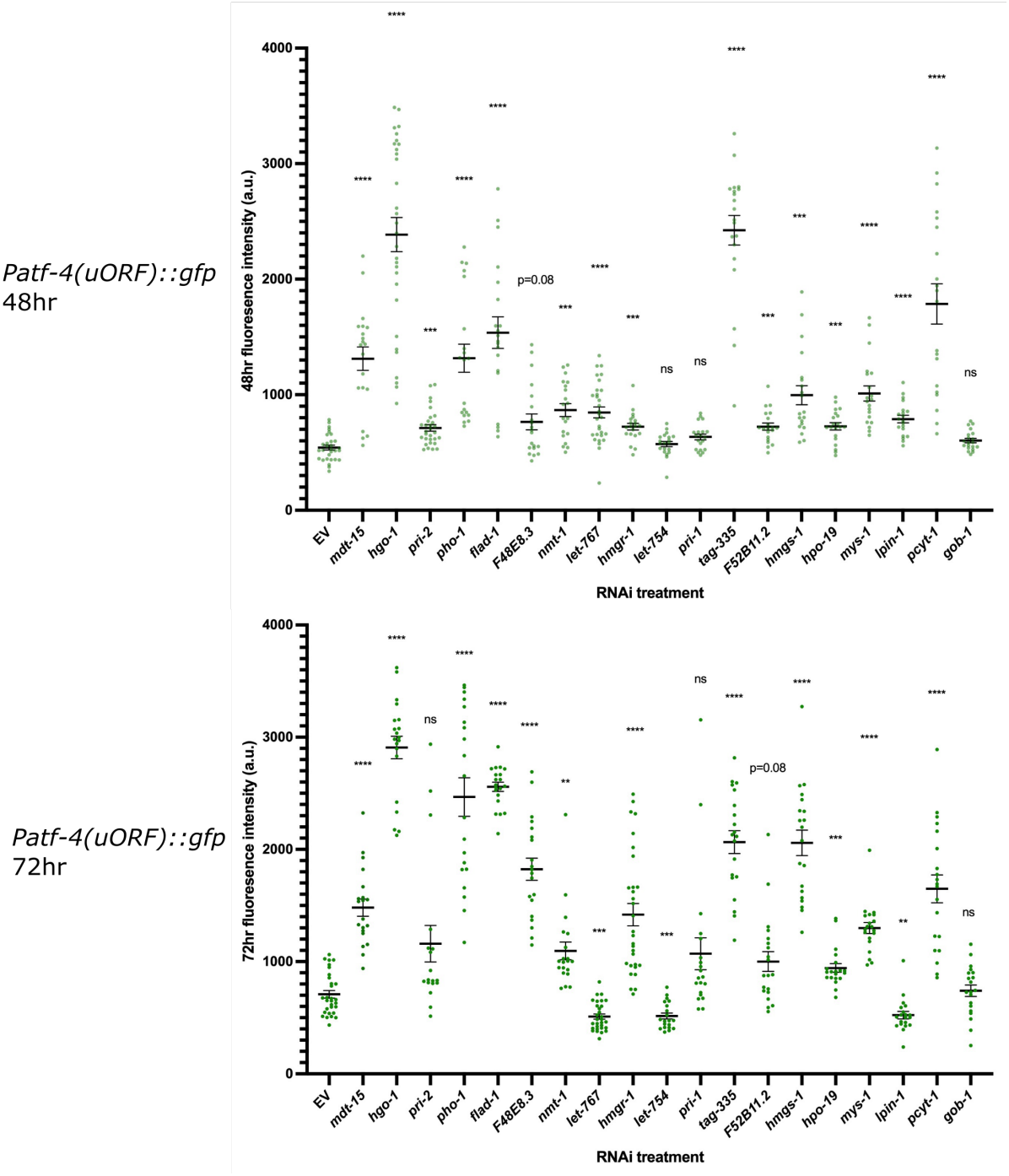

Figure 7. Summary of screen hit identities and intensities of the *Patf-4(uORF)::gfp* reporter strain.

(A) Heat map of average scores reflecting *Patf-4(uORF)::gfp* fluorescence intensity. Average score is aggregated from three biological repeats (Table S4). (B) GFP signal quantification of *Patf-4(uORF)::gfp* on EV, *mdt-15* RNAi, and 18 select hit RNAi at 44-48hr and 70-72hr from ≥ 20 individual worms (n=3 per RNAi treatment). Error bars

represent SEM. Statistical analysis: Dunnett's T3 multiple comparisons test; all comparisons are to vector RNAi (negative control).

2.1.5 Choline supplementation suppresses UPR-ER activation in 3 of 34 hits

C. elegans worms defective for the s-adenosylmethionine (SAM) synthase *sams-1* are unable to synthesize PC through the cytidine diphosphate diacylglycerol (CDP-DAG) pathway [50,52]. Moreover, knocking down *sams-1* increases lipogenic gene expression and activates the UPR-ER [50,165]. However, supplementation of dietary choline bypasses the requirement for SAM in PC synthesis and is able to rescue the morphological phenotypes of *sams-1(RNAi)* to worms and suppresses membrane lipid disturbance-induced UPR-ER activation [50,165]. Therefore, to understand if UPR-ER activation in our 34 hits was due to reduced PC levels, we tested whether choline supplementation is sufficient to suppress UPR activation in any of the hits. As expected, we observed complete rescue of *sams-1* RNAi-treated animals (Figure 8A and B). Choline supplementation also partially suppresses *mdt-15* RNAi-induced UPR-ER, consistent with observation reported previously that *mdt-15(RNAi)* worms have a reduced PC level. Additionally, we observed partial rescue of RNAi clones *hmgs-1*, and *vha-4*. Thus, 31 of 34 hits likely induce the UPR without dramatically altering PC levels (Table S1 tab "choline resc."), including *pri-1* and *pri-2* RNAi (Figure 8C).

A

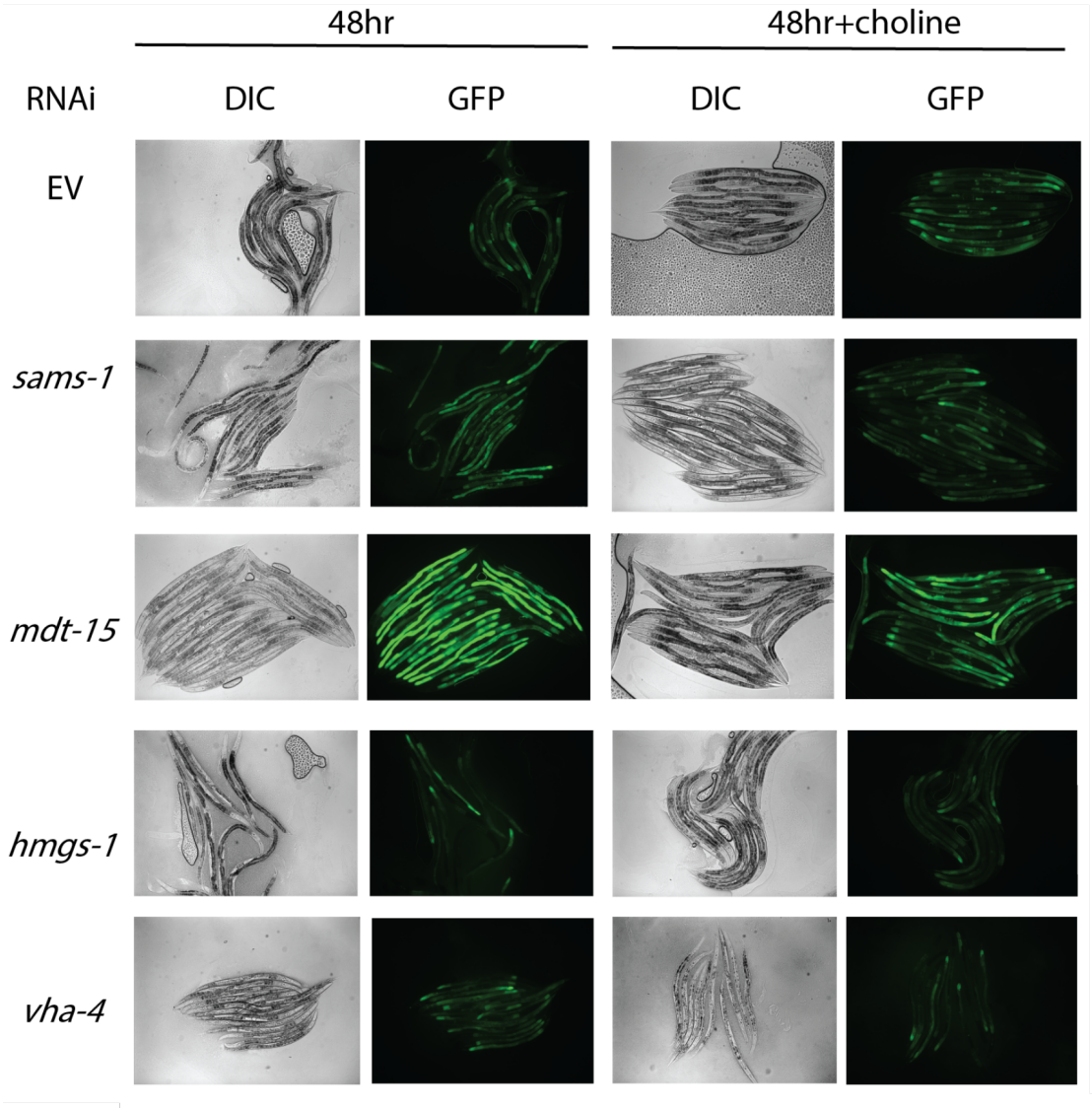
48hr
48hr+choline
RNAi
DIC
GFP
DIC
GFP
EV
sams-1
mdt-15
hmgs-1
vha-4

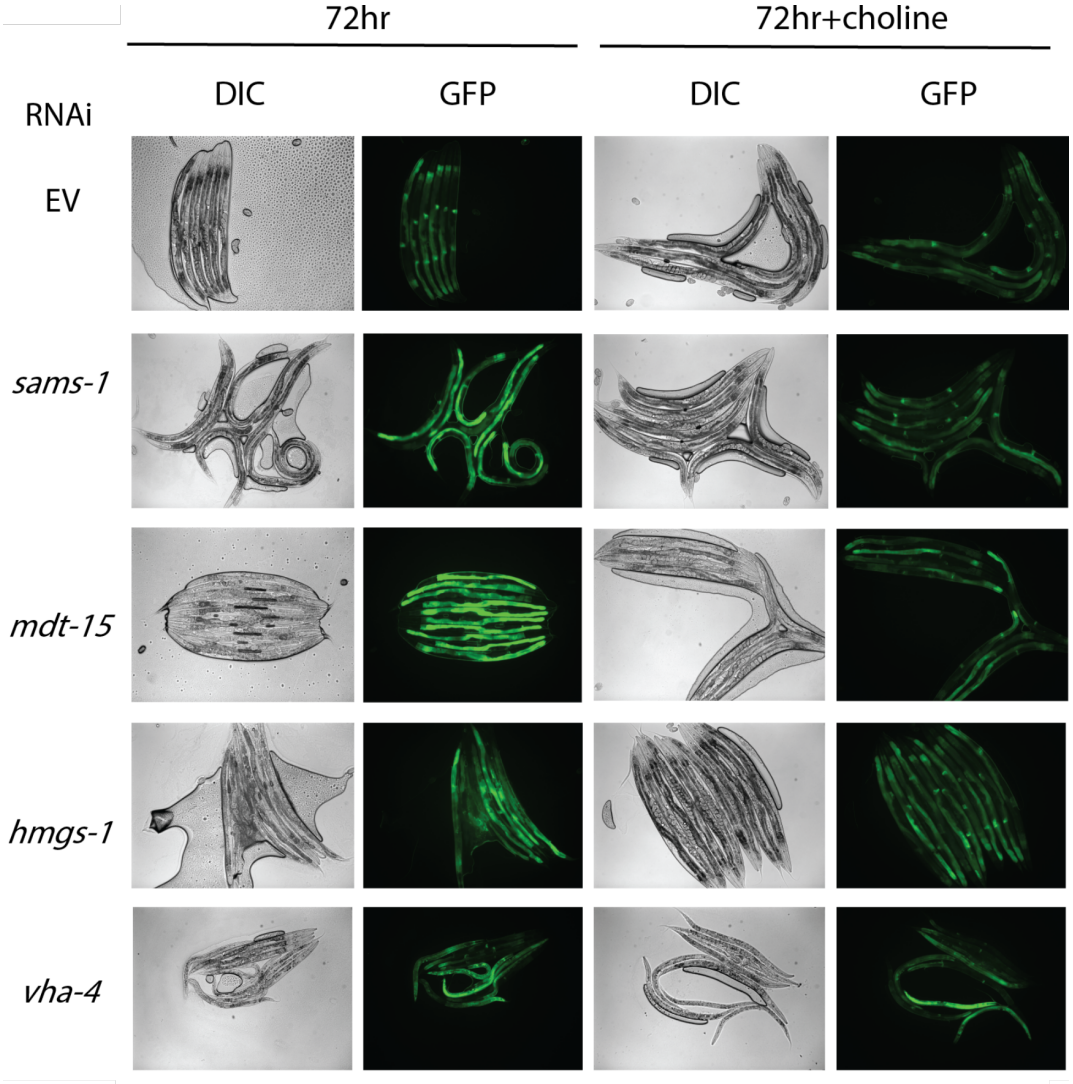
72hr
72hr+choline
RNAi
DIC
GFP
DIC
GFP
EV
sams-1
mdt-15
hmgs-1
vha-4

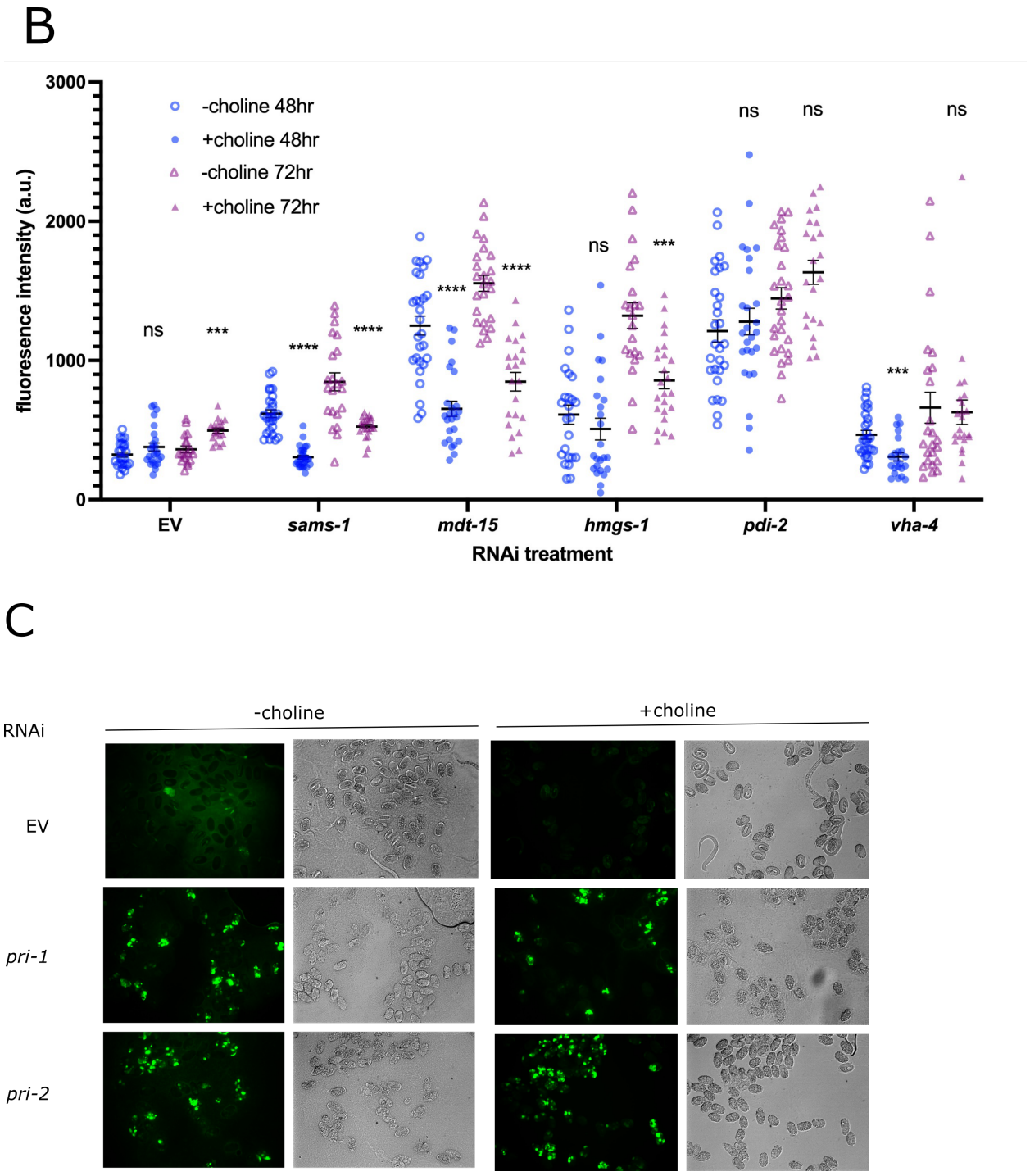

Figure 8. UPR-ER activation in select hits is rescued by dietary choline supplementation.

(A) Micrographs show control RNAi (EV), *sams-1(RNAi)*, *mdt-15(RNAi)*, *hmgs-1(RNAi)*, and *vha-4(RNAi)* worms expressing the *hsp-4p::gfp* transcriptional reporter grown without dietary supplements or with choline supplements. Fluorescence micrographs depict activation of the *hsp-4p::gfp* reporter, whereas the DIC micrographs reveal

morphological phenotypes. GFP images show partial suppression of UPR-ER with choline supplementation in *hsp-4p::gfp* worms grown on *mdt-15*, *hmgs-1*, or *vha-4* RNAi as well as the expected complete rescue of *sams-1* RNAi-treated animals, at 48hr and 72hr. (B) GFP signal quantification of *hsp-4p::gfp* on EV, *sams-1*, *mdt-15*, *hmgs-1*, and *vha-4* RNAi with or without choline at 48hr and 72hr from ≥ 20 individual worms (n=2 per RNAi treatment). Error bars represent SEM. Statistical analysis: Welch t-test; all comparisons are to vector RNAi (negative control). (C) Micrographs show control RNAi (EV), *pri-1* (RNAi) and *pri-2* (RNAi) embryos expressing the *hsp-4p::gfp* transcriptional reporter grown without dietary supplements or with choline supplements at 72hr (n=4).

2.1.6 Inactivation of yeast SPC2 homolog *spcs-2* activates UPR-ER in *C. elegans*

Yeast Ire1 retains the ability to sense LBS even if Ire1 contains a truncated LD (*IRE1ΔLD*) [81]. To systematically identify cellular perturbations inducing LBS in yeast, a genome-wide genetic screen was conducted with WT Ire1- and Ire1ΔLD-expressing query strains containing a reporter wherein GFP is driven by the UPR response element [51]. 181 hit genes whose inactivation induced the UPR-ER in both *IRE1* WT and *IRE1ΔLD* yeast strains were identified.

We asked whether the 181 genes identified in the yeast screen are linked to UPR^{LBS} activation by their homologs in *C. elegans*. We used RNAi to knock down 38 *C. elegans* genes homologous to yeast genes, and found that RNAi inactivation of one, the signal peptidase complex subunit homologue *spcs-2* (yeast homolog *SPC2*), activated the *hsp-4p::gfp* reporter (Table S2) (Figure 9). Note that of the 38 yeast homologous RNAi clones tested, three clones were of the wrong sequence (Table S2).

We also compared the 181 candidates from the yeast screen to the 34 candidates from our *C. elegans* screen to identify evolutionarily conserved processes or pathways whose impairment activates the UPR-ER in both species. Some genes whose inactivation induces the UPR-ER in *C.*

elegans are essential in yeast (e.g., fatty acid desaturation genes OLE1, protein disulfide isomerase PDI1), thus preventing us from assessing their conservation. However, impairment of Ole1 activation by Ubx2 loss induces the UPR-ER via increased saturated membrane lipids [166]. Notably, inactivation of genes in several other pathways resulted in robust UPR-ER^{LBS} induction across species, for example, genes involved in PC synthesis, genes encoding the vacuolar H^+-ATPase, and several related metabolic genes like MYST family histone acetyltransferase and succinate hydrogenase (Table S3).

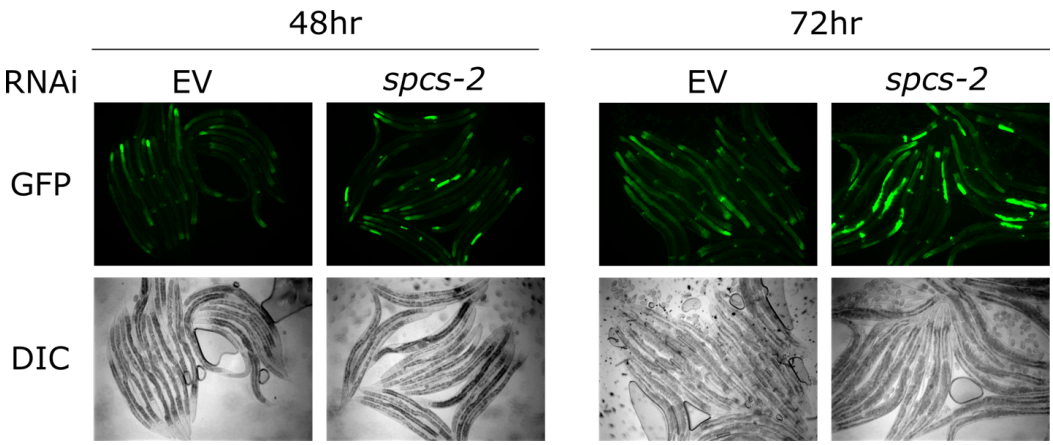

Figure 9. Inactivation of *spcs-2* activates UPR-ER.

Inactivation of *spcs*-2, the signal peptidase complex subunit homologue of yeast *SPC2*, activated the *hsp-4p::gfp* reporter in *C. elegans* at 48hr and 72hr (n=3).

2.1.7 Discussion

Since the discovery of membrane lipid as a protein misfolding-independent activator of the UPR-ER, small-scale examination of lipid metabolism gene functions in maintaining ER homeostasis have been published in various models [48,50,81]. As such, the extent of cellular perturbations activating the UPR-ER through metabolic disturbances was unknown. To address

this knowledge gap, we have performed large-scale reverse genetic screens and identified a set of genes necessary to maintain ER membrane integrity in *C. elegans*, which has homologs in conserved pathways in yeast. More detailed discussions of genes from the *C. elegans* screen and their potential mechanism in maintaining ER homeostasis are included below (see section 3.1). Our *C. elegans* screen results have provided a valuable addition to previous studies, highlighting the link between novel aspects of metabolism and ER homeostasis.

2.2 Genotoxic stress activates the UPR-ER

One interesting class of hits from our *C. elegans* screen is the primases (*pri-1* and *pri-2*). We observed that both primase subunits *pri-1* and *pri-2* induced *hsp-4p::gfp* expression in *C. elegans* embryos from adults fed RNAi for the screen (i.e. effect was strongly manifested in the F1 generation). Loss of *pri-1* and *pri-2* causes persisting replication fork stalling, which in turn leads to double stranded DNA breaks [107]. Our observation that *pri-1* and *pri-2*-induced UPR-ER activation in *C. elegans* embryos suggests a potentially interesting link between the UPR-ER induction and genotoxic stress. Although *pri-2* was not included in the final 34 hits list (it had an aggregate GFP intensity value of 2 from the screen, below the cutoff value of 3), PRI-1 and PRI-2 are subunits of the same DNA polymerase α primase complex. Additionally, in follow-up experiments, *pri-2(RNAi)* worms reproducibly phenocopied *pri-1(RNAi)* worms.

2.2.1 *pri-1/2* knockdown activates the *ire-1* pathway

Consistent with what we observed in the previous screen rounds, *pri-1* and *pri-2* RNAi knockdown by feeding RNAi with parental *C. elegans* results in *hsp-4p::gfp* induction in

embryos (Figure 10A). F1 offspring embryos from *pri-1* and *pri-2* RNAi-treated P0 adults never hatch, because these eggs arrest at early embryogenesis/pre-morphogenetic stage (Figures 10A).

Next, we asked if the induction of *hsp-4p::gfp* transcription reporter in *pri-1* (RNAi) and *pri-2* (RNAi) embryos has true biological meaning, i.e. if it correlates with endogenous mRNA changes. To test this, we used an integrated transgenic strain that carries a GFP coding sequence inserted at the 3' end of HSP-4 coding sequence just before the stop codon sequence, which will be translated to a C-terminal GFP tagged HSP-4 protein (see Methods). First, to test if this recombinant HSP-4 protein is properly expressed, translated and regulated by its canonical stressors, we examined GFP intensity in STA06 strain *hsp-4::gfp(syb2824) II* (referred to as *hsp-4::gfp* from here on) strain stressed by proteotoxicity triggered by tunicamycin and lipotoxicity triggered by *mdt-15* RNAi. We observed elevated GFP intensity in *hsp-4::gfp* worms challenged with tunicamycin and *mdt-15* RNAi (Figure 10B), proving that this fusion protein is inducible by both proteotoxicity and lipotoxicity, similar to the transcriptional *hsp-4p::gfp*. This suggests that the recombinant GFP fusion protein is subject to regulation by the endogenous *hsp-4* promoter and is not degraded to a significant extent due to misfolding and is thus relatively stable. Therefore, we proceeded to grow the translational fusion *hsp-4::gfp* reporter strain on *pri-1* and *pri-2* RNAi for 96hr and observed GFP fluorescence in the embryos as well as in the uterus region of adult worms (Figure 10C), confirming induction of the endogenous HSP-4 protein in embryos in these RNAi conditions.

Interestingly, the induction in somatic cells is weak at both time points compared to the negative control RNAi (Figures 10A and 10C). This suggests that loss of primases and subsequent replication defects likely trigger a different cellular program in early embryos than in the somatic cells of *C. elegans*.

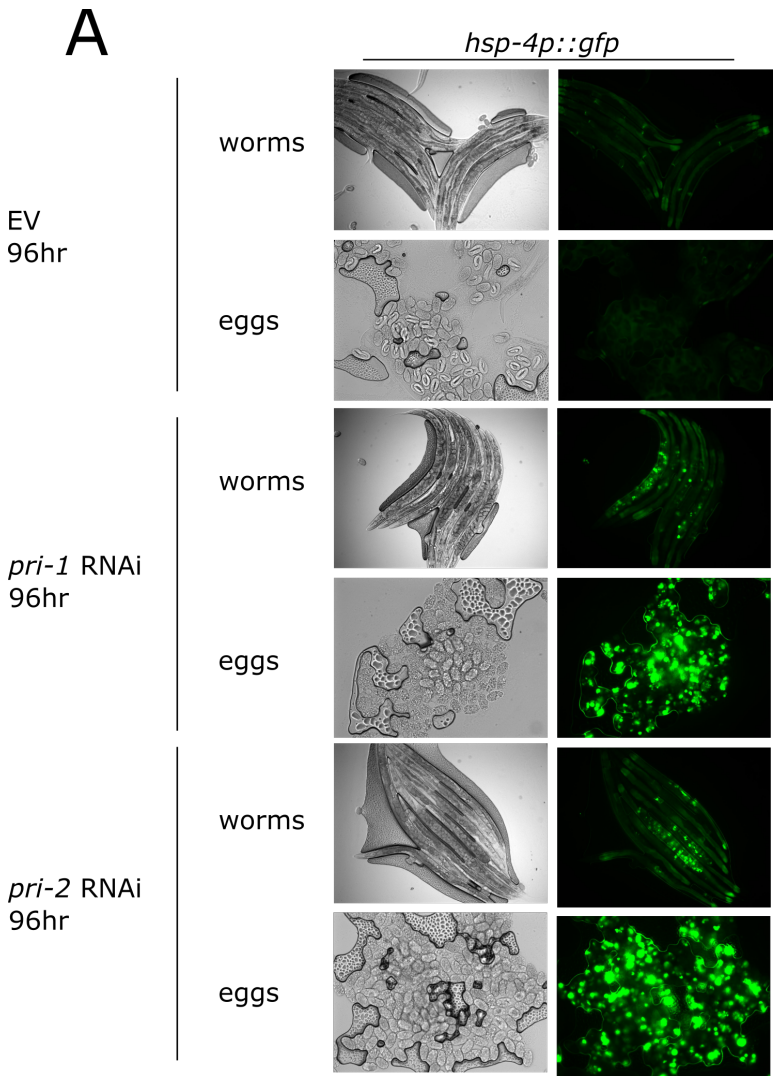
A
hsp-4p::gfp
EV
96hr
worms
eggs
pri-1 RNAi
96hr
worms
eggs
pri-2 RNAi
96hr
worms
eggs

B

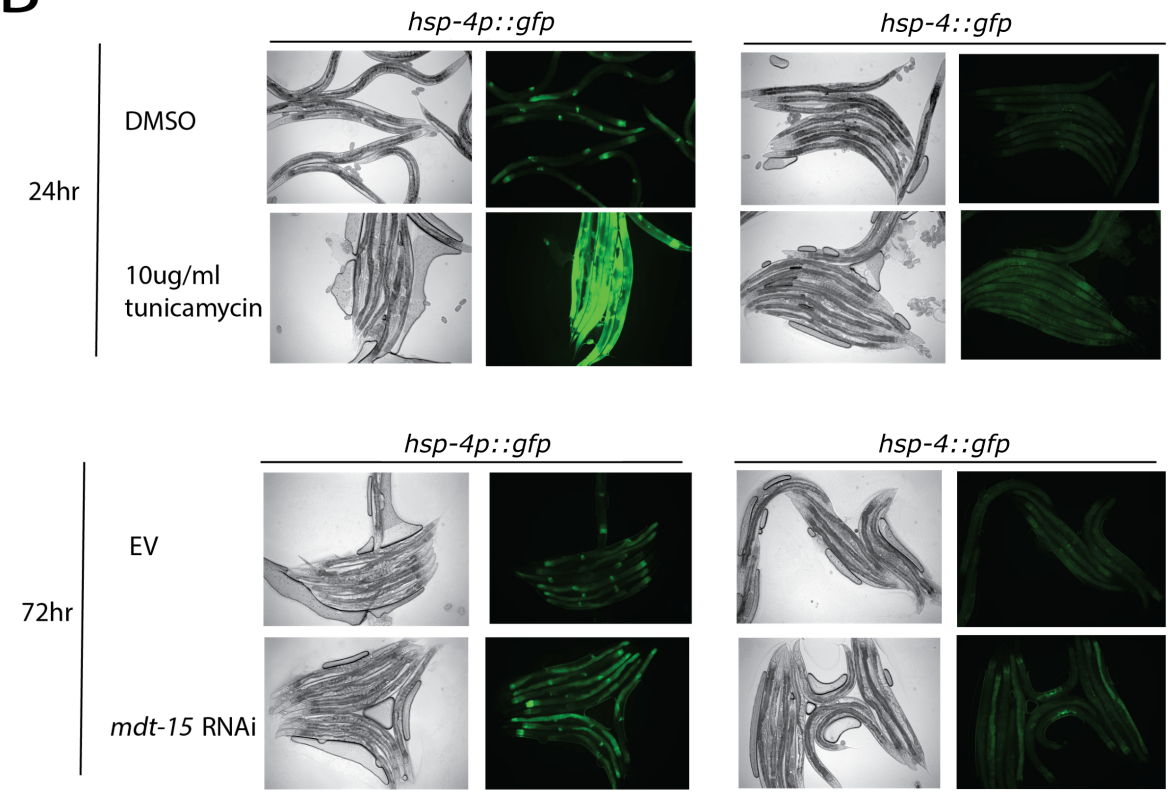
hsp-4p::gfp
hsp-4::gfp
24hr
DMSO
10ug/ml
tunicamycin
hsp-4p::gfp
hsp-4::gfp
72hr
EV
mdt-15 RNAi

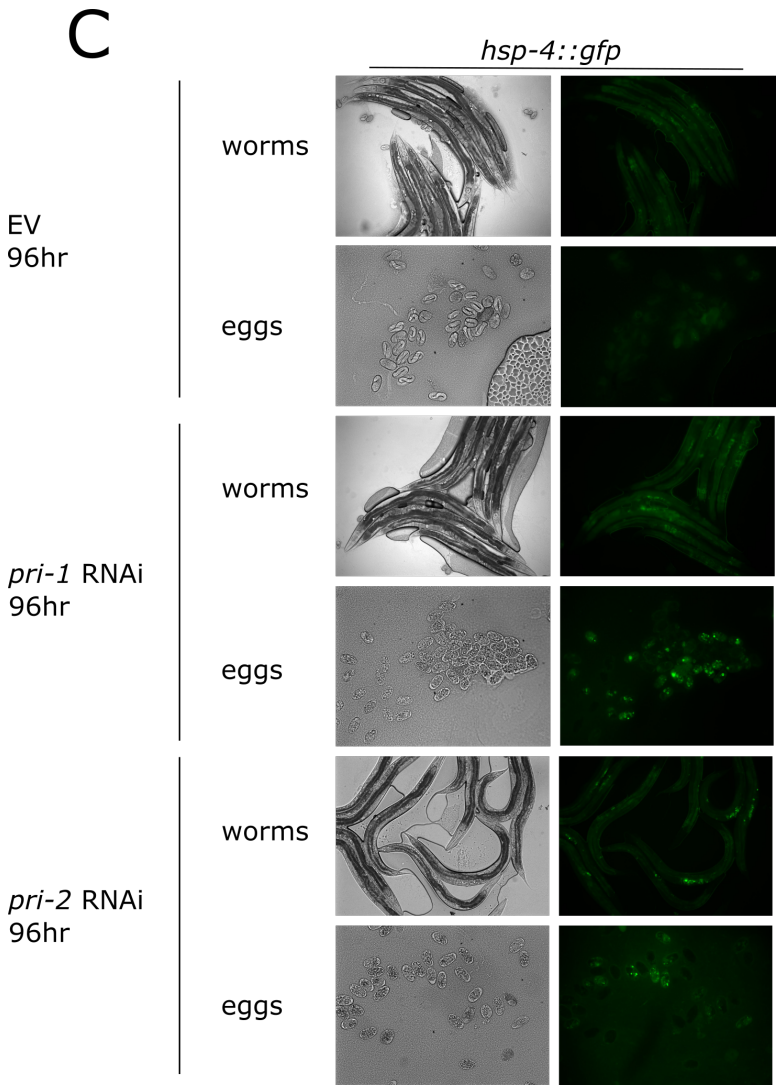

Figure 10. *pri-1/2* knockdown induces the IRE-1 branch in *C. elegans* embryos.

(A) Micrographs show GFP reporter expression in *hsp-4p::gfp* adult worms and embryos after growing on RNAi for 96hr (n=3). (B) Micrographs show GFP reporter expression in *hsp-4p::gfp* and *hsp-4::gfp* worms on DMSO and tunicamycin, as well as on control RNAi (EV) and *mdt-15* RNAi (n=1). (C) Micrographs show GFP reporter expression in *hsp-4::gfp* adult worms and embryos after growing on RNAi for 96hr (n=3).

2.2.2 *pri-1/2* knockdown activates the *pek-1* pathway

To determine if *pri-1* and *pri-2* RNAi treatments also activate the PEK-1 pathway, we fed *pri-1* and *pri-2* RNAi to *Patf-4(uORF)::gfp* worms. We observed robust activation of the GFP

reporter in embryos at 72hr and 96hr (Figure 11A). Moreover, we performed western blot to detect levels of phospho-Ser51 on eIF2α, which is a marker for activated PEK-1 [167]. Previous results showed worm sample grown on *mdt-15* RNAi has an increased level of phospho-Ser51 on eIF2α [50], we were able to reproduce this result (Figure 11B). Indeed, we observed increased phosphorylation of phospho-Ser51 on eIF2α in *pri-1(RNAi)* and *pri-2(RNAi)* embryos compared to EV embryos (Figure 11C).

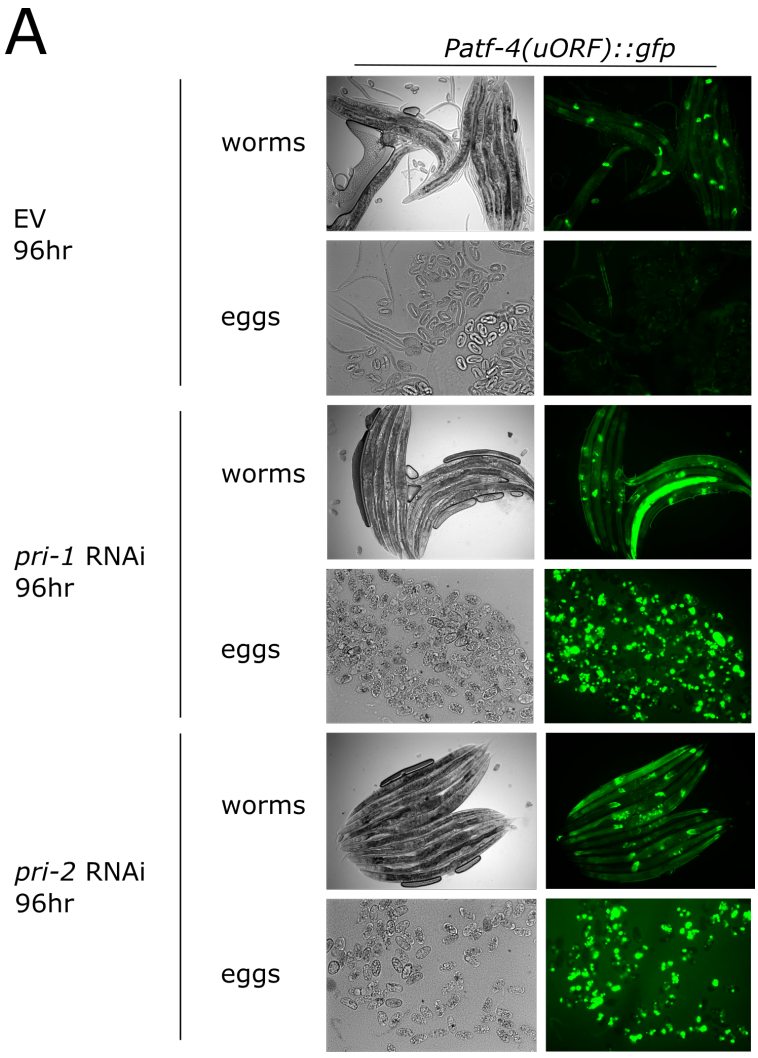

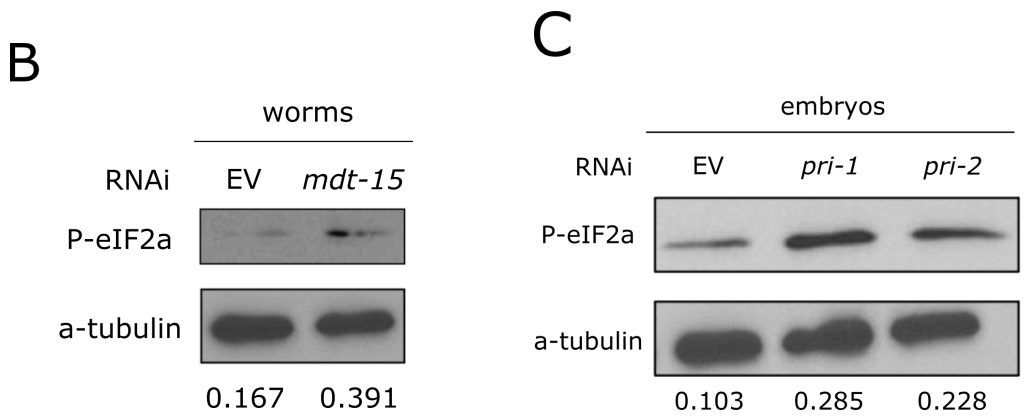

Figure 11. *pri-1/2* knockdown induces the PEK-1 branch in *C. elegans* embryos.

(A) Micrographs show GFP reporter expression in *Patf-4(uORF)::gfp* adult worms and embryos after growing on RNAi for 96hr (n=3). (B) Immunoblot depicts the levels of phospho-Ser51 eIF2α (P-eIF2α) and α-tubulin in control RNAi (EV) and *mdt-15* (RNAi) day-2 adult worms (n=2). The numbers represent the intensity of the P-eIF2α bands relative to the corresponding α-tubulin bands. (C) Immunoblot depicts the levels of phospho-Ser51 eIF2α (P-eIF2α) and α-tubulin in control RNAi (EV), *pri-1(RNAi)* and *pri-2(RNAi)* worm embryos (n=2). The numbers represent the intensity of the P-eIF2α bands relative to the corresponding α-tubulin bands.

2.2.3 *pri-1/2* knockdown induces the UPR-ER specifically

To address the question if UPR-ER induction in *pri-1* and *pri-2* RNAi-treated embryos is due to general protein misfolding, we monitored the expression of other chaperone genes in the cytosol and mitochondria, with *hsp-16.2p::gfp* and *hsp-6p::gfp* reporter strains, respectively. The rationale is that if the UPR-ER activation seen in *pri-1* and *pri-2* (RNAi) embryos is due to general protein misfolding, it will affect proper protein folding in the mitochondria and cytosol, either directly or indirectly through impaired ER proteostasis. *mdt-15* (RNAi) and *cox-5B* (RNAi) were used as positive controls for *hsp-4p::gfp* and *hsp-6p::gfp*, respectively (Figure

12A). We did not observe induction in the somatic tissues of these reporter worms, in contrast to weak induction in *hsp-4p::gfp* strain (Figure 12A), suggesting mitochondrial proteostasis is not compromised in somatic cells.

Similarly, heat stress strongly induced cytosolic protein misfolding and thus activates the *hsp-16.2p::gfp* cytosolic UPR reporter strongly throughout the embryos (Figure 12B). In contrast, *pri-1* and *pri-2* RNAi treatments did not induce the *hsp-16.2p::gfp* reporter to a significant extent, which implies large-scale cytosolic protein misfolding is not triggered by *pri-1* and *pri-2* RNAi-induced replication stress (Figure 12B).

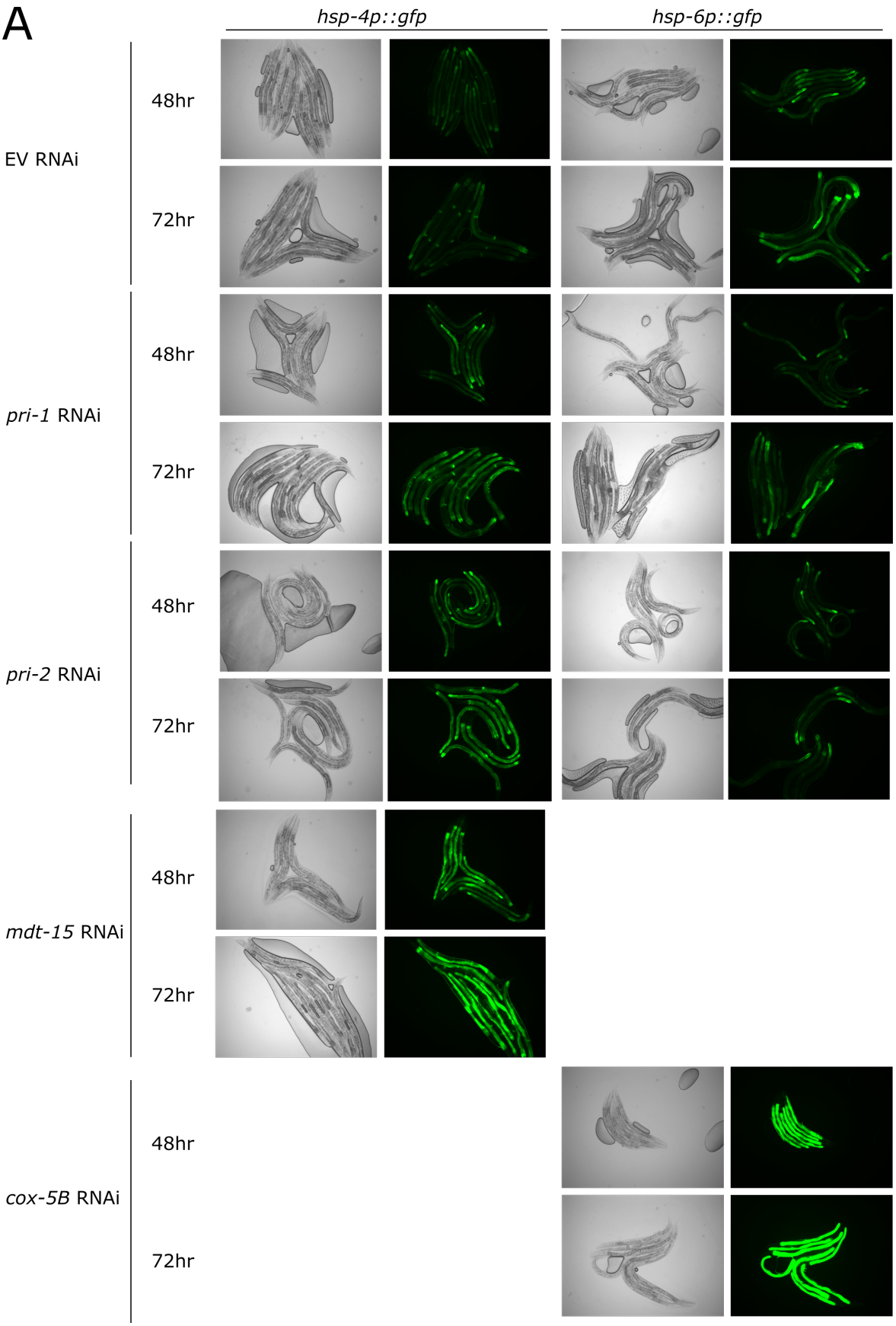
A
hsp-4p::gfp
hsp-6p::gfp
EV RNAi
48hr
72hr
pri-1 RNAi
48hr
72hr
pri-2 RNAi
48hr
72hr
mdt-15 RNAi
48hr
72hr
cox-5B RNAi
48hr
72hr

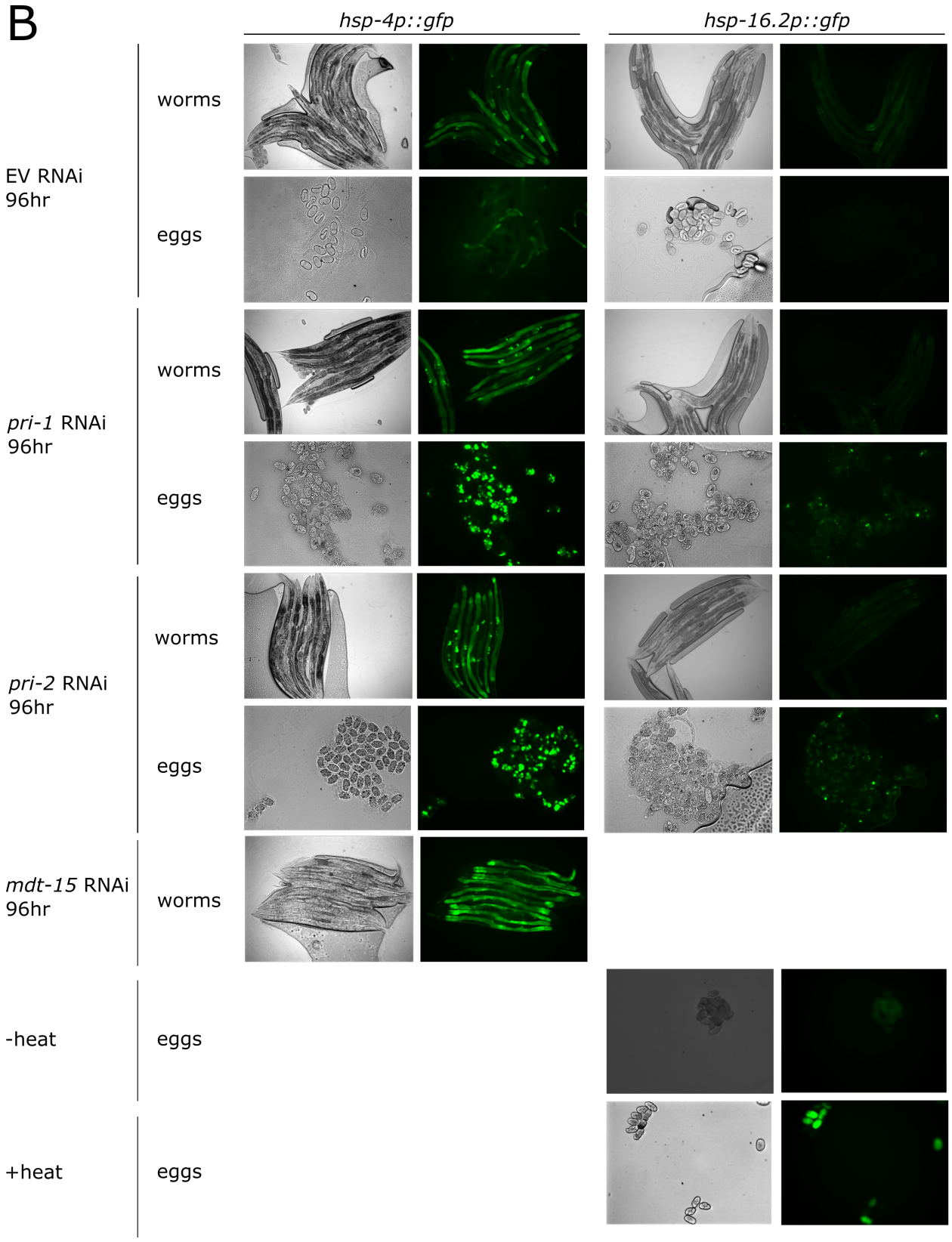
B
hsp-4p::gfp
hsp-16.2p::gfp
EV RNAi 96hr
worms
eggs
pri-1 RNAi 96hr
worms
eggs
pri-2 RNAi 96hr
worms
eggs
mdt-15 RNAi 96hr
worms
-heat
eggs
+heat
eggs

Figure 12. *pri-1/2* knockdown induces the UPR-ER but not the mitochondrial UPR or the cytosolic UPR. (A) Micrographs show worms of *hsp-4p::gfp* reporter strain grown on control RNAi (EV), *pri-1* RNAi, *pri-2* RNAi, *cox-5B* RNAi, as well as *hsp-6p::gfp* reporter strain grown on control RNAi (EV), *pri-1* RNAi, *pri-2* RNAi, *mdt-15* RNAi for 48 and 72 hours. (B) Micrographs show embryos and worms of *hsp-4p::gfp* reporter strain grown on control RNAi (EV), *pri-1* RNAi, *pri-2* RNAi, and *mdt-15* RNAi for 96 hours. As a positive control, collected *hsp-16.2p::gfp* embryos were subjected to heat shock where they were incubated at 37^{o}C for 5 minutes and recovered at 20^{o}C for 1 hour before imaging.

2.2.4 *pri-1/2* knockdown induces embryonic *hsp-4* partially independently of *xbp-1* and *ire-1*

hsp-4 induction as a part of the UPR-ER depends on *ire-1* and *xbp-1* under many stress conditions [33,168]. Thus, I tested whether these two genes were also required for *hsp-4* induction due to *pri-1* and *pri-2* RNAi by exposing *ire-1; hsp-4p::gfp* and *xbp-1; hsp-4p::gfp* worms to *pri-1* and *pri-2* RNAi. I observed weak induction of fluorescence in somatic cells of *pri-1* and *pri-2* (RNAi) worms, and strong induction in somatic cells of *mdt-15* (RNAi) worms, all dependent on either *xbp-1* or *ire-1*, as *xbp-1* or *ire-1* loss of function mutations caused complete abrogation of *hsp-4p::gfp* reporter induction (Figure 13A). Surprisingly, induction of *hsp-4* in the embryos was partially independent of the canonical IRE-1-XBP-1-HSP-4 signaling pathway (Figure 13B). This suggests that alternative pathways are activated by replication stress, which lead to *hsp-4* expression in embryos.

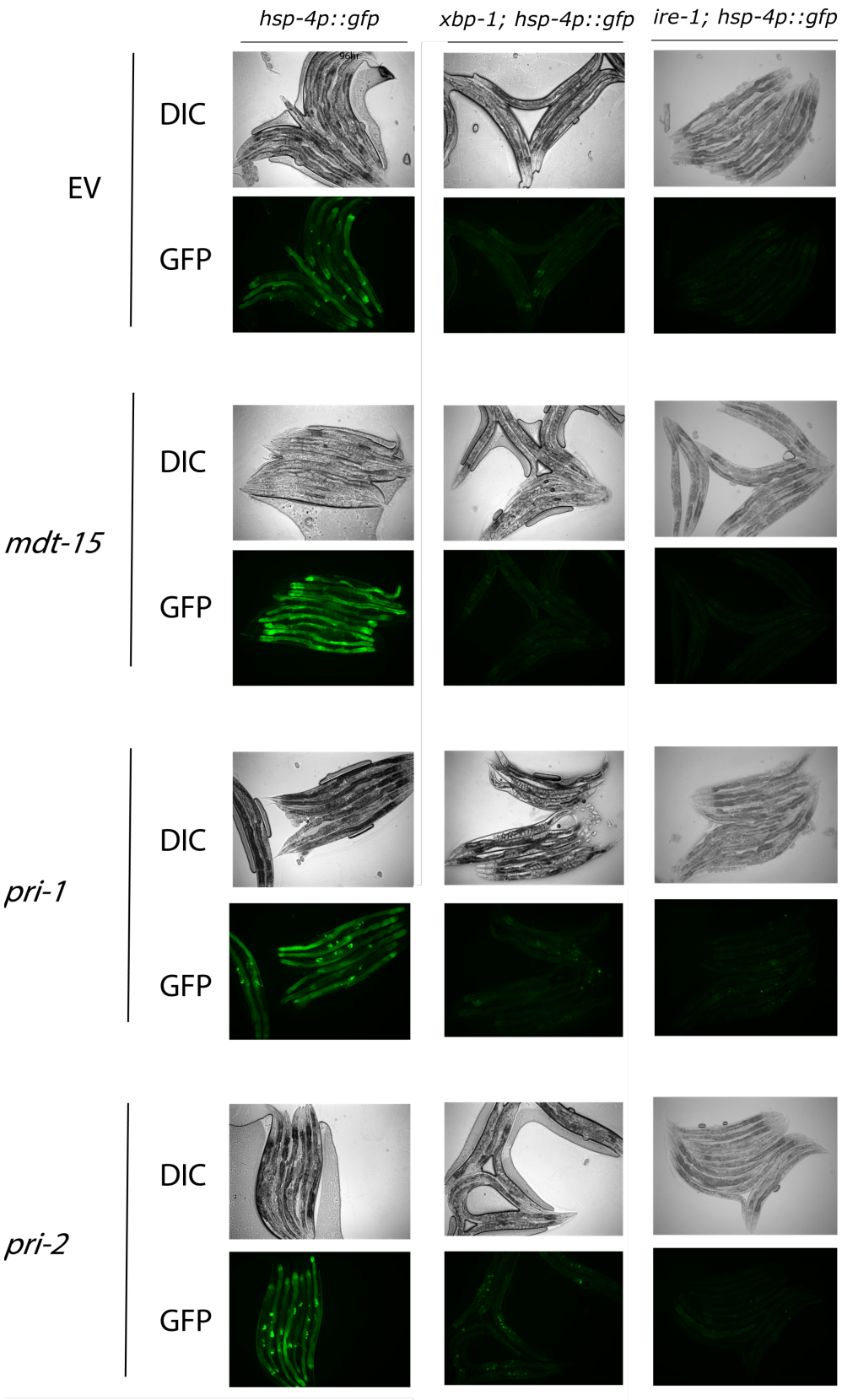
A
hsp-4p::gfp
xbp-1; hsp-4p::gfp
ire-1; hsp-4p::gfp
EV
DIC
GFP
mdt-15
DIC
GFP
pri-1
DIC
GFP
pri-2
DIC
GFP

B

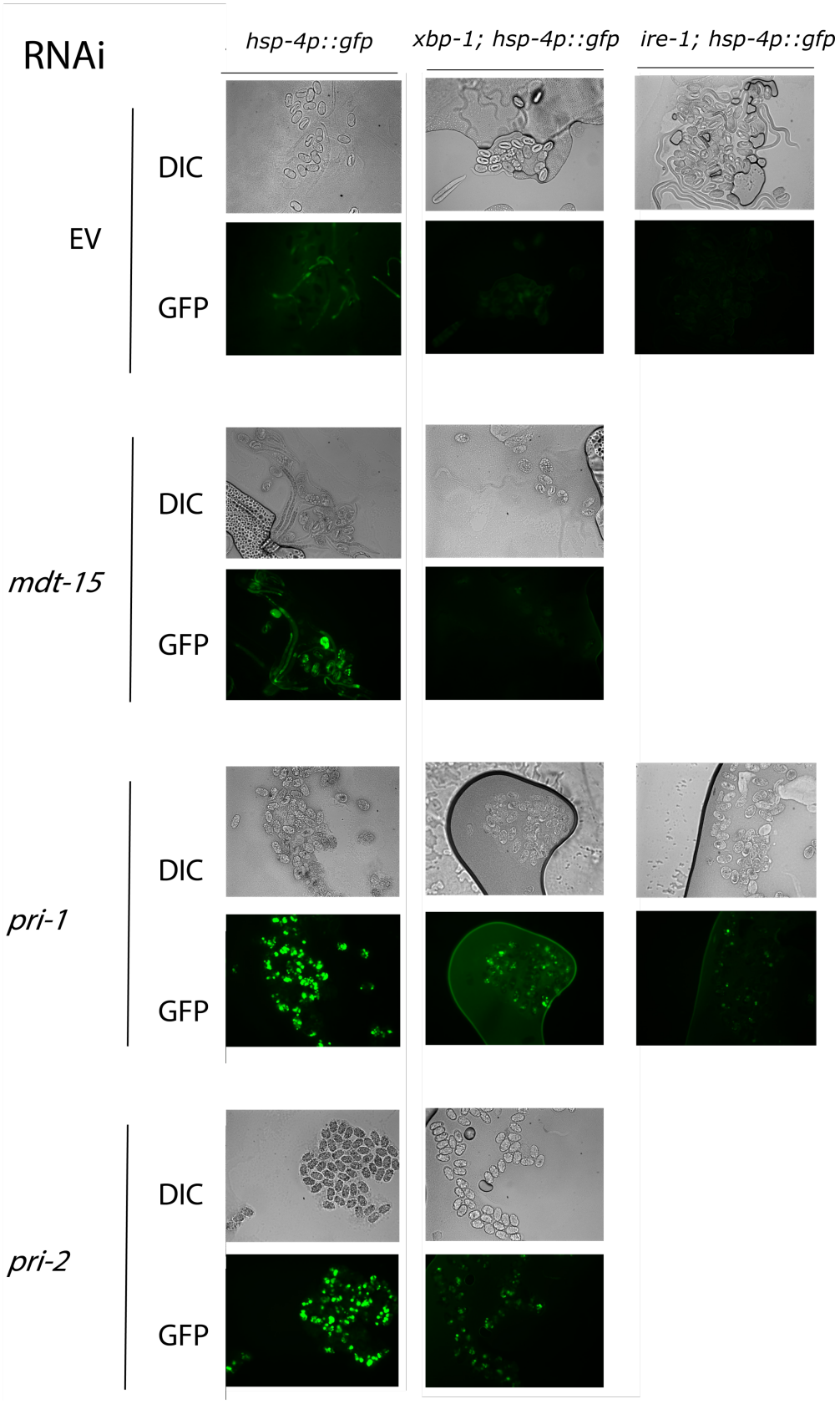
RNAi
hsp-4p::gfp
xbp-1; hsp-4p::gfp
ire-1; hsp-4p::gfp
EV
DIC
GFP
mdt-15
DIC
GFP
pri-1
DIC
GFP
pri-2
DIC
GFP

Figure 13. *pri-1/2* knockdown activates embryonic *hsp-4* through a partially *ire-1*- and *xbp-1*-independent mechanism.

(A) Micrographs depict day-2 adult worms of *hsp-4p::gfp, xbp-1(zc12); hsp-4p::gfp* and *ire-1(zc14);hsp-4p::gfp* grown on control RNAi (EV), *mdt-15* RNAi, *pri-1* RNAi, and *pri-2* RNAi for 96 hours. (B) Micrographs depict embryos laid by *hsp-4p::gfp, xbp-1(zc12); hsp-4p::gfp* and *ire-1(zc14);hsp-4p::gfp* worms grown on control RNAi (EV), *mdt-15* RNAi, *pri-1* RNAi, and *pri-2* RNAi for 96 hours.

2.2.5 UV-C treatment phenocopies *pri-1* and *pri-2* RNAi

Other than replication block-induced DSBs, ultraviolet C (UV-C) light is a known inducer of DSBs if the bipyrimidine photo-products it induced are not efficiently resolved by the nucleotide excision repair pathway [110]. Throughout the life cycle of the worm, the early developing embryo is the most sensitive to UV-C-induced DSBs, which is likely due to the lack of DNA damage checkpoints and rapid proliferation cycle [98]. Therefore, to understand the consequence of *pri-1* and *pri-2* RNAi, we tested if unrepaired DSBs induced by UV-C in early embryos can phenocopy *pri-1* and *pri-2* RNAi treatment. We irradiated day 1 adult worms with 400J/m^2 UV-C and waited 24hr before imaging the worms and the embryos. Consistent with *pri-1* and *pri-2* (RNAi) embryos, UV-C treatment activates *hsp-4p::gfp* and *Patf-4(uORF)::gfp* strongly, suggesting activation of the *ire-1* and *pek-1* branch, respectively (Figure 14A). Although the induction is weaker than the transcriptional reporter, we are able to confirm the induction of *hsp-4* with the *hsp-4::gfp* translational GFP fusion reporter as well (Figure 14A). Similar to *pri-1* and *pri-2* RNAi, the observed UV-C-induced *hsp-4* upregulation is partially independent of *ire-1* and *xbp-1* in the embryos (Figure 14A). However, the cytosolic UPR reporter *hsp-16.2p::gfp* is not strongly activated as seen in heat shock (Figure 14A and 12), suggesting that UV-C activates the UPR-ER specifically in the embryos.

Next, we looked at the somatic response to UV-C and found that it phenocopied *pri-1* and *pri-2* RNAi as well. Specifically, we found that the *pek-1* branch of the UPR-ER is activated in response to UV-C, similar to *pri-1* and *pri-2* RNAi fed day-2 adult worms (Figure 14B and 11A). In addition, the mitochondrial reporter *hsp-6p::gfp* and the cytosolic reporter *hsp-16.2p::gfp* are not activated by UV-C-induced DNA damage in adult somatic cells like *pri-1* and *pri-2* RNAi (Figure 14B and 12). However, a small difference exists between these two types of treatments. We observed weak *hsp-4* induction in the somatic tissues of day-2 adult worms fed with *pri-1* and *pri-2* (RNAi) (Figure 10A), while failing to observe such weak but visible upregulation upon UV-C exposure in day 2 adults (Figure 14B).

Collectively, these observations suggest that the cellular consequence of *pri-1* and *pri-2* RNAi is similar to UV-C irradiation in *C. elegans*, likely causing extensive DSBs which the dividing embryo is not able to tolerate or repair. The ability to reproduce these phenotypes with a different method further confirmed DNA damage as a UPR-ER inducer.

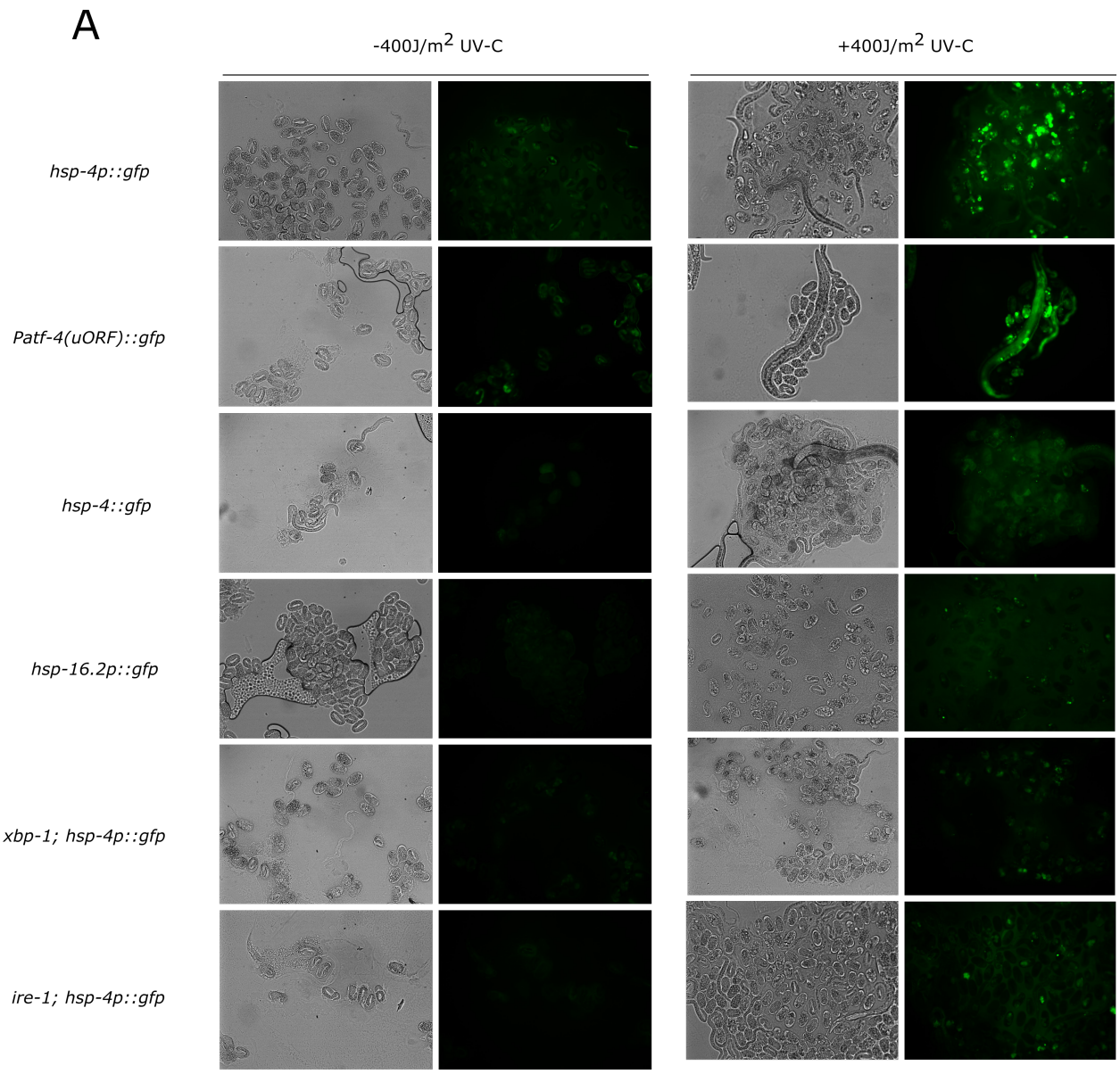
A
-400J/m2 UV-C
+400J/m2 UV-C
hsp-4p::gfp
Patf-4(uORF)::gfp
hsp-4::gfp
hsp-16.2p::gfp
xbp-1; hsp-4p::gfp
ire-1; hsp-4p::gfp

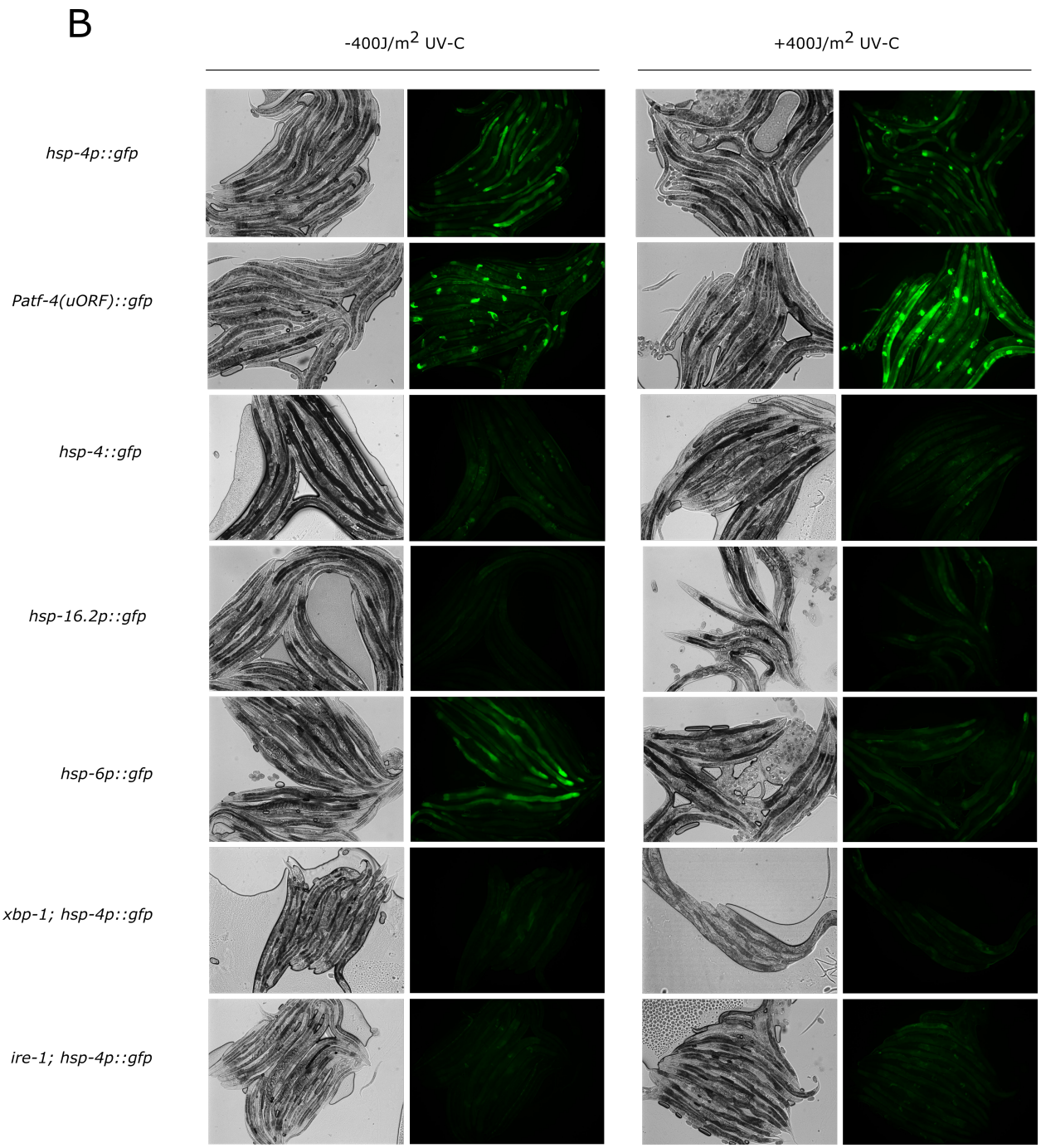

Figure 14. UV-C treatment phenocopies *pri-1* and *pri-2* RNAi

(A) Micrographs depict embryos of specified genotypes. Embryos are collected and imaged 24hr after the parental adult worms are treated with 400J/m^2 UV-C (n=2). GFP, RFP and DIC channels are merged (B) Micrographs depict adult worms of indicated genotypes, 24hr post 400J/m^2 UV-C treatment (n=2).

2.2.6 ATF-6 is partially required for *hsp-4* induction in *pri-1/2* knockdown embryos

Since ATF6α is required for the transcription of *Xbp-1* mRNA [25,37], we then asked if the *C. elegans atf-6* is also required for replication stress-induced *hsp-4* expression. We crossed the *hsp-4::gfp* fusion reporter into the *atf-6 (ok551)* deletion strain, and subjected this *atf-6; hsp-4::gfp* to *pri-1* and *pri-2* RNAi. *atf-6* loss of function itself appeared to induce *hsp-4* expression in the soma, while *mdt-15* loss aggravates UPR-ER induction after 72hr and 96hr feeding on RNAi (Figure 15). Therefore, *mdt-15* RNAi-induced *hsp-4* expression in somatic tissues does not rely on the presence of intact *atf-6*. However, in *pri-1* and *pri-2* (RNAi) embryos of the *atf-6*; *hsp-4::gfp* fusion strain, which also arrest at an early stage, the HSP-4 protein level is lower than that in the *pri-1* and *pri-2* (RNAi) embryos of the *hsp-4::gfp* strain (Figure 12). This observation indicates that the increase in HSP-4 protein levels is partially dependent on *atf-6*, regulated at mRNA or/and protein level, during replication stress in *pri-1* and *pri-2* (RNAi) early embryos.

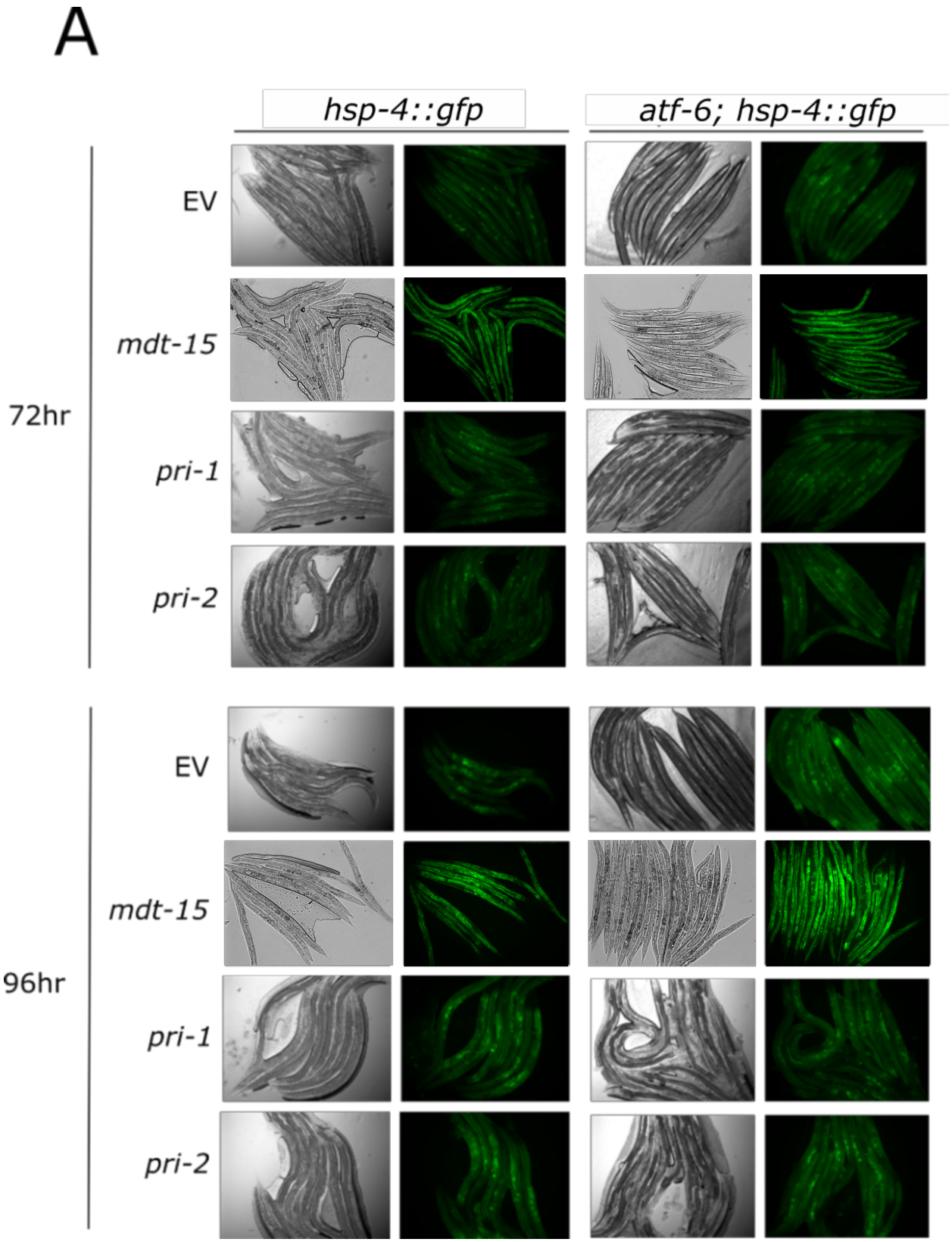
A
hsp-4::gfp
atf-6; hsp-4::gfp
72hr
EV
mdt-15
pri-1
pri-2
96hr
EV
mdt-15
pri-1
pri-2

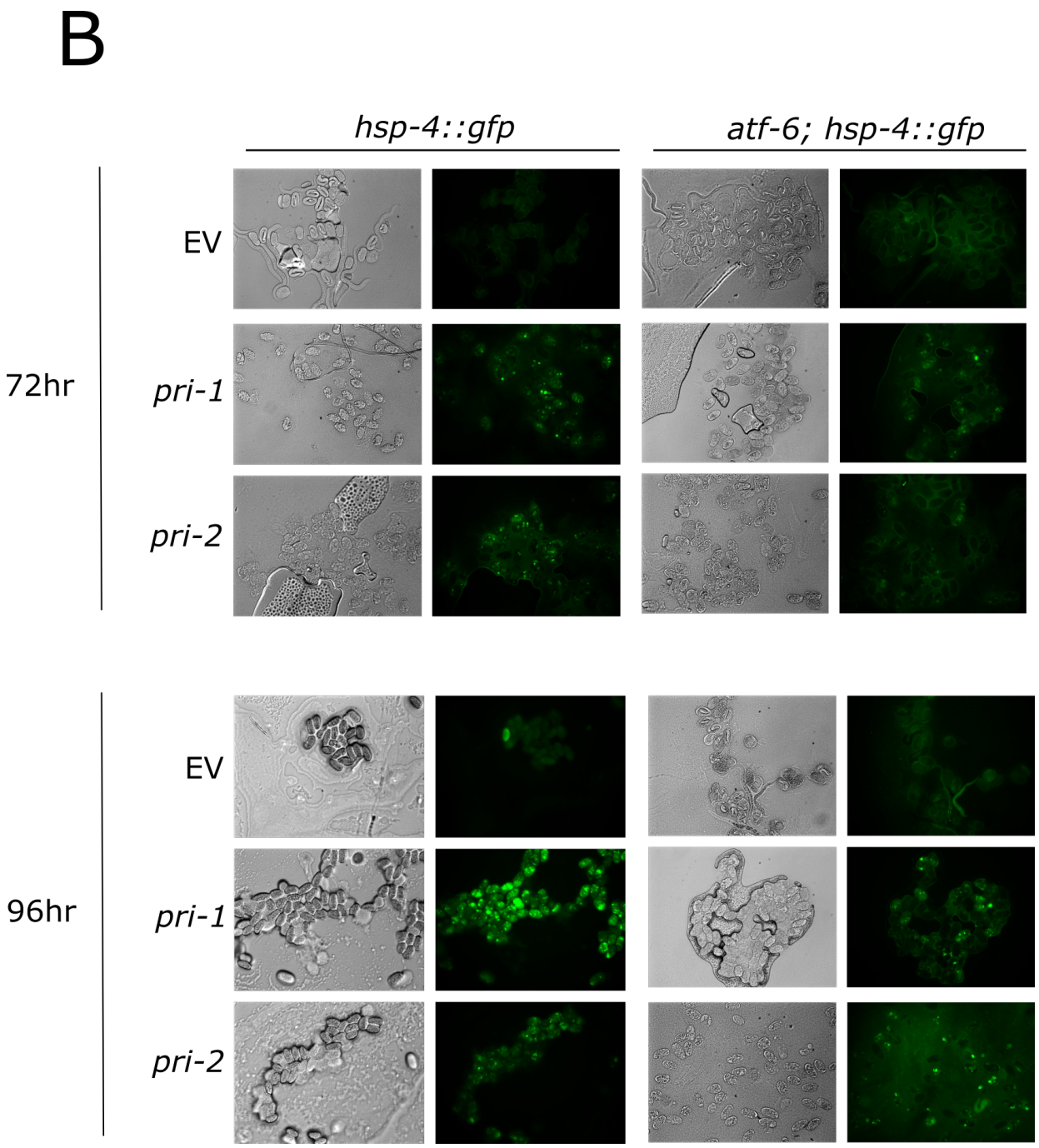

Figure 15. Activation of *hsp-4* by *pri-1/2* knockdown is partially independent of *atf-6*.

(A) Micrographs depict worms of *hsp-4::gfp* and *atf-6(ok551)*; *hsp-4::gfp* strains grown on control RNAi (EV), *pri-1* RNAi and *pri-2* RNAi for 72 and 96 hours (n=2). (A) Micrographs depict embryos laid by *hsp-4::gfp* and *atf-6(ok551)*; *hsp-4::gfp* strains grown on EV, *pri-1* RNAi and *pri-2* RNAi for 72 and 96 hours.(n=2)

2.2.7 Knocking down components of the polymerase *α* primase complex phenocopies *pri-1/2* RNAi

The *C. elegans* primase is found as a complex of four proteins: the DNA polymerase *α* catalytic subunit homolog (*pola-1*), the DNA polymerase *α* accessory subunit (*div-1*) and the two primase subunits (*pri-1* and *pri-2*). Apart from the canonical role of synthesizing short RNA primers required for initiating replication and lagging strand replication, members of the eukaryotic primase superfamily can play more complex roles in processes such as DNA repair and even possibly transcription [169]. Evidence from *C. elegans* also showed that different subunits of the same DNA polymerase alpha-primase complex in contexts outside of DNA replication [170]. Specifically, the spatiotemporal requirement for different subunits for GLP-1/Notch-mediated germ cell proliferation is different [170].

Therefore, we asked if UPR-ER activation seen in *pri-1* and *pri-2* (RNAi) embryos is associated with replication defects or other primase functions unrelated to replication. To address this question, we decided to test if RNAi knockdown of components of the same polymerase α primase complex, specifically *pola-1* and *div-1* would phenocopy *pri-1* and *pri-2* RNAi. We found that *pola-1* and *div-1* RNAi activated *hsp-4p::gfp* in embryos, similar to *pri-1* and *pri-2* RNAi treatments (Figure 16). This suggests that the induction of the UPR-ER in these conditions is most likely a result of replication stress caused by defective polymerase α primase complex function.

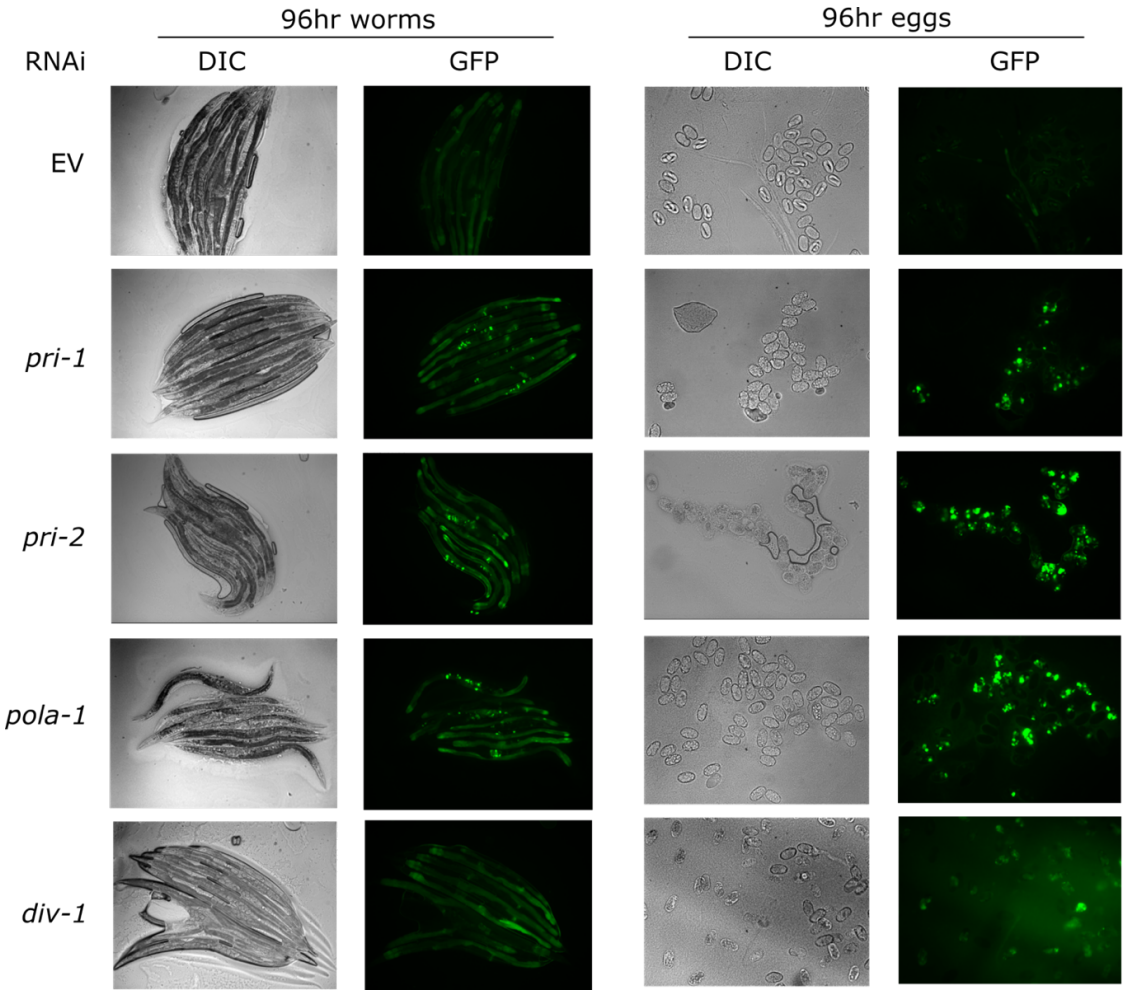

Figure 16. Polymerase *α* primase complex subunit knockdown phenocopies *pri-1/2* RNAi.

Micrographs depict *hsp-4p::gfp* worms grown on control RNAi (EV), *pri-1* RNAi, *pri-2* RNAi, *pola-1* RNAi, and *div-1* RNAi for 96 hours and their corresponding embryos collected at 96hr.

2.2.8 Knocking down DNA repair pathway components does not activate the UPR-ER in somatic cells

The above data raised the possibility that genotoxic stress activates UPR-ER. To assess if deficient DNA repair is sufficient to induce UPR-ER in *C. elegans,* we used a feeding RNAi approach to knock down specific components of various repair pathways.

The DNA lesion-inducing genes we examined include *msh-2* (mismatch repair), *xpf-1* (nucleotide excision repair), *him-1* (cohesin, whose loss results in apoptosis and high incidence of males due to chromosomal segregation defects in the mitotic and meiotic germlines of *C. elegans*, respectively [171,172]), *mus-81* (replicative repair), *dog-1* and *him-6* (RNAi causes unscheduled formation of DNA structures such as R-loops or G4 structures, which result in deletions in poly-guanine tracts and genome instability [173,174]). Additionally, we focused on a DNA damage checkpoint protein, CID-1. CID-1 loss of function reverts HU-induced developmental arrest in *C. elegans* [175]. *cid-1* RNAi enhances organismal heat stress resistance and extends lifespan and causes elevated *hsp-4* levels seen in the *hsp-4p::gfp* reporter strain [175] However, unlike the depletion of *pri-1* or *pri-2*, knockdown of neither genes activated either reporter gene in the somatic cells of *C. elegans* at 48hr or 72hr (Figure 17), except for *xpf-1*. Loss of *xpf-1* (nucleotide excision repair) weakly but significantly induced the *Patf-4(uORF)::gfp* reporter strain (Figure 17) at 48hr of RNAi treatment. Moreover, in our hands, *cid-1* RNAi failed to induce *hsp-4* in three biological repeats (Figure 17), despite having the correct RNAi sequence. Possible explanations for the discrepancy would be that the RNAi approach was modified in our approach, starting with stage synchronized L1s whereas in the original work, the authors started with embryos on RNAi. In addition, the original results were obtained with adults grown up from the progeny generation, whereas ours were observed in the parental generation adults, although we did not observe above background fluorescence in *cid-1(RNAi)* F1 worms in L3-L4 stage either.

Together, these data suggest two possible scenarios applicable to the parental worm generation. First, lesions specific to all the repair pathways tested do not activate the UPR-ER in

somatic cells. Second, the number of somatic lesions accumulated by loss of a specific DNA repair component in one generation of worms is not sufficient to trigger UPR-ER activation.

However, unlike the other DNA repair genes tested by RNAi, inactivation of the cohesion homolog *him-1* activates the embryonic UPR-ER (Figure 17E). Loss of *him-1* in *C. elegans* embryos results in hypersensitivity to UV and X rays [176]. In one study, *him-1* (RNAi) embryos displayed chromosomal segregation defects and 98% embryonic lethality [171]. This links gross morphological chromosome defects, as another type of DNA damage, to UPR-ER activation in *C. elegans* embryos, implying that the linking mechanisms are potentially more general. However, unlike *pri-1* and *pri-2* (RNAi) embryos, the *him-1* RNAi phenotype is relatively weak, in terms of percentage of embryonic lethality and the uniformity of UPR-ER activation.

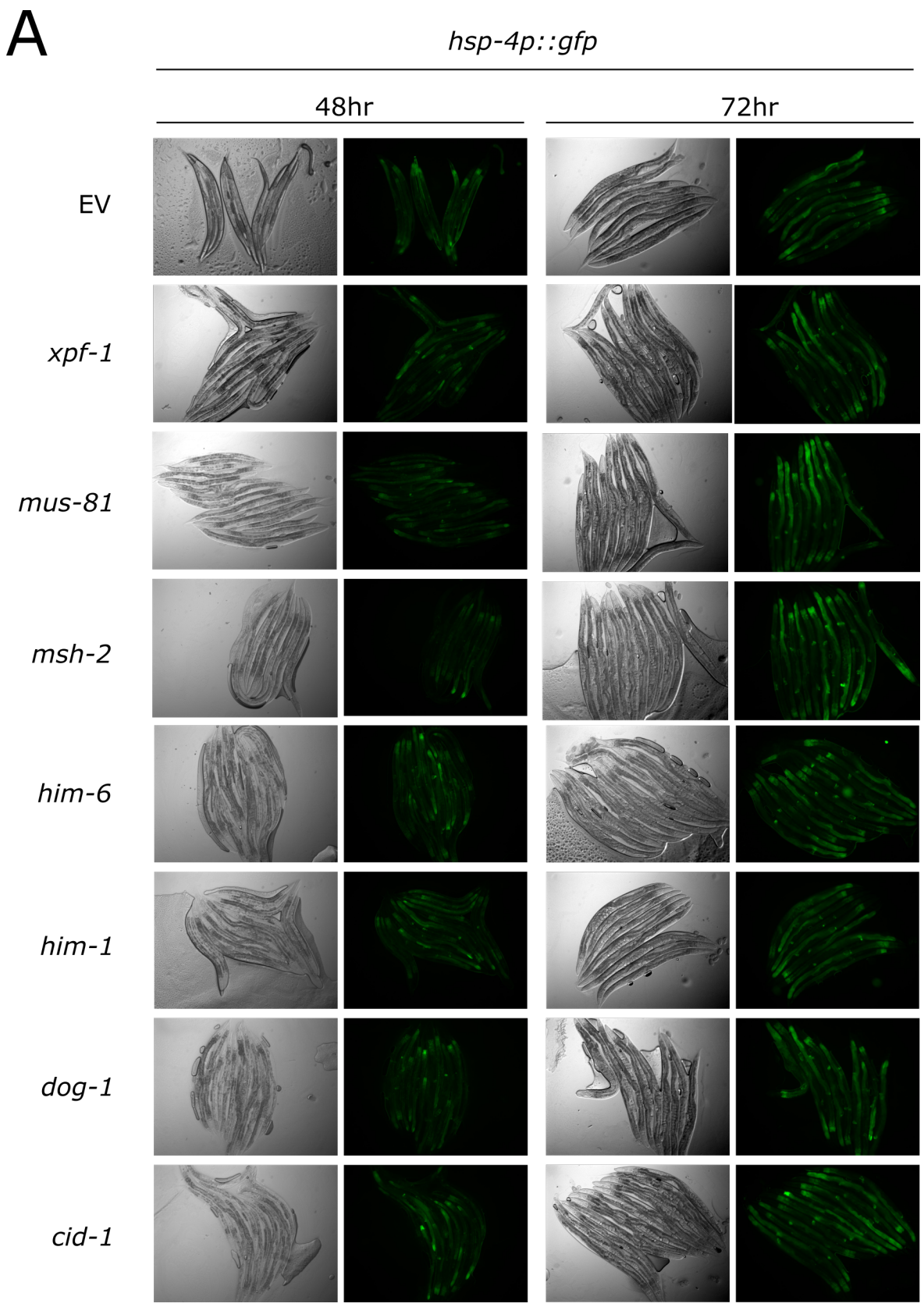
A
hsp-4p::gfp
48hr
72hr
EV
xpf-1
mus-81
msh-2
him-6
him-1
dog-1
cid-1

B

hsp-4p::gfp

48hr

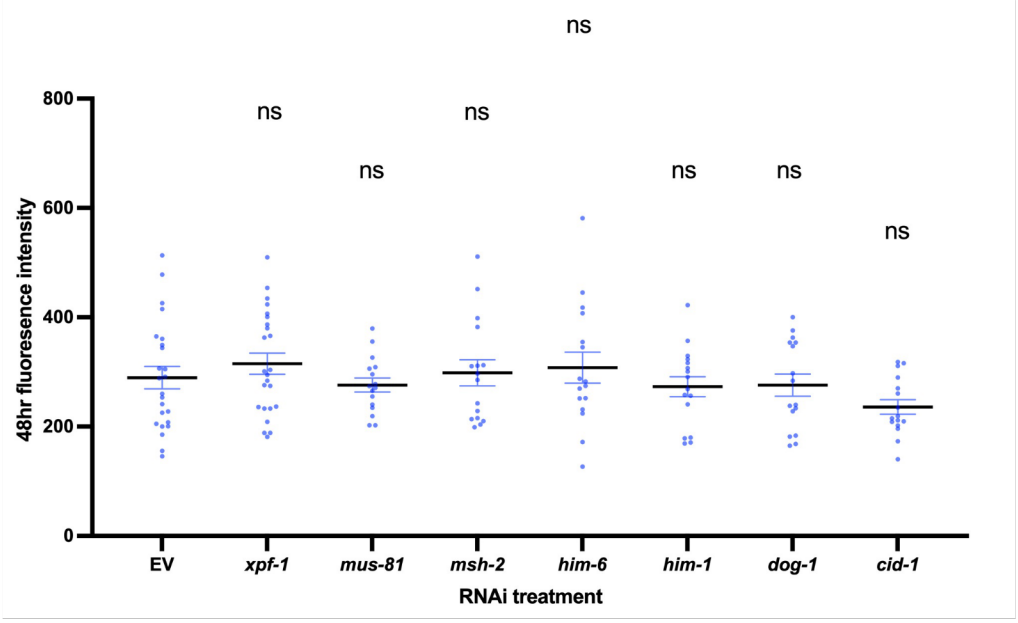

72hr

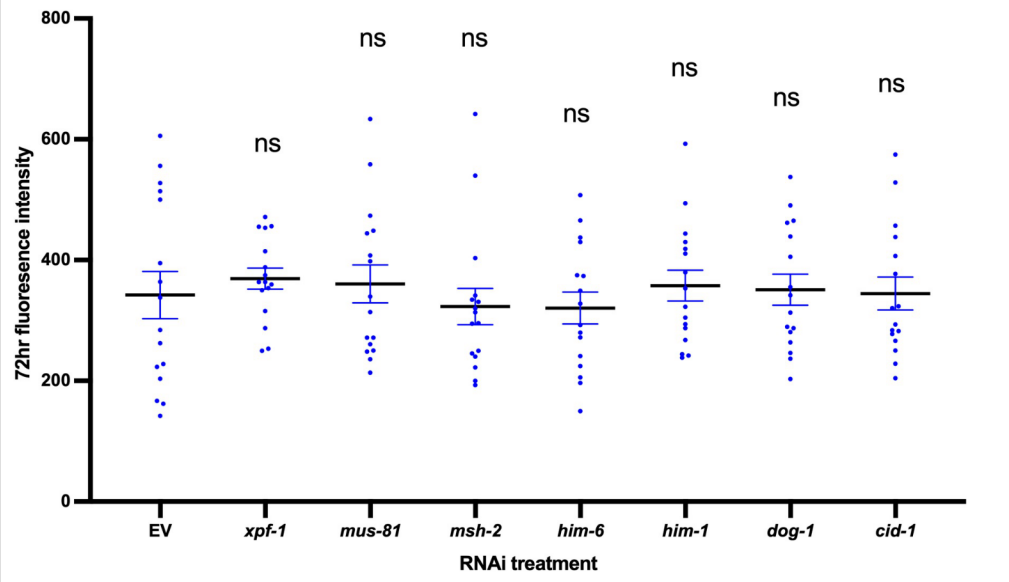

C

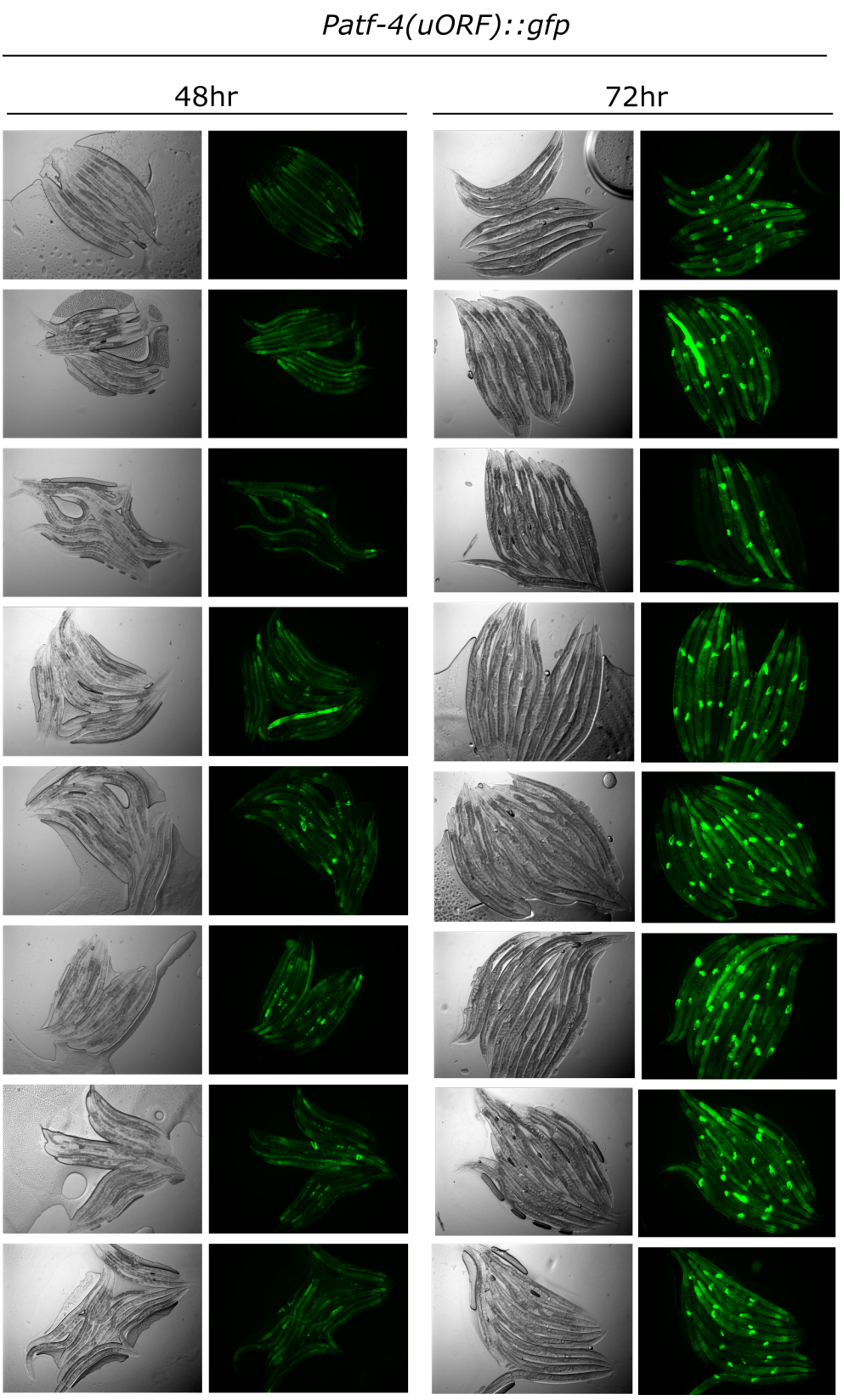
Patf-4(uORF)::gfp
48hr
72hr
EV
xpf-1
mus-81
msh-2
him-6
him-1
dog-1
cid-1

D

Patf-4(uORF)::gfp

48hr

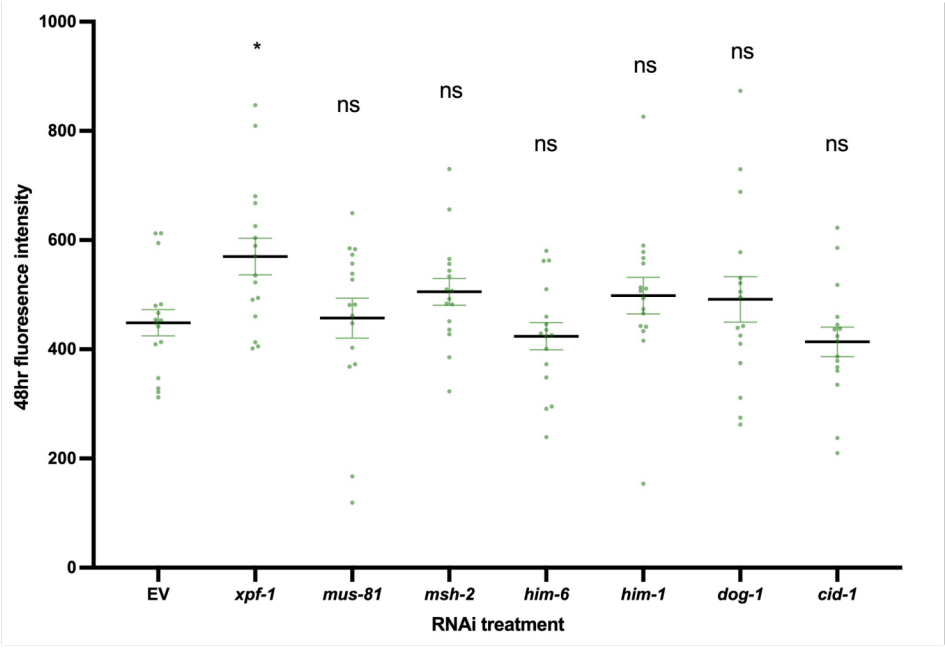

72hr

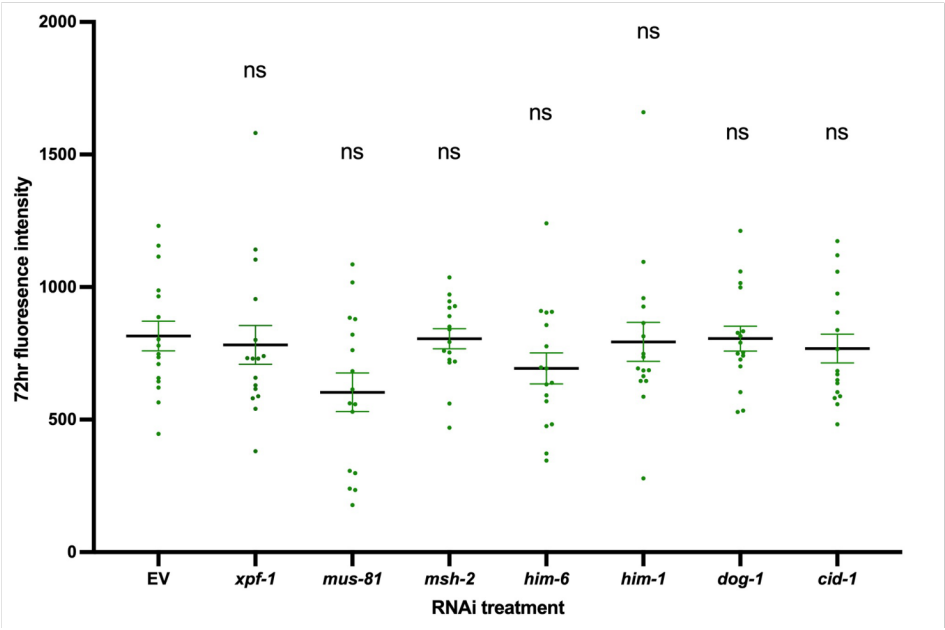

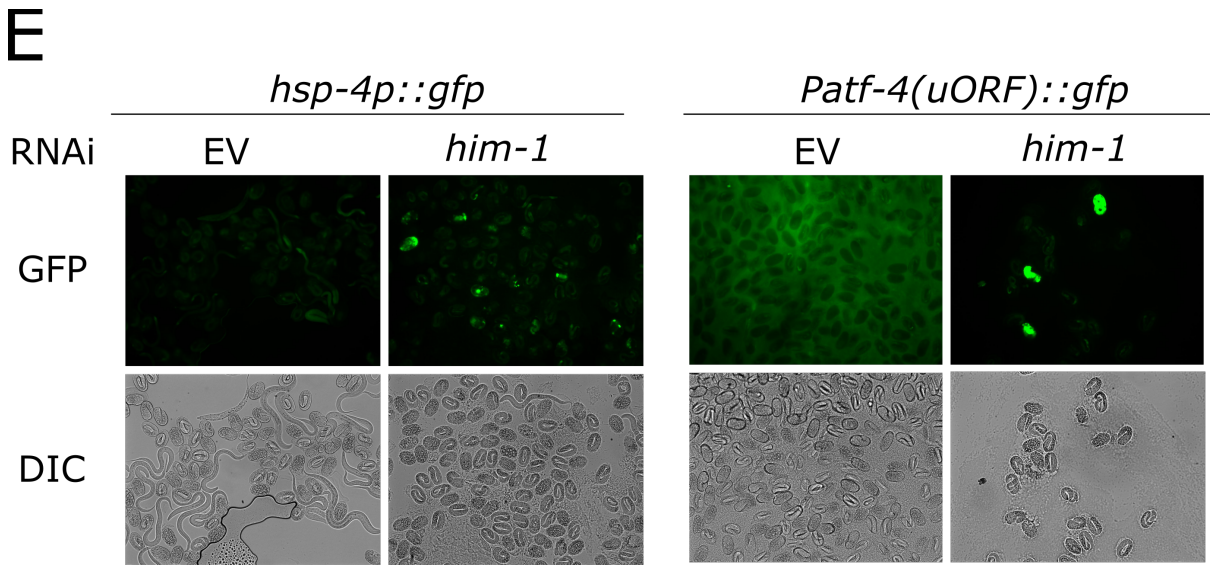

Figure 17. Knockdown of DNA repair pathway components failed to activate the UPR-ER.

(A) Representative micrographs depict worms of *hsp-4p::gfp* (n=3 per RNAi treatment) grown on control RNAi (EV), *xpf-1* RNAi, *mus-81* RNAi, *msh-2* RNAi, *him-6* RNAi, *him-1* RNAi, *dog-1* RNAi, and *cid-1* RNAi for 48hr and 72hr. (B) GFP signal quantification of *hsp-4p::gfp* grown on RNAi for 48hr and 72hr. Error bars represent SEM. Statistical analysis: Dunnett's T3 multiple comparisons test; all comparisons are to vector RNAi (negative control). (C) Representative micrographs depict worms of *Patf-4(uORF)::gfp* (n=2 per RNAi treatment) grown on control RNAi (EV), *xpf-1* RNAi, *mus-81* RNAi, *msh-2* RNAi, *him-6* RNAi, *him-1* RNAi, *dog-1* RNAi, and *cid-1* RNAi for 48hr and 72hr. (D) GFP signal quantification of *Patf-4(uORF)::gfp* on RNAi at 48hr and 72hr from ≥ 16 individual worms (n=2 per RNAi treatment). Error bars represent SEM. Statistical analysis: Dunnett's T3 multiple comparisons test; all comparisons are to vector RNAi (negative control). (E) Representative micrographs depict embryos of *hsp-4p::gfp* and *Patf-4(uORF)::gfp* (n=3 per RNAi treatment) harvested after 96hr of growing the parental generation on control RNAi (EV) and *him-1* RNAi for 96hr.

2.2.9 IRE-1 is required for germline protection against hydroxyurea (HU)-induced replication stress.

Based on the observations that UPR-ER is activated in both somatic cells and embryos upon *pri-1* and *pri-2* RNAi treatment, we asked if the three branches of UPR-ER play a

protective role against replication stress. We used hydroxyurea (HU), a widely used chemical that inhibits ribonucleotide reductase, which reduces ribonucleosides into deoxyribonucleosides for DNA synthesis. The mechanism of action is conserved in *C. elegans*, as HU exposure leads to S-phase arrest, evident from oversized nuclei in the mitotic compartment of the germline and extends the duration of the first cell cycle in early embryos in wild-type *C. elegans* [177,178]. In addition, it was reported that 24hr exposure of L4 hermaphrodites to HU is sufficient to trigger significant germline apoptosis as seen in the decrease in the number of germline nuclei by two-fold [179]. By comparing the number of eggs laid per HU-exposed worm during the 4hr recovery period on OP50 to the number of eggs per unstressed worms of the same genotype. we found that loss of *ire-1* decreases fecundity, indicating weakened germline resistance to replication stress upon HU exposure. However, the loss of *pek-1* or *atf-6* does not seem to have significantly detrimental effects (Figure 18A and B). Moreover, to assess the effect of prolonged replication stress in germline development, we subjected worms to chronic 10mM HU exposure from L1. The downstream effector of the *ire-1* pathway, *xbp-1* also had protective roles in protecting adult germline from replication stress (Figure 18A and B), further highlighting the importance of IRE-1 branch in replication stress protection in the *C. elegans* germline.

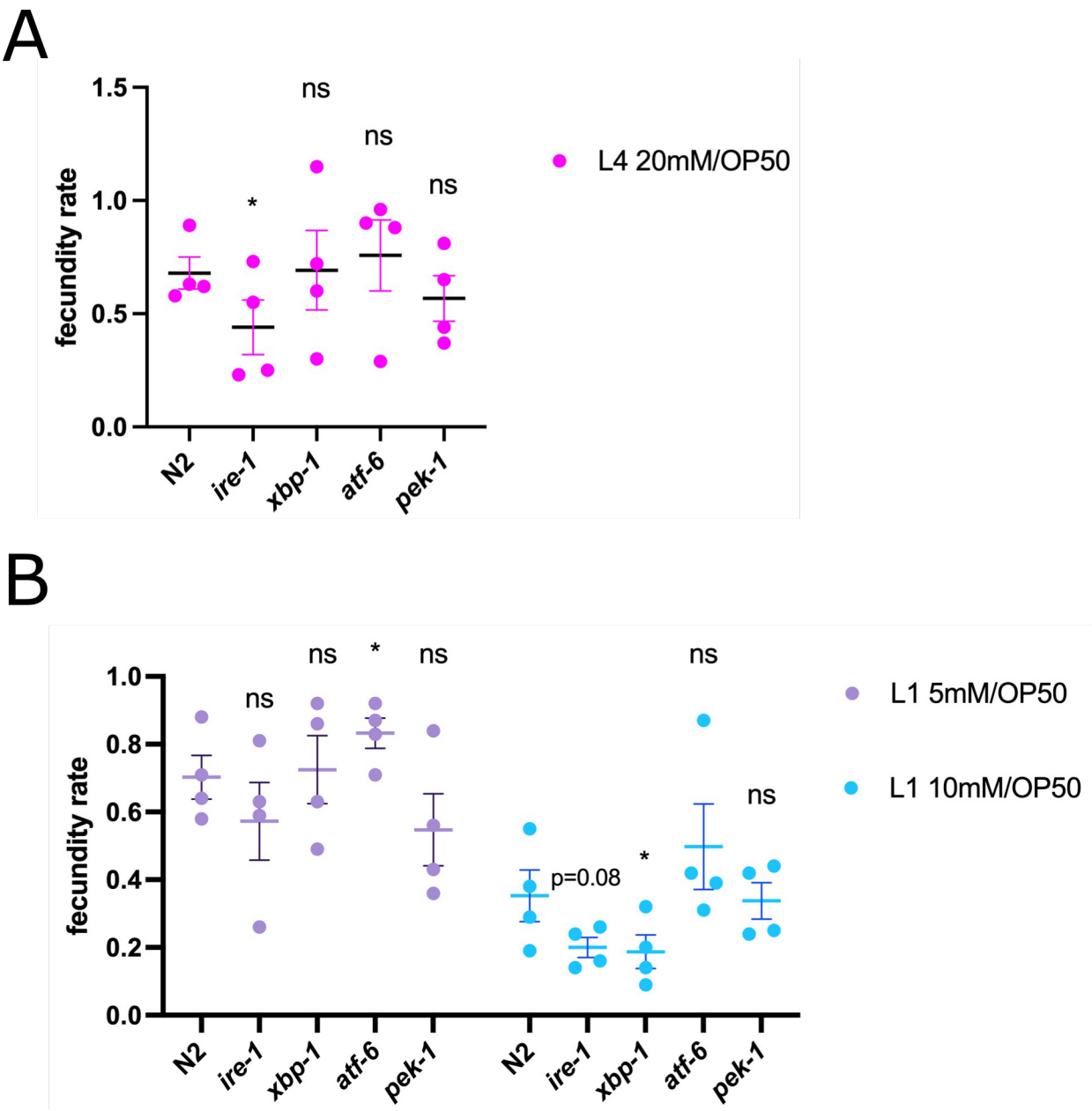

Figure 18. *ire-1* is required for germline protection against HU-induced replication stress.

Each dot represents fecundity rate, which is calculated as follows: (average number of eggs laid during 4hr recovery on OP50 per HU-treated worm)/(average number of eggs laid on OP50 in 4hr per untreated worm). Data points are pooled from four biological repeats, with each biological repeat containing four technical repeats of five worms of each genotype and condition. (two-way repeated measures (RM) ANOVA). (A) Stage-synchronized late L4 worms were transferred from OP50 to 20mM HU and maintained for 24hr before being transferred to OP50 plates for egg

laying. (B) Stage-synchronized L1 worms were placed onto NGM-l plates containing 5mM or 10mM HU, maintained for 72hr before being transferred to OP50 plates for egg laying. (one-way RM ANOVA).

2.2.10 *ire-1* and *pek-1* are required for somatic protection against hydroxyurea (HU)-induced replication stress.

Next, we aimed to answer whether the UPR-ER branches can protect somatic growth and development during prolonged HU exposure. To provide a quantitative measure of how HU-induced replication stress affects somatic development, we measured the body area of worms grown on 15mM HU from L1 stage after 72 hours. Although *ire-1* and *xbp-1* worms have a smaller body size than N2 grown under unstressed conditions (without HU) (Figure 19A), after normalization to average body size under unstressed condition for each genotype, we found that replication stress significantly hampers the somatic growth of *ire-1* and *pek-1* worms (Figure 19B). This suggests that both the *ire-1* and *pek-1* branches are important for worms to tolerate and/or resolve prolonged replication stress to achieve normal somatic growth, while the *atf-6* branch is dispensable for such a role. Finally, we observed that loss of either *ire-1* or *pek-1* leads to a developmental delay seen with the decreased ratio of 15mM HU-exposed worms grown past L4 stage at 48hr, compared to the HU-exposed N2 control (Figure 19D). Yet, loss of any UPR-ER branch does not cause a significant developmental delay under unstressed conditions (Figure 19C). In contrast, *atf-6* loss does not have a negative effect on developmental speed for *C. elegans* challenged with HU-induced replication stress.

Collectively, these data show that the *ire-1* and *pek-1* branches are required to maintain somatic resistance to replication stress. In contrast, the *atf-6* branch is dispensable for both roles in adaptation to HU-triggered replication stress.

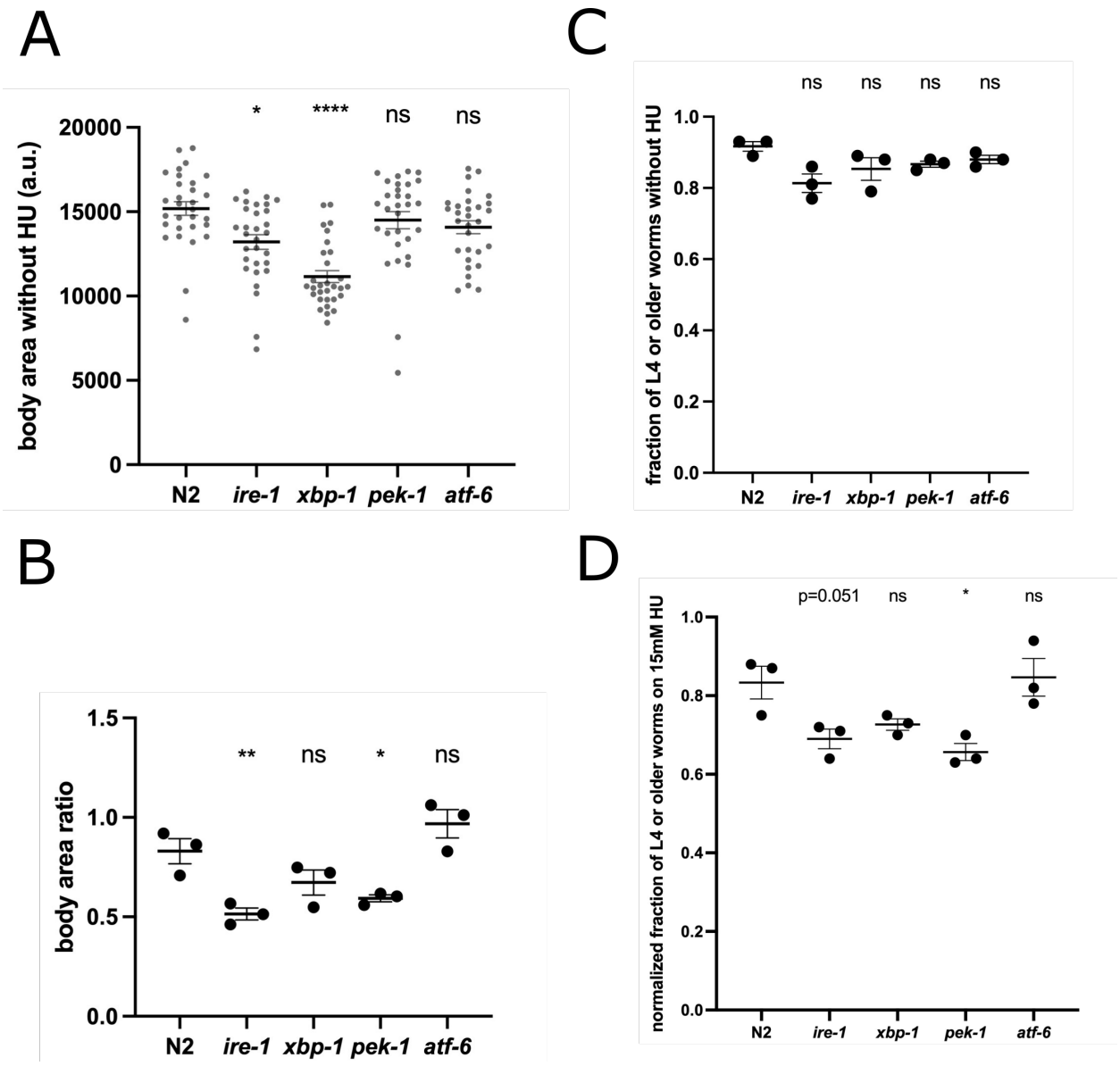

Figure 19. *ire-1* and *pek-1* are required for germline protection against HU-induced replication stress.

(A) Each dot represents the body size of an individual worm under unstressed conditions at 72hr (n=3, with at least 10 worms quantified per repeat). (B) Each dot represents average body area ratio, which is calculated as follows: (average body area of worms on 15mM HU)/(average body area of worms on DMSO) (n=3) (one-way RM ANOVA). (C) Each dot represents % worms grown past L4 on DMSO at 48hr (one-way RM ANOVA). (D) Each dot represents normalized % worms past L4 on 15mM HU, which is calculated as follows: (% of worms past L4 on

15mM HU)/(% of worms past L4 without HU) (n=3) (one-way RM ANOVA). Error bars represent SEM, and * indicates $p<0.05$

Chapter 3: Discussion and Conclusion

Recently, perturbations to membrane lipid composition have been found to be direct activators of the UPR-ER in a number of models including yeast, cell line, and *C. elegans* [48,50,180]. However, the extent of cellular perturbations activating the UPR through metabolic alterations independent of proteotoxicity was unknown. To address this knowledge gap, we performed large-scale genetic screens to identify 34 metabolic genes necessary to maintain ER homeostasis integrity in *C. elegans*. Our data provided several interesting and potentially protein-misfolding independent metabolic links to ER homeostasis, such as *nmt-1*, *hgo-1* and *let-767* (discussed in detail below). Moreover, we observed an interesting feedback relationship between genotoxicity and UPR-ER activation, but the detailed signaling mechanism between them requires further investigations.

3.1 Metabolic alterations that activate the UPR-ER and their potential mechanisms

Our functional genomic screen identified several genes that activate the UPR-ER [51]. Consistent with previous studies, we identified genes that induce proteotoxicity independent UPR-ER^{LBS}, such as the FA desaturases *fat-6* and *fat-7* [50], the PC synthesis enzymes *pcyt-1* and *sams-1* [165], *lpin-1*, which is linked to the synthesis of ω-6 PUFA-containing PLs [181–183], and the mevalonate pathway components *hmgs-1* and *hmgr-1* [184,185] (Figure 20). We also found several other metabolic genes whose inactivation may activate the UPR-ER^{LBS}, but via unclear mechanisms. For some genes, possible mechanisms are discussed below.

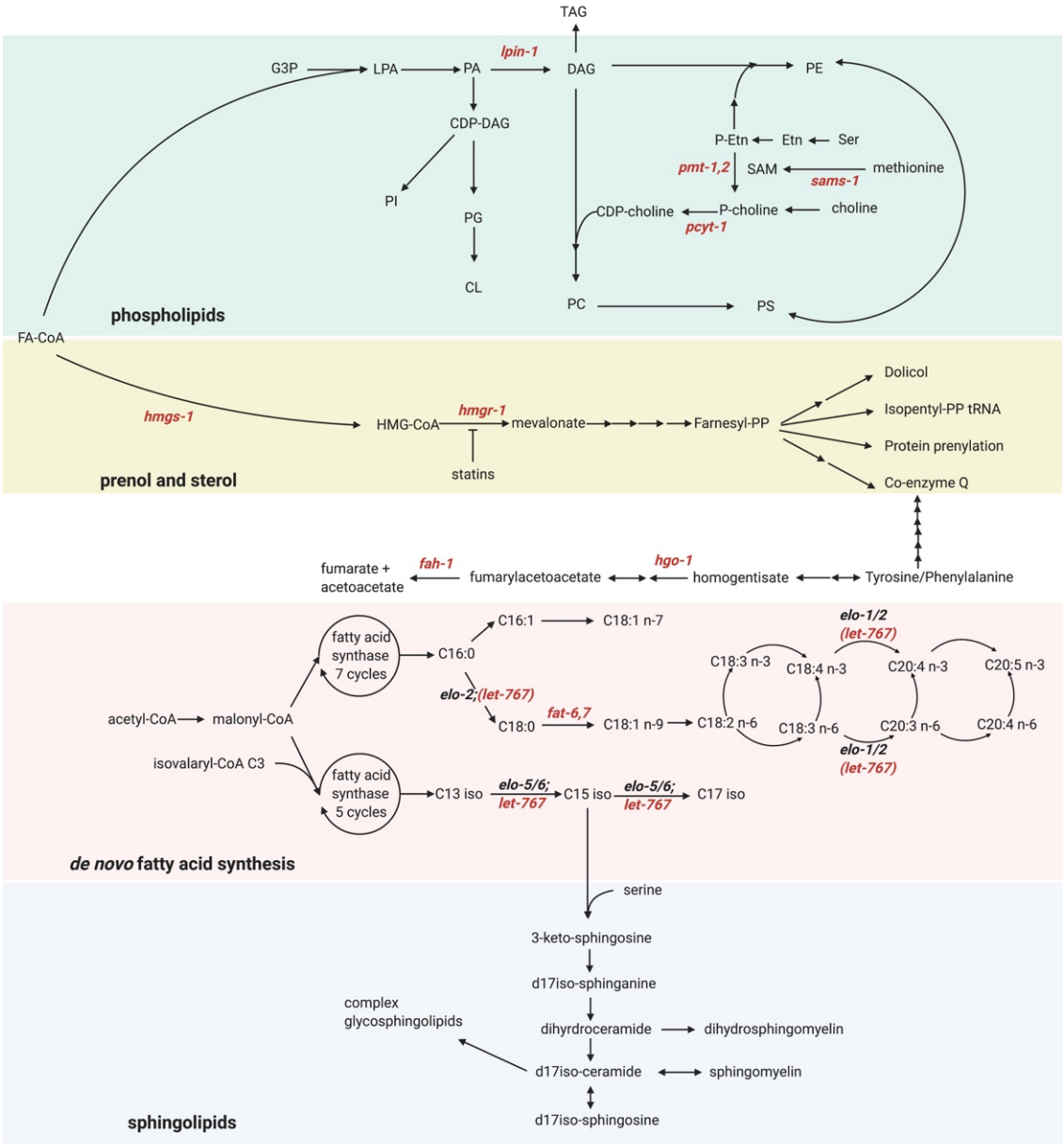

Figure 20. Overview of lipid synthesis pathways in *C. elegans* (adapted with permission from [145])

Abbreviated schematics depicts the metabolic pathways of major classes of lipids in C. elegans with genes that induce the UPR-ER when inactivated colored in red. Abbreviations: TAG: triacylglycerol; G3P: glucose-3 phosphate; LPA: lysophosphatidic acid; PA: phosphatidic acid; DAG: diacylglycerol; CDP-DAG: cytidine diphosphate diacylglycerol; PG: phosphatidylglycerol; PI: phosphatidylinositol; CL: cardiolipin; PC: phosphatidylcholine; CDP-Cho: cytidine diphosphate choline; PS: phosphatidylserine; PE:

phosphatidylethanolamine; Etn: ethanolamine; P-Etn: phosphoethanolamine; Ser: serine; SAM: s-adenosyl methionine. HMG-CoA: 3-hydroxy-3-methyl-glutaryl-coenzyme A. (Created with BioRender.com, Toronto, Ontario, Canada).

3.1.1 Loss of myristoylation on conserved *nmt-1* protein targets may cause UPR-ER activation

nmt-1 encodes N-myristoyl transferase, which irreversibly attaches a myristate (C14 FA) group to the N-terminal glycine residue of proteins involved in signal transduction. A global N-myristoylated proteome consisting of >100 proteins in human cells has been determined by quantitative proteomics studies [186]. Intriguingly, like in *C. elegans*, chemical inhibition of N-myristoyl transferase activity in human cell lines upregulates proteins involved in ER stress [187], suggesting that myristoylation is required for ER homeostasis via conserved protein targets. Identifying targets of *C. elegans* NMT-1 using comparative proteomics followed by genetic validation studies may pinpoint NMT-1 downstream targets whose myristoylation is involved in maintaining ER homeostasis.

3.1.2 Phenylalanine build-up may cause membrane lipid changes and UPR-ER activation

Another interesting gene is *hgo-1*, which encodes for homogentisate 1,2-dioxygenase; HGO-1 breaks down aromatic amino acids (tyrosine and phenylalanine; Figure 20). *hgo-1* loss not only activates the UPR-ER, but also results in increased oxidative stress [188]. Moreover, inactivation of the fumarylacetoacetate hydrolase *fah-1*, an enzyme downstream of *hgo-1* in the tyrosine/phenylamine metabolism pathway, also causes UPR-ER induction (Figure 20). This suggests that this breakdown pathway may be essential to preventing ER stress. *fah-1* RNAi

results in growth defects and *hsp-4* upregulation in *C. elegans* due to toxic upstream metabolite buildup, and the growth defect is suppressed in *fah-1/hgo-1* double RNAi treated worms [189]. However, *hgo-1* RNAi also induced *hsp-4* expression, suggesting that the growth defect can be uncoupled from UPR-ER activation in tyrosine/phenylalanine metabolism pathway mutants. Remarkably, inhibition of phenylalanine hydroxylase, the initial enzyme in the aromatic amino acid catabolism pathway, has been implicated in changing FA composition, which cannot be rescued by tyrosine supplementation [190,191]. Collectively, these studies point to phenylalanine build-up as a potential cause for UPR-ER activation, consistent with previous reports that phenylalanine increases membrane permeability by insertion into the membrane in liposomes [192]. However, whether phenylalanine induces the UPR-ER via alterations in membrane properties in vivo has not been tested. Untargeted or semi-targeted lipidomics profiling could reveal novel insights into if and how this phenylalanine catabolism pathway induces the UPR-ER.

3.1.3 Multiple lipid precursors synthesis pathways are disrupted upon loss of *let-767*

Finally, *let-767*, whose inactivation also induces the UPR-ER and causes developmental arrest, is a 3-ketoacyl-CoA reductase localized to the ER. *let-767* is necessary for the production of long-chain and mono-methyl branched-chain FAs [193] (Figure 20), both important precursors for sphingolipid synthesis in *C. elegans* [193,194]. Yet how *let-767* maintains ER homeostasis is unknown. LET-767 possesses steroid-modifying activity in worms [195], but this function is dispensable for normal development [193]. GC-MS analysis of FA profiles revealed that *let-767* RNAi caused a decrease in C15iso and C17iso monomethyl branched-chain FAs and sphingolipids [193,194,196]. Consistently, iso-15:0, iso-17:0, and iso-19:0 monomethyl

branched-chain FAs are sufficient to rescue the developmental arrest caused by *let-767* RNAi [193]. Interestingly, a recent study showed that *let-767* RNAi results in severely disturbed ER morphology, which can be rescued by supplementation with wildtype worm lysate, which likely contains a complete panel of essential lipids [197]. This suggests that LET-767 disruption induces ER stress through an unknown mechanism [198], independently of branched-chain FA synthesis. Perhaps, defective synthesis of long-chain FAs and/or sphingolipids, both of which have been linked to UPR-ER regulation [150], is the culprit. Indeed, very long-chain FAs (>20C) can increase membrane saturation [199], which activates the UPR-ER^{LBS} [50]. Targeted lipidomics in *let-767* depleted worms would be a powerful approach to quantify changes in different very long-chain FA levels in sphingolipids, possibly after ER membrane extraction [200].

3.2 DNA damage caused by stalled replication fork is an activator of UPR-ER

3.2.1 UPR-ER in such context may be independent of global protein misfolding

Knocking down *pri-1* and *pri-2* or irradiation with UV-C activates UPR-ER in the soma and in the embryo, but only in select embryonic cells (Figure 10, 11 and 14). Assuming that RNAi efficiency is similar in the replicating cells of early embryo, such specific activation argues against general non-specific protein misfolding. Instead, selective UPR-ER activation in embryos is more likely an adaptive mechanism triggered by altered spatial and temporal localization of cellular factors after *pri-1* and *pri-2* knockdown, like mis-localization of fate-determining factors such as PIE-1, UNC-120, and HLH-1 seen in *div-1* knockdown embryos. [201,202].

3.2.1.1 Exclusive activation of the UPR-ER reporter

The UPR-ER, the cytosolic UPR and the mitochondrial UPR pathways are interconnected. Conditions that impair general protein folding such as oxidative stress and protein degradation defects were known to induce all three branches of the UPR in *C. elegans* [203–205]. However, in contrast to the robust *hsp-4* induction by *pri-1* and *pri-2* RNAi or UV-C irradiation, we did not observe such induction of the cytosolic UPR reporter gene *hsp-16.2* (Figure 12 and 14), indicating that cytosolic proteostasis is not disturbed to a large extent by replication stress.

The mitochondrial UPR reporter gene *hsp-6* is not induced by *pri-1* and *pri-2* RNAi or UV-C either, in somatic worm cells (Figure 12A and 14B). This suggests that stalled replication fork does not cause protein misfolding in the mitochondria. Another caveat is that mitochondrial biogenesis occurs during the later phases of embryo development, as revealed by tissue-specific mitochondrial biogenesis reporters [206]. Moreover, proper mitochondrial proliferation is a pre-requisite for the biological meaning of *hsp-6p::gfp* induction and mitochondrial stress [206]. Therefore, we did not look at *hsp-6* induction in embryos as *pri-1* and *pri-2* RNAi or UV-C treated embryos arrest at an early stage, where mitochondrial biogenesis has not taken place.

3.2.2 Replication stress induces non-canonical *ire-1*- and *xbp-1*-independent *hsp-4* expression in embryos

Although *hsp-4* expression is widely used as a reporter for IRE-1-XBP-1 pathway activity, we observed partially *ire-1*-dependent and *xbp-1*-dependent activation of *hsp-4* by *pri-1* and *pri-2* RNAi in embryos (Figure 13). This is surprising because IRE-1 is the only known UPR

sensor to cleave *xbp-1u* mRNA into *xbp-1s*, which is then translated into the protein that upregulates *hsp-4* expression (Figure 1) [20,21,66]. *atf-6* loss of function also failed to completely abolish *hsp-4* induction, even though ATF-6 activation is required for *xbp-1u* transcription [25,37]. In somatic cells, IRE-1-XBP-1 independent, transient *hsp-4* induction occurs during the differentiation of stem-like seam cells into alae-secreting cells [207]. Although the factor required for this induction remains unidentified, the transcriptional factor B-Lymphocyte–Induced Maturation Protein 1 (BLMP-1) is required to suppress *hsp-4* in this context [207]. To our knowledge, our data is the first report of a partially UPR-ER independent mechanism of *hsp-4* induction in *C. elegans* embryos.

3.3 IRE-1 and PEK-1 of the UPR-ER are required for resistance to genotoxicity

Drawing on results published in different models, the bidirectional regulation between the DDR and the UPR-ER has begun to emerge [114,121]. Yeast data showed IRE1 is required for survival on HU [122]. We found that in *C. elegans*, the IRE-1 branch is required for protection of germline and soma during prolonged HU exposure initiated at an early developmental stage (Figure 18B and 19). In contrast, short-term acute HU exposure at a later developmental stage is tolerated well (Figure 18A), similar to what has been reported with treating *ire-1* worms at L4 stage with *rad-51* RNAi to induce DNA damage [208].

Few lines of published evidence exist for roles of the other two branches in resistance to genotoxicity. We observed that although *pek-1* is required for somatic resistance to HU, it is dispensable for germline resistance, unlike *ire-1* (Figure 18 and 19). In contrast, the *atf-6* branch is not required for soma or germline protection in genotoxic stress (Figure 18 and 19).

3.4 Caveats and considerations

3.4.1 Use of RNAi

Feeding RNAi is routinely used with *C. elegans* to circumvent mutations that are lethal or cause other severe effects, as well as to study large sets of genes in a high-throughput manner. Because we wished to study more than a thousand genes simultaneously and because many metabolic genes are essential, RNAi was therefore our method of choice. Feeding single RNAi generally yielded reproducible results, although effect size varied sometimes, requiring careful scoring of animals [209]. Indeed, with regards to the screen using *hsp-4p::gfp* as readout, a range of GFP intensity was usually observed for a given RNAi treatment.

3.4.2 Use of transcriptional GFP reporters

Comparing the GFP signal intensity of the transcriptional and the translational *hsp-4* reporters (grown on *mdt-15* RNAi or tunicamycin; Figure 10B), we observed a GFP intensity difference between the two, with the transcriptional reporter appearing to be more robust and sensitive. Even if the translational reporter may not provide accurately endogenous HSP-4 levels, the difference between the two reporter systems should be considered. We outline two reasons that may explain this discrepancy. First, unlike the translational reporter *hsp-4::gfp*, which was generated with CRISPR-Cas9 genome editing of the endogenous *hsp-4* locus, the widely-used *hsp-4p::gfp* transcriptional reporter strain was generated by integrating a multicopy extrachromosomal array of the *hsp-4p::gfp* transgene (GFP ORF fused to the promoter sequence of *hsp-4*) into the genome via irradiation [24].Therefore, the integrated transgene may be overexpressed at basal level and in response to stress. In addition, although the translational

reporter was generated by targeted gene editing method, fusing a GFP to the C terminus of the HSP-4 protein may affect the stability and hence the level of fa usion protein. Therefore, although the transcriptional reporters are convenient for screening purposes, follow-up endogenous validation methods such as a translational reporter strain or qRT-PCR are necessary to understand the true strength of a gene induction.

3.5 Conclusions

We used RNA interference (RNAi) to inactivate 1247 metabolic genes in *Caenorhabditis elegans* with the IRE-1 branch specific transcriptional reporter, *hsp-4p::gfp* to identify proteotoxicity-independent metabolic pathways that affect ER homeostasis, After screening and rigorous validation efforts, we obtained 34 high-confidence *xbp-1*-dependent hits that also activate the PEK-1 branch. Next, we used quantitative real-time PCR to show that 11 of 15 tested RNAi clones induce the endogenous UPR-ER in wild-type worms. Then we tested whether dietary choline supplementation, which suppresses UPR-ER in worms defective for PC synthesis pathway, is sufficient to suppress UPR-ER activation in our hits. Of the 34 hits, 3 were partially rescued by dietary supplementation of choline along with the complete rescue of *sams-1* RNAi-treated animals, suggesting that the majority of the hits does not activate the UPR-ER via defective PC synthesis. Finally, we performed follow-up studies on one of the hit pathways on DNA replication. In early embryos, DNA replication stress by the loss of primases or UV-C treatment induces UPR-ER activation, but not the mechanistically distinct cytosolic or mitochondrial UPRs, in a partially *ire-1*-, *xbp-1*-, and *atf-6*-dependent manner. This suggests that replication stress does not trigger global protein misfolding. Interestingly, genomic instability caused by loss of DNA repair pathways such as mismatch repair and nucleotide excision repair,

did not activate the UPR-ER, suggesting that molecular events specific to replication stress activate *hsp-4* and the UPR-ER in the embryo. Finally, we found that the IRE-1 branch of the UPR-ER is required for germline and somatic resistance to prolonged replication stress, while the PEK-1 is only required for germline resistance. ATF-6 of the three branches is dispensable for both roles. In sum, by identifying new genes that affect UPR-ER homeostasis in *C. elegans*, my project provides new insights into UPR-ER regulation and may serve as a starting point for the discovery of drug targets for human diseases featuring UPR-ER dysfunction and replication stress.

Chapter 4: Materials and Methods

4.1 Worm strains

Table 1 List of worm strains used in this thesis

Strain	Genotype	note
SJ4005	*zcIs4 [hsp-4p::gfp] V*	Obtained from CGC
SJ17	*xbp-1(zc12) III;zcIs4 [hsp-4p::gfp] V*	Obtained from CGC
SJ4100	*zcIs13 [hsp-6p::gfp] V*	Obtained from CGC
TJ375	*gpIs1 [hsp-16.2p::gfp]*	Obtained from CGC
LD1499	P*atf-4*(uORF)::*gfp*::*unc-54*(3'UTR)	A gift from Dr. Collin Ewald,
	xbp-1(tm2482) III	Obtained from NBRP. Backcrossed x2
RB545	*pek-1(ok275) V*	Obtained from CGC. Backcrossed x2 to lab WT N2.
RB925	*ire-1(ok799) II*	Obtained from CGC
RB772	*atf-6(ok551) X*	Obtained from CGC. Backcrossed x2 to lab WT N2.
VC1099	*hsp-4(gk514) II*	obtained from CGC (outcrossed x1). Backcrossed x1 to lab WT N2.
STA06	*hsp-4::gfp(syb2824) II*	Obtained from SunyBiotech Co., Ltd. Backcrossed x2

4.2 Worm growth conditions

We cultured *C. elegans* strains on nematode growth medium (NGM)-lite (0.2% NaCl, 0.4% tryptone, 0.3% KH_2PO_4, 0.05% K_2HPO_4) agar plates with *E. coli* OP50 as food source, except for RNAi, for which HT115 strain was used. To developmentally synchronize worm populations, gravid adult worms were bleached with sodium hypochlorite solution to extract

embryos, which were washed twice with M9 onto an unseeded NGM-lite plate to allow hatching overnight. When imaging worms, adult worms were bleached for no longer than 10 minutes until the auto-fluorescent mother bodies have disappeared for easier fluorescence scoring. The resulting synchronized L1 larvae were transferred onto OP50 NGM-lite plates or RNAi plates (NGM-lite plates containing 25 μg/mL carbenicillin, 2 mM IPTG, and 12.5 μg/mL tetracycline) to allow development.

For RT-qPCR (reverse transcription quantitative PCR) experiments, worms were harvested and washed in M9 at the indicated incubation time (usually 43-44 and 71-72 hours) at 20°C after placing L1 larvae on food. For imaging experiments, worms were allowed to grow for 48 and 72 hours at 20°C to reach late L4 and day-1 adulthood, respectively.

4.3 Metabolic RNAi sublibrary construction

Sublibrary construction Individual RNAi clones from Ahringer library was picked into each well containing 80ul of lysogeny broth (LB)with tetracycline (25ug/ml) and carbenicillin (12.5ug/ml) on a 96-well plate. The RNAi bacteria were allowed to grow for approximately 40 hours before the addition of 75ul of 30% sterile glycerol solution and stored at -80℃.

4.4 Feeding RNA interference

Feeding RNA interference (RNAi) was performed using NGM-lite RNAi plates (NGM-lite plates containing 25 μg/mL carbenicillin, 2 mM IPTG, and 12.5 μg/mL tetracycline) and seeded twice with the appropriate HT115 RNAi bacteria. Synchronous L1 worms were placed on RNAi plates and grown until they reached the desired developmental stage.

4.5 Sanger Sequencing

the plasmid DNA of the 38 high-confidence clones was extracted using QIAGEN Plasmid Mini Kit before sending for sequencing using M13 Forward primer. The identities of RNAi clones were verified by comparing plasmid sequencing results to the NCBI nucleotide database using the BLAST tool

4.6 RNA isolation and real-time quantitative PCR

Approximately 1000-2000 developmentally synchronized L4 larvae were collected, washed twice with M9, and then flash frozen in an ethanol/dry ice bath. For RNA isolation, Trizol was added to the thawed worm pellets, which were then subjected to two rounds of sonication (Fisher Scientific Sonic Dismembrator Model 500, 30 cycles, 0.1 second pulse on, 0.5 second pulse off). Purification of the sonicated mix was achieved by BCP extraction, isopropanol precipitation, and clean-up with the RNAeasy Mini Kit (#74106, Qiagen) including digestion with DNAse (#79254, Qiagen). cDNA synthesis was performed with Superscript III reverse transcriptase (#1405708, Invitrogen). Specifically, cDNA was generated from 2 μg of isolated RNA using Superscript III reverse transcriptase (#1708235, Invitrogen), random primers (#1597109, Invitrogen), 0.1M DTT (#1405708, Invitrogen), dNTPs (#R0186, Fermentas), and RNAseOUT (#1685480, Invitrogen) in XX microliter total volume. qPCR was performed in 96 well plates, using custom primer pairs from IDT (primer sequences are listed in Table 2). Newly designed primer pairs were first tested for primer specificity and efficiency, using serially diluted *C. elegans* cDNA samples; primers that failed this test were discarded and new primers were ordered. Each qPCR reaction mix contained 3μl of RNase/DNase free H_2O, 5μl of Sybr Green Master mix (#4385612, Applied Biosystems), 1μl of 5μM primer pair mix, and 1μl of 1:10

diluted cDNA. Each sample/gene combination was tested in technical triplicate and biological triplicates on an Applied Biosystems StepOnePlus machine.

Table 2. List of primer sequences used for RT-qPCR

Gene	Forward	Reverse
hsp-4	CGAGCGAGCTATTGAGTGGC	CCGAGTAAAGTTTGGAGACG
xbp-1u	CCGATCCACCTCCATCAAC	ACCGTCTGCTCCTTCCTCAATG
xbp-1s	TGCCTTTGAATCAGCAGTGG	ACCGTCTGCTCCTTCCTCAATG
Y41C4A.11	GCCATGGATTTTGACTGCTT	CGTGGATTTTTCGGAGACC
act-1	GCTGGACGTGATCTTACTGATTACC	GTAGCAGAGCTTCTCCTTGATGTC
ubc-2	AGGGAGGTGTCTTCTTCCTCAC	CGGATTTGGATCACAGAGCAGC
tba-1	GTACACTCCACTGATCTCTGCTGACAAG	CTCTGTACAAGAGGCAAACAGC

4.7 DIC and fluorescence microscopy

Worms were mounted onto 2% (w/v) agarose pads containing a drop of 20 mM sodium azide (NaN_3) for microscopy (magnification 10x unless stated in the figure legend). Eggs were scraped off from plates onto 2% (w/v) agarose pads containing a drop of M9 for microscopy (20x magnification). The worms were imaged using DIC and fluorescence optics through a CoolSnap HQ camera (Photometrics, Tucson, AZ, USA) on a Zeiss Axioplan 2 compound microscope (Carl Zeiss Microscopy, Thornwood, NY, USA). All GFP images were taken at the same exposure time of 300ms. Using the ImageJ software, the images in the GFP channel were adjusted to the same brightness and contrast levels for subsequent display and quantification purposes. Analysis of overall fluorescence intensity of individual worms was performed by

tracing the outline of worms on the corresponding DIC images, then normalized for area and background fluorescence.

4.8 Protein extraction and immunoblots

Whole-worm protein extracts were generated by sonication in RIPA (Radioimmunoprecipitation assay) lysis buffer with cOmplete^{TM} Protease Inhibitor Cocktail (#4693116001, Roche) and β-glycerophosphate. Protein concentrations were determined using the RC DC Protein Assay kit (#500-0121, Bio-Rad), and SDS-PAGE analysis and immunoblotting were performed as described [50] with anti Ser51-Phospho-eIF2α rabbit antibody (#9721, Cell Signaling Technologies), Anti-α-tubulin mouse antibody (# T9026 Sigma), and anti-rabbit HRP conjugated (#7074, NEB) and anti-mouse HRP conjugated secondary antibodies (#7076, Cell Signaling Technologies). Detection was done using ECL (#32109, Pierce).

4.9 UV-C exposure

Synchronized population of day-1 adult *C. elegans* was placed on NGM-l plates seeded with a thin layer of OP50 lawn. Uncovered NGM-l plates were then placed in Stratalinker 2400 UV Crosslinker (Stratagene) and irradiated with wavelength 254 nm light at 400J/m^2 energy level. After 24hr of recovery at 20^{o}C , worms and embryos laid were mounted and imaged.

4.10 Hydroxyurea treatment

For L1 recovery experiments, an age-synchronized L1 population was grown on regular OP50 NGM-lite or NMG-lite plates containing either 5 or 10mM HU for 72hr. Then, worms

were transferred to regular OP50-seeded NGM-lite plates for recovery and egg laying. After 4hr, the number of eggs was counted for each genotype in each condition, as indicated.

For L4 recovery experiments, synchronized L1 worms for were grown for 48hr on OP50. Then the age-synchronized L4 population was transferred to and maintained on either NMG-lite plates or NMG-lite plates containing 20mM HU for 24hr. Then, adults were transferred to OP50 plates for recovery and egg laying. After 4hr, the number of eggs was counted for each genotype and condition.

For developmental speed measurements, synchronized L1 population was grown on regular OP50 NGM-lite or NMG-lite plates containing 15mM HU for 48hr. Then the number of L4 or older worms and the total number of worms were counted for each genotype and condition.

For body size quantification experiments, synchronized L1 population was grown on regular OP50 NGM-lite or NMG-lite plates containing 15mM HU for 72hr, before >10 worms for each genotype and condition were mounted and imaged.

4.11 Statistics

In graphs, error bars denote SEM, derived from at least three biological replicates, unless otherwise indicated. p values were calculated using two-tailed Student's t test unless otherwise indicated in the figure legends and reported as values in figures. Scatter plots were plotted using GraphPad Prism 8.

Bibliography

1. Haucke, V.; Di Paolo, G. Lipids and lipid modifications in the regulation of membrane traffic. *Curr. Opin. Cell Biol.* **2007**, *19*, 426–35, doi:10.1016/j.ceb.2007.06.003.
2. Havel, R.J.; Eder, H.A.; Bragdon, J.H. The distribution and chemical composition of ultracentrifugally separated lipoproteins in human serum. *J. Clin. Invest.* **1955**, *34*, 1345–1353, doi:10.1172/JCI103182.
3. Fahy, E.; Subramaniam, S.; Brown, H.A.; Glass, C.K.; Merrill, A.H.; Murphy, R.C.; Raetz, C.R.H.; Russell, D.W.; Seyama, Y.; Shaw, W.; et al. A comprehensive classification system for lipids. *J. Lipid Res.* **2005**, *46*, 839–861, doi:10.1194/jlr.E400004-JLR200.
4. Witting, M.; Schmitt-Kopplin, P. The Caenorhabditis elegans lipidome: A primer for lipid analysis in Caenorhabditis elegans. *Arch. Biochem. Biophys.* **2016**, *589*, 27–37, doi:10.1016/j.abb.2015.06.003.
5. Sara Woodman; Kyoungtae Kim Membrane Lipids: Implication for Diseases and Membrane Trafficking. *SM J. Biol.* **2017**, *3*.
6. Van Meer, G.; De Kroon, A.I.P.M. Lipid map of the mammalian cell. *J. Cell Sci.* **2011**, *124*, 5–8, doi:10.1242/jcs.071233.
7. Vance, J.E. Phospholipid Synthesis and Transport in Mammalian Cells. *Traffic* **2015**, *16*, 1–18, doi:10.1111/tra.12230.
8. Potting, C.; Tatsuta, T.; König, T.; Haag, M.; Wai, T.; Aaltonen, M.J.; Langer, T. TRIAP1/PRELI Complexes Prevent Apoptosis by Mediating Intramitochondrial Transport of Phosphatidic Acid. *Cell Metab.* **2013**, *18*, 287–295, doi:10.1016/j.cmet.2013.07.008.
9. Mesmin, B. Mitochondrial lipid transport and biosynthesis: A complex balance. *J. Cell Biol.* **2016**, *214*, 9–11, doi:10.1083/jcb.201606069.
10. Wang, R.; Li, B.; Lam, S.M.; Shui, G. Integration of lipidomics and metabolomics for in-depth understanding of cellular mechanism and disease progression. *J. Genet. Genomics* **2020**, *47*, 69–83, doi:10.1016/j.jgg.2019.11.009.
11. Senft, D.; Ronai, Z.A. UPR, autophagy, and mitochondria crosstalk underlies the ER stress response. *Trends Biochem. Sci.* **2015**, *40*, 141–148, doi:10.1016/j.tibs.2015.01.002.
12. Adams, C.J.; Kopp, M.C.; Larburu, N.; Nowak, P.R.; Ali, M.M.U. Structure and molecular mechanism of ER stress signaling by the unfolded protein response signal activator IRE1. *Front. Mol. Biosci.* **2019**, *6*, 11, doi:10.3389/fmolb.2019.00011.
13. Oakes, S.A.; Papa, F.R. The Role of Endoplasmic Reticulum Stress in Human Pathology. *Annu. Rev. Pathol. Mech. Dis* **2015**, *10*, 173–94, doi:10.1146/annurev-pathol-012513-104649.
14. Hetz, C.; Papa, F.R. The Unfolded Protein Response and Cell Fate Control. *Mol. Cell* **2018**, *69*, 169–181, doi:10.1016/j.molcel.2017.06.017.
15. Lindholm, D.; Korhonen, L.; Eriksson, O.; Kõks, S. Recent insights into the role of unfolded protein response in ER stress in health and disease. *Front. Cell Dev. Biol.* **2017**, *5*, 48, doi:10.3389/fcell.2017.00048.
16. Diehl, J.A.; McQuiston, A. Recent insights into PERK-dependent signaling from the stressed endoplasmic reticulum. *F1000Research* **2017**, *6*, 1897, doi:10.12688/f1000research.12138.1.
17. Hillary, R.F.; Fitzgerald, U. A lifetime of stress: ATF6 in development and homeostasis.

J. Biomed. Sci. **2018**, *25*, 48, doi:10.1186/s12929-018-0453-1.
18. Walter, P.; Ron, D. The unfolded protein response: from stress pathway to homeostatic regulation. *Science* **2011**, *334*, 1081–6, doi:10.1126/science.1209038.
19. Nikawa, J. -I; Yamashita, S. IRE1 encodes a putative protein kinase containing a membrane-spanning domain and is required for inositol phototrophy in Saccharomyces cerevisiae. *Mol. Microbiol.* **1992**, *6*, 1441–1446, doi:10.1111/j.1365-2958.1992.tb00864.x.
20. Cox, J.S.; Shamu, C.E.; Walter, P. Transcriptional induction of genes encoding endoplasmic reticulum resident proteins requires a transmembrane protein kinase. *Cell* **1993**, *73*, 1197–1206, doi:10.1016/0092-8674(93)90648-A.
21. Morl, K.; Ma, W.; Gething, M.J.; Sambrook, J. A transmembrane protein with a cdc2+ CDC28-related kinase activity is required for signaling from the ER to the nucleus. *Cell* **1993**, *74*, 743–756, doi:10.1016/0092-8674(93)90521-Q.
22. Carrara, M.; Prischi, F.; Nowak, P.R.; Ali, M.M. Crystal structures reveal transient PERK luminal domain tetramerization in endoplasmic reticulum stress signaling. *EMBO J.* **2015**, *34*, 1589–1600, doi:10.15252/embj.201489183.
23. Lu, Y.; Liang, F.X.; Wang, X. A Synthetic Biology Approach Identifies the Mammalian UPR RNA Ligase RtcB. *Mol. Cell* **2014**, *55*, 758–770, doi:10.1016/j.molcel.2014.06.032.
24. Calfon, M.; Zeng, H.; Urano, F.; Till, J.H.; Hubbard, S.R.; Harding, H.P.; Clark, S.G.; Ron, D. IRE1 couples endoplasmic reticulum load to secretory capacity by processing the XBP-1 mRNA. **2002**, *415*, 92–96, doi:10.1038/415092a.
25. Yoshida, H.; Matsui, T.; Yamamoto, A.; Okada, T.; Mori, K. XBP1 mRNA is induced by ATF6 and spliced by IRE1 in response to ER stress to produce a highly active transcription factor. *Cell* **2001**, *107*, 881–891, doi:10.1016/S0092-8674(01)00611-0.
26. Travers, K.J.; Patil, C.K.; Wodicka, L.; Lockhart, D.J.; Weissman, J.S.; Walter, P. Functional and Genomic Analyses Reveal an Essential Coordination between the Unfolded Protein Response and ER-Associated Degradation. *Cell* **2000**, *101*, 249–258, doi:10.1016/S0092-8674(00)80835-1.
27. Hetz, C.; Glimcher, L.H. Fine-Tuning of the Unfolded Protein Response: Assembling the IRE1α Interactome. *Mol. Cell* **2009**, *35*, 551–561, doi:10.1016/j.molcel.2009.08.021.
28. Bertolotti, A.; Zhang, Y.; Hendershot, L.M.; Harding, H.P.; Ron, D. Dynamic interaction of BiP and ER stress transducers in the unfolded-protein response. *Nat. Cell Biol.* **2000**, *2*, 326–332, doi:10.1038/35014014.
29. Ho, N.; Xu, C.; Thibault, G. From the unfolded protein response to metabolic diseases – lipids under the spotlight. *J. Cell Sci.* **2018**, *131*, 199307, doi:10.1242/jcs.199307.
30. Novoa, I.; Zeng, H.; Harding, H.P.; Ron, D. Feedback inhibition of the unfolded protein response by GADD34-mediated dephosphorylation of eIF2α. *J. Cell Biol.* **2001**, *153*, 1011–1021, doi:10.1083/jcb.153.5.1011.
31. Rousakis, A.; Vlassis, A.; Vlanti, A.; Patera, S.; Thireos, G.; Syntichaki, P. The general control nonderepressible-2 kinase mediates stress response and longevity induced by target of rapamycin inactivation in Caenorhabditis elegans. *Aging Cell* **2013**, *12*, 742–751, doi:10.1111/acel.12101.
32. Statzer, C.; Venz, R.; Bland, M.; Robida-Stubbs, S.; Meng, J.; Patel, K.; Emsley, R.; Petrovic, D.; Liu, P.; Morantte, I.; et al. ATF-4 and hydrogen sulfide signalling mediate longevity from inhibition of translation or mTORC1. *bioRxiv* **2020**, doi:10.1101/2020.11.02.364703.

33. Shen, X.; Ellis, R.E.; Lee, K.; Liu, C.Y.; Yang, K.; Solomon, A.; Yoshida, H.; Morimoto, R.; Kurnit, D.M.; Mori, K.; et al. Complementary signaling pathways regulate the unfolded protein response and are required for C. elegans development. *Cell* **2001**, *107*, 893–903, doi:10.1016/S0092-8674(01)00612-2.
34. Harding, H.P.; Zhang, Y.; Bertolotti, A.; Zeng, H.; Ron, D. Perk is essential for translational regulation and cell survival during the unfolded protein response. *Mol. Cell* **2000**, *5*, 897–904, doi:10.1016/S1097-2765(00)80330-5.
35. Harding, H.P.; Zeng, H.; Zhang, Y.; Jungries, R.; Chung, P.; Plesken, H.; Sabatini, D.D.; Ron, D. Diabetes mellitus and exocrine pancreatic dysfunction in Perk-/- mice reveals a role for translational control in secretory cell survival. *Mol. Cell* **2001**, *7*, 1153–1163, doi:10.1016/S1097-2765(01)00264-7.
36. Delépine, M.; Nicolino, M.; Barrett, T.; Golamaully, M.; Mark Lathrop, G.; Julier, C. EIF2AK3, encoding translation initiation factor 2-α kinase 3, is mutated in patients with Wolcott-Rallison syndrome. *Nat. Genet.* **2000**, *25*, 406–409, doi:10.1038/78085.
37. Lee, K.; Tirasophon, W.; Shen, X.; Michalak, M.; Prywes, R.; Okada, T.; Yoshida, H.; Mori, K.; Kaufman, R.J. IRE1-mediated unconventional mRNA splicing and S2P-mediated ATF6 cleavage merge to regulate XBP1 in signaling the unfolded protein response. *Genes Dev.* **2002**, *16*, 452–466, doi:10.1101/gad.964702.
38. Yamamoto, K.; Sato, T.; Matsui, T.; Sato, M.; Okada, T.; Yoshida, H.; Harada, A.; Mori, K. Transcriptional Induction of Mammalian ER Quality Control Proteins Is Mediated by Single or Combined Action of ATF6α and XBP1. *Dev. Cell* **2007**, *13*, 365–376, doi:10.1016/j.devcel.2007.07.018.
39. Shoulders, M.D.; Ryno, L.M.; Genereux, J.C.; Moresco, J.J.; Tu, P.G.; Wu, C.; Yates, J.R.; Su, A.I.; Kelly, J.W.; Wiseman, R.L. Stress-Independent Activation of XBP1s and/or ATF6 Reveals Three Functionally Diverse ER Proteostasis Environments. *Cell Rep.* **2013**, *3*, 1279–1292, doi:10.1016/j.celrep.2013.03.024.
40. Waldherr, S.M.; Strovas, T.J.; Vadset, T.A.; Liachko, N.F.; Kraemer, B.C. Constitutive XBP-1s-mediated activation of the endoplasmic reticulum unfolded protein response protects against pathological tau. *Nat. Commun.* **2019**, *10*, 4443, doi:10.1038/s41467-019-12070-3.
41. Wu, J.; Rutkowski, D.T.; Dubois, M.; Swathirajan, J.; Saunders, T.; Wang, J.; Song, B.; Yau, G.D.Y.; Kaufman, R.J. ATF6α Optimizes Long-Term Endoplasmic Reticulum Function to Protect Cells from Chronic Stress. *Dev. Cell* **2007**, *13*, 351–364, doi:10.1016/j.devcel.2007.07.005.
42. Shen, X.; Ellis, R.E.; Sakaki, K.; Kaufman, R.J. Genetic Interactions Due to Constitutive and Inducible Gene Regulation Mediated by the Unfolded Protein Response in C. elegans. *PLoS Genet.* **2005**, *1*, e37, doi:10.1371/journal.pgen.0010037.
43. Wang, S.; Hu, B.; Ding, Z.; Dang, Y.; Wu, J.; Li, D.; Liu, X.; Xiao, B.; Zhang, W.; Ren, R.; et al. ATF6 safeguards organelle homeostasis and cellular aging in human mesenchymal stem cells. *Cell Discov.* **2018**, *4*, 1–19, doi:10.1038/s41421-017-0003-0.
44. Kohl, S.; Zobor, D.; Chiang, W.C.; Weisschuh, N.; Staller, J.; Menendez, I.G.; Chang, S.; Beck, S.C.; Garrido, M.G.; Sothilingam, V.; et al. Mutations in the unfolded protein response regulator ATF6 cause the cone dysfunction disorder achromatopsia. *Nat. Genet.* **2015**, *47*, 757–765, doi:10.1038/ng.3319.
45. Ariyama, H.; Kono, N.; Matsuda, S.; Inoue, T.; Arai, H. Decrease in Membrane

Phospholipid Unsaturation Induces Unfolded Protein Response. *J. Biol. Chem.* **2010**, *285*, 22027–22035, doi:10.1074/jbc.M110.126870.
46. Pineau, L.; Ferreira, T. Lipid-induced ER stress in yeast and β cells: parallel trails to a common fate. *FEMS Yeast Res.* **2010**, *10*, 1035–1045, doi:10.1111/j.1567-1364.2010.00674.x.
47. Pineau, L.; Colas, J.; Dupont, S.; Beney, L.; Fleurat-Lessard, P.; Berjeaud, J.-M.; Bergès, T.; Ferreira, T. Lipid-Induced ER Stress: Synergistic Effects of Sterols and Saturated Fatty Acids. *Traffic* **2009**, *10*, 673–690, doi:10.1111/j.1600-0854.2009.00903.x.
48. Volmer, R.; van der Ploeg, K.; Ron, D. Membrane lipid saturation activates endoplasmic reticulum unfolded protein response transducers through their transmembrane domains. *Proc. Natl. Acad. Sci.* **2013**, *110*, 4628–4633, doi:10.1073/pnas.1217611110.
49. Sommerweiss, D.; Gorski, T.; Richter, S.; Garten, A.; Kiess, W. Oleate rescues INS-1E β-cells from palmitate-induced apoptosis by preventing activation of the unfolded protein response. *Biochem. Biophys. Res. Commun.* **2013**, *441*, 770–776, doi:10.1016/j.bbrc.2013.10.130.
50. Hou, N.S.; Gutschmidt, A.; Choi, D.Y.; Pather, K.; Shi, X.; Watts, J.L.; Hoppe, T.; Taubert, S. Activation of the endoplasmic reticulum unfolded protein response by lipid disequilibrium without disturbed proteostasis in vivo. *Proc. Natl. Acad. Sci.* **2014**, *111*, E2271–E2280, doi:10.1073/pnas.1318262111.
51. Ho, N.; Yap, W.S.; Xu, J.; Wu, H.; Koh, J.H.; Goh, W.W. Bin; George, B.; Chong, S.C.; Taubert, S.; Thibault, G. Stress sensor Ire1 deploys a divergent transcriptional program in response to lipid bilayer stress. *J. Cell Biol.* **2020**, *219*, e201909165, doi:10.1083/JCB.201909165.
52. Hong Koh, J.; Wang, L.; Beaudoin-Chabot, C.; Thibault, G.; Koh, J.H.; Wang, L.; Beaudoin-Chabot, C.; Thibault, G. Lipid bilayer stress-activated IRE-1 modulates autophagy during endoplasmic reticulum stress. *J. Cell Sci.* **2018**, *131*, 217992, doi:10.1242/jcs.217992.
53. Thibault, G.; Shui, G.; Kim, W.; McAlister, G.C.; Ismail, N.; Gygi, S.P.; Wenk, M.R.; Ng, D.T.W. The Membrane Stress Response Buffers Lethal Effects of Lipid Disequilibrium by Reprogramming the Protein Homeostasis Network. *Mol. Cell* **2012**, *48*, 16–27, doi:10.1016/j.molcel.2012.08.016.
54. Fu, S.; Yang, L.; Li, P.; Hofmann, O.; Dicker, L.; Hide, W.; Lin, X.; Watkins, S.M.; Ivanov, A.R.; Hotamisligil, G.S. Aberrant lipid metabolism disrupts calcium homeostasis causing liver endoplasmic reticulum stress in obesity. *Nature* **2011**, *473*, 528–531, doi:10.1038/nature09968.
55. Jo, H.; Shim, J.; Lee, J.H.; Lee, J.; Kim, J.B. IRE-1 and HSP-4 Contribute to Energy Homeostasis via Fasting-Induced Lipases in C. elegans. *Cell Metab.* **2009**, *9*, 440–448, doi:10.1016/j.cmet.2009.04.004.
56. Koh, J.H.; Wang, L.; Beaudoin-Chabot, C.; Thibault, G. Lipid perturbation-activated IRE-1 modulates autophagy and lipolysis during endoplasmic reticulum stress. *bioRxiv* **2018**, doi:10.1101/285379.
57. Kyriakakis, E.; Charmpilas, N.; Tavernarakis, N. Differential adiponectin signalling couples ER stress with lipid metabolism to modulate ageing in C. Elegans. *Sci. Rep.* **2017**, *7*, 1–13, doi:10.1038/s41598-017-05276-2.
58. Taylor, R.C.; Dillin, A. XBP-1 Is a cell-nonautonomous regulator of stress resistance and

longevity. *Cell* **2013**, *153*, 1435, doi:10.1016/j.cell.2013.05.042.
59. Özbey, N.P.; Imanikia, S.; Krueger, C.; Hardege, I.; Morud, J.; Sheng, M.; Schafer, W.R.; Casanueva, M.O.; Taylor, R.C. Tyramine Acts Downstream of Neuronal XBP-1s to Coordinate Inter-tissue UPRER Activation and Behavior in C. elegans. *Dev. Cell* **2020**, *55*, 754–770, doi:10.1016/j.devcel.2020.10.024.
60. Karagöz, G.E.; Acosta-Alvear, D.; Walter, P. The unfolded protein response: Detecting and responding to fluctuations in the protein-folding capacity of the endoplasmic reticulum. *Cold Spring Harb. Perspect. Biol.* **2019**, *11*, a033886, doi:10.1101/cshperspect.a033886.
61. Credle, J.J.; Finer-Moore, J.S.; Papa, F.R.; Stroud, R.M.; Walter, P. On the mechanism of sensing unfolded protein in the endoplasmic reticulum. *Proc. Natl. Acad. Sci. U. S. A.* **2005**, *102*, 18773–18784, doi:10.1073/pnas.0509487102.
62. Gardner, B.M.; Walter, P. Unfolded proteins are Ire1-activating ligands that directly induce the unfolded protein response. *Science (80-.).* **2011**, *333*, 1891–1894, doi:10.1126/science.1209126.
63. Karagöz, G.E.; Acosta-Alvear, D.; Nguyen, H.T.; Lee, C.P.; Chu, F.; Walter, P. An unfolded protein-induced conformational switch activates mammalian IRE1. *Elife* **2017**, *6*, doi:10.7554/eLife.30700.
64. Wang, P.; Li, J.; Tao, J.; Sha, B. The luminal domain of the ER stress sensor protein PERK binds misfolded proteins and thereby triggers PERK oligomerization. *J. Biol. Chem.* **2018**, *293*, 4110–4121, doi:10.1074/jbc.RA117.001294.
65. Preissler, S.; Ron, D. Early events in the endoplasmic reticulum unfolded protein response. *Cold Spring Harb. Perspect. Biol.* **2019**, *11*, a033894, doi:10.1101/cshperspect.a033894.
66. Kopp, M.C.; Nowak, P.R.; Larburu, N.; Adams, C.J.; Ali, M.M.U. In vitro FRET analysis of IRE1 and BiP association and dissociation upon endoplasmic reticulum stress. *Elife* **2018**, *7*, doi:10.7554/eLife.30257.
67. Carrara, M.; Prischi, F.; Nowak, P.R.; Kopp, M.C.; Ali, M.M.U. Noncanonical binding of BiP ATPase domain to Ire1 and Perk is dissociated by unfolded protein CH1 to initiate ER stress signaling. *Elife* **2015**, *2015*, doi:10.7554/eLife.03522.
68. Okamura, K.; Kimata, Y.; Higashio, H.; Tsuru, A.; Kohno, K. Dissociation of Kar2p/BiP from an ER sensory molecule, Ire1p, triggers the unfolded protein response in yeast. *Biochem. Biophys. Res. Commun.* **2000**, *279*, 445–450, doi:10.1006/bbrc.2000.3987.
69. Oikawa, D.; Kimata, Y.; Kohno, K.; Iwawaki, T. Activation of mammalian IRE1α upon ER stress depends on dissociation of BiP rather than on direct interaction with unfolded proteins. *Exp. Cell Res.* **2009**, *315*, 2496–2504, doi:10.1016/j.yexcr.2009.06.009.
70. Amin-Wetzel, N.; Neidhardt, L.; Yan, Y.; Mayer, M.P.; Ron, D. Unstructured regions in IRE1α specify BiP-mediated destabilisation of the luminal domain dimer and repression of the UPR. *Elife* **2019**, *8*, doi:10.7554/eLife.50793.
71. Heschl, M.F.P.; Baillie, D.L. The HSP70 multigene family of Caenorhabditis elegans. *Comp. Biochem. Physiol. -- Part B Biochem.* 1990, *96*, 633–637.
72. Kapulkin, V.; Hiester, B.G.; Link, C.D. Compensatory regulation among ER chaperones in C. elegans. *FEBS Lett.* **2005**, *579*, 3063–3068, doi:10.1016/j.febslet.2005.04.062.
73. Özcan, U.; Yilmaz, E.; Özcan, L.; Furuhashi, M.; Vaillancourt, E.; Smith, R.O.; Görgün, C.Z.; Hotamisligil, G.S. Chemical chaperones reduce ER stress and restore glucose

homeostasis in a mouse model of type 2 diabetes. *Science (80-.).* **2006**, *313*, 1137–1140, doi:10.1126/science.1128294.
74. Mai, C.T.; Le, Q.G.; Ishiwata-Kimata, Y.; Takagi, H.; Kohno, K.; Kimata, Y. 4-Phenylbutyrate suppresses the unfolded protein response without restoring protein folding in Saccharomyces cerevisiae. *FEMS Yeast Res.* **2018**, *18*, 16, doi:10.1093/femsyr/foy016.
75. Nissar, A.U.; Sharma, L.; Mudasir, M.A.; Nazir, L.A.; Umar, S.A.; Sharma, P.R.; Vishwakarma, R.A.; Tasduq, S.A. Chemical chaperone 4-phenyl butyric acid (4-PBA) reduces hepatocellular lipid accumulation and lipotoxicity through induction of autophagy. *J. Lipid Res.* **2017**, *58*, 1855–1868, doi:10.1194/jlr.M077537.
76. Arai, Y.; Choi, B.; Kim, B.J.; Rim, W.; Park, S.; Park, H.; Ahn, J.; Lee, S.H. Tauroursodeoxycholic acid (TUDCA) counters osteoarthritis by regulating intracellular cholesterol levels and membrane fluidity of degenerated chondrocytes. *Biomater. Sci.* **2019**, *7*, 3178–3189, doi:10.1039/c9bm00426b.
77. Lee, H.; Lee, G.; Kim, H.; Lee, Y.; Chae, H. Phosphatidylinositol 3-kinase-δ controls endoplasmic reticulum membrane fluidity and permeability in fungus-induced allergic inflammation in mice. *Br. J. Pharmacol.* **2020**, *177*, 1556–1567, doi:10.1111/bph.14917.
78. Wei, Y.; Wang, D.; Gentile, C.L.; Pagliassotti, M.J. Reduced endoplasmic reticulum luminal calcium links saturated fatty acid-mediated endoplasmic reticulum stress and cell death in liver cells. *Mol. Cell. Biochem.* **2009**, *331*, 31–40, doi:10.1007/s11010-009-0142-1.
79. Bi, J.; Wang, W.; Liu, Z.; Huang, X.; Jiang, Q.; Liu, G.; Wang, Y. Seipin promotes adipose tissue fat storage through the ER Ca^{2+}-ATPase SERCA. *Cell Metab.* **2014**, *19*, 861–871, doi:10.1016/J.CMET.2014.03.028.
80. Kitai, Y.; Ariyama, H.; Kono, N.; Oikawa, D.; Iwawaki, T.; Arai, H. Membrane lipid saturation activates IRE1a without inducing clustering. *Genes to Cells* **2013**, *18*, 798–809, doi:10.1111/gtc.12074.
81. Promlek, T.; Ishiwata-Kimata, Y.; Shido, M.; Sakuramoto, M.; Kohno, K.; Kimata, Y. Membrane aberrancy and unfolded proteins activate the endoplasmic reticulum stress sensor Ire1 in different ways. *Mol. Biol. Cell* **2011**, *22*, 3520–32, doi:10.1091/mbc.E11-04-0295.
82. Daniele, J.R.; Higuchi-Sanabria, R.; Durieux, J.; Monshietehadi, S.; Ramachandran, V.; Tronnes, S.U.; Kelet, N.; Sanchez, M.; Metcalf, M.G.; Garcia, G.; et al. UPRER promotes lipophagy independent of chaperones to extend life span. *Sci. Adv.* **2020**, *6*, e1441, doi:10.1126/sciadv.aaz1441.
83. Deguil, J.; Pineau, L.; Rowland Snyder, E.C.; Dupont, S.; Beney, L.; Gil, A.; Frapper, G.; Ferreira, T. Modulation of Lipid-Induced ER Stress by Fatty Acid Shape. *Traffic* **2011**, *12*, 349–362, doi:10.1111/j.1600-0854.2010.01150.x.
84. Shyu, P.; Ng, B.S.H.; Ho, N.; Chaw, R.; Seah, Y.L.; Marvalim, C.; Thibault, G. Membrane phospholipid alteration causes chronic ER stress through early degradation of homeostatic ER-resident proteins. *Sci. Rep.* **2019**, *9*, 8637, doi:10.1038/s41598-019-45020-6.
85. Boslem, E.; Weir, J.M.; Macintosh, G.; Sue, N.; Cantley, J.; Meikle, P.J.; Biden, T.J. Alteration of endoplasmic reticulum lipid rafts contributes to lipotoxicity in pancreatic β-cells. *J. Biol. Chem.* **2013**, *288*, 26569–26582, doi:10.1074/jbc.M113.489310.
86. Sharpe, H.J.; Stevens, T.J.; Munro, S. A Comprehensive Comparison of Transmembrane

Domains Reveals Organelle-Specific Properties. *Cell* **2010**, *142*, 158–169, doi:10.1016/j.cell.2010.05.037.
87. Imanikia, S.; Sheng, M.; Castro, C.; Griffin, J.L.; Taylor, R.C. XBP-1 Remodels Lipid Metabolism to Extend Longevity. *Cell Rep.* **2019**, *28*, 581-589.e4, doi:10.1016/j.celrep.2019.06.057.
88. Singh, S.; Trikha, S.; Bhowmick, D.C.; Sarkar, A.A.; Jeremic, A.M. Role of cholesterol and phospholipids in amylin misfolding, aggregation and etiology of islet amyloidosis. *Adv. Exp. Med. Biol.* **2015**, *855*, 95–116, doi:10.1007/978-3-319-17344-3_4.
89. Bogdanov, M.; Dowhan, W. Phospholipid-assisted protein folding: Phosphatidylethanolamine is required at a late step of the conformational maturation of the polytopic membrane protein lactose permease. *EMBO J.* **1998**, *17*, 5255–5264, doi:10.1093/emboj/17.18.5255.
90. Lee, J.S.; Mendez, R.; Heng, H.H.; Yang, Z.Q.; Zhang, K. Pharmacological ER stress promotes hepatic lipogenesis and lipid droplet formation. *Am. J. Transl. Res.* **2012**, *4*, 102–113.
91. Kim, S.; Kwon, D.; Kwak, J.-H.; Lee, S.; Lee, Y.-H.; Yun, J.; Son, T.; Jung, Y.-S. Tunicamycin-Induced ER Stress is Accompanied with Oxidative Stress via Abrogation of Sulfur Amino Acids Metabolism in the Liver. *Int. J. Mol. Sci.* **2018**, *19*, 4114, doi:10.3390/ijms19124114.
92. Qin, X.Y.; Su, T.; Yu, W.; Kojima, S. Lipid desaturation-associated endoplasmic reticulum stress regulates MYCN gene expression in hepatocellular carcinoma cells. *Cell Death Dis.* **2020**, *11*, 66, doi:10.1038/s41419-020-2257-y.
93. Bik, E.; Mielniczek, N.; Jarosz, M.; Denbigh, J.; Budzynska, R.; Baranska, M.; Majzner, K. Tunicamycin induced endoplasmic reticulum changes in endothelial cells investigated: In vitro by confocal Raman imaging. *Analyst* **2019**, *144*, 6561–6569, doi:10.1039/c9an01456j.
94. Reinhard, J.; Mattes, C.; Väth, K.; Radanović, T.; Surma, M.A.; Klose, C.; Ernst, R. A Quantitative Analysis of Cellular Lipid Compositions During Acute Proteotoxic ER Stress Reveals Specificity in the Production of Asymmetric Lipids. *Front. Cell Dev. Biol.* **2020**, *8*, 756, doi:10.3389/fcell.2020.00756.
95. Jackson, S.P.; Bartek, J. The DNA-damage response in human biology and disease. *Nature* 2009, *461*, 1071–1078.
96. Wang, K.; Li, L.; Zhang, Y.; Gao, D. Crosstalk between signaling pathways and DNA damage response. *Genome Instab. Dis.* **2020**, *1*, 81–91, doi:10.1007/s42764-019-00005-7.
97. Srinivas, U.S.; Tan, B.W.Q.; Vellayappan, B.A.; Jeyasekharan, A.D. ROS and the DNA damage response in cancer. *Redox Biol.* 2019, *25*, 101084.
98. O'Neil, N.; Rose, A. DNA repair. *WormBook* 2006, 1–12.
99. Stergiou, L.; Hengartner, M.O. Death and more: DNA damage response pathways in the nematode C. elegans. *Cell Death Differ.* **2004**, *11*, 21–28, doi:10.1038/sj.cdd.4401340.
100. Vermezovic, J.; Stergiou, L.; Hengartner, M.O.; D'Adda Di Fagagna, F. Differential regulation of DNA damage response activation between somatic and germline cells in Caenorhabditis elegans. *Cell Death Differ.* **2012**, *19*, 1847–1855, doi:10.1038/cdd.2012.69.
101. Sonneville, R.; Querenet, M.; Craig, A.; Gartner, A.; Julian Blow, J. The dynamics of replication licensing in live Caenorhabditis elegans embryos. *J. Cell Biol.* **2012**, *196*, 233–

246, doi:10.1083/jcb.201110080.
102. Schübeler, D.; Scalzo, D.; Kooperberg, C.; van Steensel, B.; Delrow, J.; Groudine, M. Genome-wide DNA replication profile for Drosophila melanogaster: A link between transcription and replication timing. *Nat. Genet.* **2002**, *32*, 438–442, doi:10.1038/ng1005.
103. Dileep, V.; Gilbert, D.M. Single-cell replication profiling to measure stochastic variation in mammalian replication timing. *Nat. Commun.* **2018**, *9*, 1–8, doi:10.1038/s41467-017-02800-w.
104. Strobino, M.; Wenda, J.M.; Padayachy, L.; Steiner, F.A. Loss of histone H3.3 results in DNA replication defects and altered origin dynamics in C. elegans. *Genome Res.* **2020**, *31*, 1740–1751, doi:10.1101/gr.260794.120.
105. Rose, A. Replication and repair. *WormBook* 2014, 1–16.
106. Blackford, A.N.; Jackson, S.P. Molecular Cell Review ATM, ATR, and DNA-PK: The Trinity at the Heart of the DNA Damage Response. *Mol. Cell* **2017**, *66*, 801–817, doi:10.1016/j.molcel.2017.05.015.
107. Zeman, M.K.; Cimprich, K.A. Causes and consequences of replication stress. *Nat. Cell Biol.* 2014, *16*, 2–9.
108. Lans, H.; Vermeulen, W. Tissue specific response to DNA damage: C. elegans as role model. *DNA Repair (Amst).* **2015**, *32*, 141–148, doi:10.1016/j.dnarep.2015.04.025.
109. Lans, H.; Marteijn, J.A.; Schumacher, B.; Hoeijmakers, J.H.J.; Jansen, G.; Vermeulen, W. Involvement of Global Genome Repair, Transcription Coupled Repair, and Chromatin Remodeling in UV DNA Damage Response Changes during Development. *PLoS Genet.* **2010**, *6*, e1000941, doi:10.1371/journal.pgen.1000941.
110. Stergiou, L.; Eberhard, R.; Doukoumetzidis, K.; Hengartner, M.O. NER and HR pathways act sequentially to promote UV-C-induced germ cell apoptosis in Caenorhabditis elegans. *Cell Death Differ.* **2011**, *18*, 897–906, doi:10.1038/cdd.2010.158.
111. Maklakov, A.A.; Immler, S. The Expensive Germline and the Evolution of Ageing. *Curr. Biol.* 2016, *26*, R577–R586.
112. Holway, A.H.; Kim, S.H.; La Volpe, A.; Michael, W.M. Checkpoint silencing during the DNA damage response in Caenorhabditis elegans embryos. *J. Cell Biol.* **2006**, *172*, 999–1008, doi:10.1083/jcb.200512136.
113. Brauchle, M.; Baumer, K.; Gönczy, P. Differential activation of the DNA replication checkpoint contributes to asynchrony of cell division in C. elegans embryos. *Curr. Biol.* **2003**, *13*, 819–827, doi:10.1016/S0960-9822(03)00295-1.
114. González-Quiroz, M.; Blondel, A.; Sagredo, A.; Hetz, C.; Chevet, E.; Pedeux, R. When Endoplasmic Reticulum Proteostasis Meets the DNA Damage Response. *Trends Cell Biol.* 2020, *30*, 881–891.
115. Tao, R.; Chen, H.; Gao, C.; Xue, P.; Yang, F.; Han, J.D.J.; Zhou, B.; Chen, Y.G. Xbp1-mediated histone H4 deacetylation contributes to DNA double-strand break repair in yeast. *Cell Res.* **2011**, *21*, 1619–1633, doi:10.1038/cr.2011.58.
116. Zheng, P.; Chen, Q.; Tian, X.; Qian, N.; Chai, P.; Liu, B.; Hu, J.; Blackstone, C.; Zhu, D.; Teng, J.; et al. DNA damage triggers tubular endoplasmic reticulum extension to promote apoptosis by facilitating ER-mitochondria signaling. *Cell Res.* **2018**, *28*, 833–854, doi:10.1038/s41422-018-0065-z.
117. Lee, J.H.; Mand, M.R.; Kao, C.H.; Zhou, Y.; Ryu, S.W.; Richards, A.L.; Coon, J.J.; Paull, T.T. ATM directs DNA damage responses and proteostasis via genetically separable

pathways. *Sci. Signal.* **2018**, *11*, doi:10.1126/scisignal.aan5598.
118. Hotokezaka, Y.; Katayama, I.; Nakamura, T. ATM-associated signalling triggers the unfolded protein response and cell death in response to stress. *Commun. Biol.* **2020**, *3*, 1–11, doi:10.1038/s42003-020-1102-2.
119. Ermolaeva, M.A.; Segref, A.; Dakhovnik, A.; Ou, H.L.; Schneider, J.I.; Utermöhlen, O.; Hoppe, T.; Schumacher, B. DNA damage in germ cells induces an innate immune response that triggers systemic stress resistance. *Nature* **2013**, *501*, 416–420, doi:10.1038/nature12452.
120. Deng, J.; Bai, X.; Tang, H.; Pang, S. DNA damage promotes ER stress resistance through elevation of unsaturated phosphatidylcholine in Caenorhabditis elegans. *J. Biol. Chem.* **2021**, *296*, 100095, doi:10.1074/jbc.ra120.016083.
121. Chevet, E.; Hetz, C.; Samali, A. Endoplasmic reticulum stress–activated cell reprogramming in oncogenesis. *Cancer Discov.* 2015, *5*, 586–597.
122. Henry, K.A.; Blank, H.M.; Hoose, S.A.; Polymenis, M. The unfolded protein response is not necessary for the G1/S transition, but it is required for chromosome maintenance in Saccharomyces cerevisiae. *PLoS One* **2010**, *5*, 1–10, doi:10.1371/journal.pone.0012732.
123. Argemí, J.; Kress, T.R.; Chang, H.C.Y.; Ferrero, R.; Bértolo, C.; Moreno, H.; González-Aparicio, M.; Uriarte, I.; Guembe, L.; Segura, V.; et al. X-box Binding Protein 1 Regulates Unfolded Protein, Acute-Phase, and DNA Damage Responses During Regeneration of Mouse Liver. *Gastroenterology* **2017**, *152*, 1203-1216.e15, doi:10.1053/j.gastro.2016.12.040.
124. Acosta-Alvear, D.; Zhou, Y.; Blais, A.; Tsikitis, M.; Lents, N.H.; Arias, C.; Lennon, C.J.; Kluger, Y.; Dynlacht, B.D. XBP1 Controls Diverse Cell Type- and Condition-Specific Transcriptional Regulatory Networks. *Mol. Cell* **2007**, *27*, 53–66, doi:10.1016/j.molcel.2007.06.011.
125. Lyu, X.; Zhang, M.; Li, G.; Cai, Y.; Li, G.; Qiao, Q. Interleukin-6 production mediated by the <scp>IRE</scp> 1- <scp>XBP</scp> 1 pathway confers radioresistance in human papillomavirus-negative oropharyngeal carcinoma. *Cancer Sci.* **2019**, *110*, 2471–2484, doi:10.1111/cas.14094.
126. Dufey, E.; Bravo-San Pedro, J.M.; Eggers, C.; González-Quiroz, M.; Urra, H.; Sagredo, A.I.; Sepulveda, D.; Pihán, P.; Carreras-Sureda, A.; Hazari, Y.; et al. Genotoxic stress triggers the activation of IRE1α-dependent RNA decay to modulate the DNA damage response. *Nat. Commun.* **2020**, *11*, 1–13, doi:10.1038/s41467-020-15694-y.
127. Deng, X.; Hofmann, E.R.; Villanueva, A.; Hobert, O.; Capodieci, P.; Veach, D.R.; Yin, X.; Campodonico, L.; Glekas, A.; Cordon-Cardo, C.; et al. Caenorhabditis elegans ABL-1 antagonizes p53-mediated germline apoptosis after ionizing irradiation. *Nat. Genet.* **2004**, *36*, 906–912, doi:10.1038/ng1396.
128. van Haaften, G.; Romeijn, R.; Pothof, J.; Koole, W.; Mullenders, L.H.F.; Pastink, A.; Plasterk, R.H.A.; Tijsterman, M. Identification of Conserved Pathways of DNA-Damage Response and Radiation Protection by Genome-Wide RNAi. *Curr. Biol.* **2006**, *16*, 1344–1350, doi:10.1016/j.cub.2006.05.047.
129. Volkova, N. V.; Meier, B.; González-Huici, V.; Bertolini, S.; Gonzalez, S.; Vöhringer, H.; Abascal, F.; Martincorena, I.; Campbell, P.J.; Gartner, A.; et al. Mutational signatures are jointly shaped by DNA damage and repair. *Nat. Commun.* **2020**, *11*, 1–15, doi:10.1038/s41467-020-15912-7.

130. Natarajan, B.; Gaur, R.; Hemmingsson, O.; Kao, G.; Naredi, P. Depletion of the ER chaperone ENPL-1 sensitizes C. elegans to the anticancer drug cisplatin . *Worm* **2013**, *2*, e24059, doi:10.4161/worm.24059.
131. Edifizi, D.; Nolte, H.; Babu, V.; Castells-Roca, L.; Mueller, M.M.; Brodesser, S.; Krüger, M.; Schumacher, B. Multilayered Reprogramming in Response to Persistent DNA Damage in C. elegans. *Cell Rep.* **2017**, *20*, 2026–2043, doi:10.1016/j.celrep.2017.08.028.
132. Bobrovnikova-Marjon, E.; Grigoriadou, C.; Pytel, D.; Zhang, F.; Ye, J.; Koumenis, C.; Cavener, D.; Diehl, J.A. PERK promotes cancer cell proliferation and tumor growth by limiting oxidative DNA damage. *Oncogene* **2010**, *29*, 3881–3895, doi:10.1038/onc.2010.153.
133. Dadey, D.Y.A.; Kapoor, V.; Khudanyan, A.; Urano, F.; Kim, A.H.; Thotala, D.; Hallahan, D.E. The ATF6 pathway of the ER stress response contributes to enhanced viability in glioblastoma. *Oncotarget* **2016**, *7*, 2080–2092, doi:10.18632/oncotarget.6712.
134. Kim, W.; Underwood, R.S.; Greenwald, I.; Shaye, D.D. Ortholist 2: A new comparative genomic analysis of human and caenorhabditis elegans genes. *Genetics* **2018**, *210*, 445–461, doi:10.1534/genetics.118.301307.
135. Kaletta, T.; Hengartner, M.O. Finding function in novel targets: C. elegans as a model organism. *Nat. Rev. Drug Discov.* **2006**, *5*, 387–399, doi:10.1038/nrd2031.
136. Lee, K.P.K.K.; Dey, M.; Neculai, D.; Cao, C.; Dever, T.E.; Sicheri, F. Structure of the Dual Enzyme Ire1 Reveals the Basis for Catalysis and Regulation in Nonconventional RNA Splicing. *Cell* **2008**, *132*, 89–100, doi:10.1016/j.cell.2007.10.057.
137. Yoshida, H.; Matsui, T.; Yamamoto, A.; Okada, T.; Mori, K. XBP1 mRNA is induced by ATF6 and spliced by IRE1 in response to ER stress to produce a highly active transcription factor. *Cell* **2001**, *107*, 881–891, doi:10.1016/S0092-8674(01)00611-0.
138. Venz, R.; Korosteleva, A.; Jongsma, E.; Ewald, C.Y. Combining Auxin-Induced Degradation and RNAi Screening Identifies Novel Genes Involved in Lipid Bilayer Stress Sensing in Caenorhabditis elegans. *GENES GENOM GENET* **2020**, *10*, 3921–3928, doi:10.1534/g3.120.401635.
139. Harding, H.P.; Novoa, I.; Zhang, Y.; Zeng, H.; Wek, R.; Schapira, M.; Ron, D. Regulated translation initiation controls stress-induced gene expression in mammalian cells. *Mol. Cell* **2000**, *6*, 1099–1108, doi:10.1016/S1097-2765(00)00108-8.
140. Ye, J.; Rawson, R.B.; Komuro, R.; Chen, X.; Davé, U.P.; Prywes, R.; Brown, M.S.; Goldstein, J.L. ER stress induces cleavage of membrane-bound ATF6 by the same proteases that process SREBPs. *Mol. Cell* **2000**, *6*, 1355–1364, doi:10.1016/S1097-2765(00)00133-7.
141. Harayama, T.; Riezman, H. Understanding the diversity of membrane lipid composition. *Nat. Rev. Mol. Cell Biol.* **2018**, *19*, 281–296, doi:10.1038/nrm.2017.138.
142. Wortmann, S.B.; Espeel, M.; Almeida, L.; Reimer, A.; Bosboom, D.; Roels, F.; de Brouwer, A.P.M.; Wevers, R.A. Inborn errors of metabolism in the biosynthesis and remodelling of phospholipids. *J. Inherit. Metab. Dis.* **2014**, *38*, 99–110, doi:10.1007/s10545-014-9759-7.
143. Jones, K.T.; Ashrafi, K. Caenorhabditis elegans as an emerging model for studying the basic biology of obesity. *DMM Dis. Model. Mech.* 2009, *2*, 224–229.
144. Zhang, Y.; Zou, X.; Ding, Y.; Wang, H.; Wu, X.; Liang, B. Comparative genomics and functional study of lipid metabolic genes in Caenorhabditis elegans. *BMC Genomics* **2013**,

14, 164, doi:10.1186/1471-2164-14-164.
145. Watts, J.L.; Ristow, M. Lipid and carbohydrate metabolism in Caenorhabditis elegans. *Genetics* **2017**, *207*, 413–446, doi:10.1534/genetics.117.300106.
146. Singh, J.; Aballay, A. Endoplasmic reticulum stress caused by lipoprotein accumulation suppresses immunity against bacterial pathogens and contributes to immunosenescence. *MBio* **2017**, *8*, e00778-17, doi:10.1128/mBio.00778-17.
147. Marza, E.; Taouji, S.; Barroso, K.; Raymond, A.; Guignard, L.; Bonneu, M.; Pallares-Lupon, N.; Dupuy, J.; Fernandez-Zapico, M.E.; Rosenbaum, J.; et al. Genome-wide screen identifies a novel p97/CDC-48-dependent pathway regulating ER-stress-induced gene transcription. *EMBO Rep.* **2015**, *16*, 332–340, doi:10.15252/embr.201439123.
148. Rieckher, M.; Bujarrabal, A.; Doll, M.A.; Soltanmohammadi, N.; Schumacher, B. A simple answer to complex questions: Caenorhabditis elegans as an experimental model for examining the DNA damage response and disease genes. *J. Cell. Physiol.* **2017**, *233*, 2781, doi:10.1002/jcp.25979.
149. Xu, J.; Taubert, S. Beyond Proteostasis: Lipid Metabolism as a New Player in ER Homeostasis. *Metabolites* **2021**, *11*, 52, doi:10.3390/metabo11010052.
150. Tam, A.B.; Roberts, L.S.; Chandra, V.; Rivera, I.G.; Nomura, D.K.; Forbes, D.J.; Niwa, M. The UPR Activator ATF6 Responds to Proteotoxic and Lipotoxic Stress by Distinct Mechanisms. *Dev. Cell* **2018**, *46*, 327–343, doi:10.1016/j.devcel.2018.04.023.
151. Jonikas, M.C.; Collins, S.R.; Denic, V.; Oh, E.; Quan, E.M.; Schmid, V.; Weibezahn, J.; Schwappach, B.; Walter, P.; Weissman, J.S.; et al. Comprehensive Characterization of Genes Required for Protein Folding in the Endoplasmic Reticulum. *Science (80-.).* **2009**, *323*, 1693–1697, doi:10.1126/science.1167983.
152. Hetz, C.; Chevet, E.; Oakes, S.A. Proteostasis control by the unfolded protein response. *Nat. Cell Biol.* **2015**, *17*, 829–838, doi:10.1038/ncb3184.
153. Gardner, B.M.; Pincus, D.; Gotthardt, K.; Gallagher, C.M.; Walter, P. Endoplasmic Reticulum Stress Sensing in the Unfolded Protein Response. *Cold Spring Harb. Perspect. Biol.* **2013**, *5*, a013169–a013169, doi:10.1101/cshperspect.a013169.
154. Petranovic, D.; Tyo, K.; Vemuri, G.N.; Nielsen, J. Prospects of yeast systems biology for human health: integrating lipid, protein and energy metabolism. *FEMS Yeast Res.* **2010**, *10*, 1046–1059, doi:10.1111/j.1567-1364.2010.00689.x.
155. Karaskov, E.; Scott, C.; Zhang, L.; Teodoro, T.; Ravazzola, M.; Volchuk, A. Chronic Palmitate But Not Oleate Exposure Induces Endoplasmic Reticulum Stress, Which May Contribute to INS-1 Pancreatic β-Cell Apoptosis. *Endocrinology* **2006**, *147*, 3398–3407, doi:10.1210/en.2005-1494.
156. Ozcan, U.; Cao, Q.; Yilmaz, E.; Lee, A.-H.; Iwakoshi, N.N.; Ozdelen, E.; Tuncman, G.; Görgün, C.; Glimcher, L.H.; Hotamisligil, G.S. Endoplasmic Reticulum Stress Links Obesity, Insulin Action, and Type 2 Diabetes. *Science (80-.).* **2004**, *306*, 457–461, doi:10.1126/science.1103160.
157. Papsdorf, K.; Brunet, A. Linking Lipid Metabolism to Chromatin Regulation in Aging. *Trends Cell Biol.* **2018**, 1–20, doi:10.1016/j.tcb.2018.09.004.
158. Yilmaz, L.S.; Walhout, A.J.M. A Caenorhabditis elegans Genome-Scale Metabolic Network Model. *Cell Syst.* **2016**, *2*, 297–311, doi:10.1016/j.cels.2016.04.012.
159. Fukasawa, M.; Varlamov, O.; Eng, W.S.; Söllner, T.H.; Rothman, J.E. Localization and activity of the SNARE Ykt6 determined by its regulatory domain and palmitoylation.

Proc. Natl. Acad. Sci. U. S. A. **2004**, *101*, 4815–4820, doi:10.1073/pnas.0401183101.
160. Mörck, C.; Olsen, L.; Kurth, C.; Persson, A.; Storm, N.J.; Svensson, E.; Jansson, J.O.; Hellqvist, M.; Enejder, A.; Faergeman, N.J.; et al. Statins inhibit protein lipidation and induce the unfolded protein response in the non-sterol producing nematode Caenorhabditis elegans. *Proc. Natl. Acad. Sci. U. S. A.* **2009**, *106*, 18285–18290, doi:10.1073/pnas.0907117106.
161. Sato, Y.; Kojima, R.; Okumura, M.; Hagiwara, M.; Masui, S.; Maegawa, K.I.; Saiki, M.; Horibe, T.; Suzuki, M.; Inaba, K. Synergistic cooperation of PDI family members in peroxiredoxin 4-driven oxidative protein folding. *Sci. Rep.* **2013**, *3*, 1–13, doi:10.1038/srep02456.
162. Sun, J.; Liu, Y.; Aballay, A. Organismal regulation of XBP-1-mediated unfolded protein response during development and immune activation. *EMBO Rep.* 2012, *13*, 855–860.
163. Bischof, L.J.; Kao, C.Y.; Los, F.C.O.; Gonzalez, M.R.; Shen, Z.; Briggs, S.P.; Van Der Goot, F.G.; Aroian, R. V. Activation of the unfolded protein response is required for defenses against bacterial pore-forming toxin in vivo. *PLoS Pathog.* **2008**, *4*, doi:10.1371/journal.ppat.1000176.
164. B'Chir, W.; Maurin, A.C.; Carraro, V.; Averous, J.; Jousse, C.; Muranishi, Y.; Parry, L.; Stepien, G.; Fafournoux, P.; Bruhat, A. The eIF2α/ATF4 pathway is essential for stress-induced autophagy gene expression. *Nucleic Acids Res.* **2013**, *41*, 7683–7699, doi:10.1093/nar/gkt563.
165. Walker, A.K.; Jacobs, R.L.; Watts, J.L.; Rottiers, V.; Jiang, K.; Finnegan, D.M.; Shioda, T.; Hansen, M.; Yang, F.; Niebergall, L.J.; et al. A conserved SREBP-1/phosphatidylcholine feedback circuit regulates lipogenesis in metazoans. *Cell* **2011**, *147*, 840–852, doi:10.1016/j.cell.2011.09.045.
166. Surma, M.A.; Klose, C.; Peng, D.; Shales, M.; Mrejen, C.; Stefanko, A.; Braberg, H.; Gordon, D.E.; Vorkel, D.; Ejsing, C.S.; et al. A lipid E-MAP identifies Ubx2 as a critical regulator of lipid saturation and lipid bilayer stress. *Mol. Cell* **2013**, *51*, 519–530, doi:10.1016/j.molcel.2013.06.014.
167. Nukazuka, A.; Fujisawa, H.; Inada, T.; Oda, Y.; Takagi, S. Semaphorin controls epidermal morphogenesis by stimulating mRNA translation via eIF2α in Caenorhabditis elegans. *Genes Dev.* **2008**, *22*, 1025–1036, doi:10.1101/gad.1644008.
168. Richardson, C.E.; Kooistra, T.; Kim, D.H. An essential role for XBP-1 in host protection against immune activation in C. elegans. *Nature* **2010**, *463*, 1092–1095, doi:10.1038/nature08762.
169. Guilliam, T.A.; Keen, B.A.; Brissett, N.C.; Doherty, A.J. Primase-polymerases are a functionally diverse superfamily of replication and repair enzymes. *Nucleic Acids Res.* **2015**, *43*, 6651–6664, doi:10.1093/nar/gkv625.
170. Yoon, D.S.; Cha, D.S.; Alfhili, M.A.; Keiper, B.D.; Lee, M.H. Subunits of the DNA polymerase alpha-primase complex promote Notch-mediated proliferation with discrete and shared functions in C. elegans germline. *FEBS J.* **2018**, *285*, 2590–2604, doi:10.1111/febs.14512.
171. Chan, R.C.; Chan, A.; Jeon, M.; Wu, T.F.; Pasqualone, D.; Rougvie, A.E.; Meyer, B.J. Chromosome cohesion is regulated by a clock gene paralogue TIM-1. *Nature* **2003**, *423*, 1002–1009, doi:10.1038/nature01697.
172. McLellan, J.L.; O'Neil, N.J.; Barrett, I.; Ferree, E.; van Pel, D.M.; Ushey, K.;

Sipahimalani, P.; Bryan, J.; Rose, A.M.; Hieter, P. Synthetic lethality of cohesins with PARPs and replication fork mediators. *PLoS Genet.* **2012**, *8*, 1002574, doi:10.1371/journal.pgen.1002574.
173. Cheung, I.; Schertzer, M.; Rose, A.; Lansdorp, P.M. Disruption of dog-1 in Caenorhabditis elegans triggers deletions upstream of guanine-rich DNA. *Nat. Genet.* **2002**, *31*, 405–409, doi:10.1038/ng928.
174. Youds, J.L.; O'Neil, N.J.; Rose, A.M. Homologous recombination is required for genome stability in the absence of DOG-1 in Caenorhabditis elegans. *Genetics* **2006**, *173*, 697–708, doi:10.1534/genetics.106.056879.
175. Olsen, A.; Vantipalli, M.C.; Lithgow, G.J. Checkpoint proteins control survival of the postmitotic cells in Caenorhabditis elegans. *Science (80-.).* **2006**, *312*, 1381–1385, doi:10.1126/science.1124981.
176. Hartman' And, P.S.; Herman, R.K. *RADIATION-SENSITIVE MUTANTS OF CAENORHABDITIS ELEGANS*; 1982;
177. Garcia-Muse, T.; Boulton, S.J. Distinct modes of ATR activation after replication stress and DNA double-strand breaks in Caenorhabditis elegans. *EMBO J.* **2005**, *24*, 4345–4355, doi:10.1038/sj.emboj.7600896.
178. Stevens, H.; Williams, A.B.; Michael, W.M. Cell-Type Specific Responses to DNA Replication Stress in Early C. elegans Embryos. *PLoS One* **2016**, *11*, e0164601, doi:10.1371/journal.pone.0164601.
179. MacQueen, A.J.; Villeneuve, A.M. Nuclear reorganization and homologous chromosome pairing during meiotic prophase require C. elegans chk-2. *Genes Dev.* **2001**, *15*, 1674–1687, doi:10.1101/gad.902601.
180. Halbleib, K.; Pesek, K.; Covino, R.; Hofbauer, H.F.; Wunnicke, D.; Hänelt, I.; Hummer, G.; Ernst, R. Activation of the Unfolded Protein Response by Lipid Bilayer Stress. *Mol. Cell* **2017**, *67*, 673-684.e8, doi:10.1016/j.molcel.2017.06.012.
181. He, J.; Zhang, F.; Tay, L.W.R.; Boroda, S.; Nian, W.; Levental, K.R.; Levental, I.; Harris, T.E.; Chang, J.T.; Du, G.; et al. Lipin-1 regulation of phospholipid synthesis maintains endoplasmic reticulum homeostasis and is critical for triple-negative breast cancer cell survival. *FASEB J.* **2017**, *31*, 2893–2904, doi:10.1096/fj.201601353R.
182. Golden, A.; Liu, J.; Cohen-Fix, O. Inactivation of the C. elegans lipin homolog leads to ER disorganization and to defects in the breakdown and reassembly of the nuclear envelope. *J. Cell Sci.* **2009**, *122*, 1970–1978, doi:10.1242/jcs.044743.
183. Jung, Y.; Kwon, S.; Ham, S.; Lee, D.; Park, H.H.; Yamaoka, Y.; Jeong, D.; Artan, M.; Altintas, O.; Park, S.; et al. Caenorhabditis elegans Lipin 1 moderates the lifespan-shortening effects of dietary glucose by maintaining ω-6 polyunsaturated fatty acids. *Aging Cell* **2020**, *19*, e13150, doi:10.1111/acel.13150.
184. Sapir, A.; Tsur, A.; Koorman, T.; Ching, K.; Mishra, P.; Bardenheier, A.; Podolsky, L.; Bening-Abu-Shach, U.; Boxem, M.; Chou, T.F.; et al. Controlled sumoylation of the mevalonate pathway enzyme HMGS-1 regulates metabolism during aging. *Proc. Natl. Acad. Sci. U. S. A.* **2014**, *111*, E3880–E3889, doi:10.1073/pnas.1414748111.
185. Chen, J.-C.C.; Wu, M.-L.L.; Huang, K.-C.C.; Lin, W.-W.W. HMG-CoA reductase inhibitors activate the unfolded protein response and induce cytoprotective GRP78 expression. *Cardiovasc. Res.* **2008**, *80*, 138–150, doi:10.1093/cvr/cvn160.
186. Thinon, E.; Serwa, R.A.; Broncel, M.; Brannigan, J.A.; Brassat, U.; Wright, M.H.; Heal,

W.P.; Wilkinson, A.J.; Mann, D.J.; Tate, E.W. Global profiling of co- and post-translationally N-myristoylated proteomes in human cells. *Nat. Commun.* **2014**, *5*, 4919, doi:10.1038/ncomms5919.
187. Thinon, E.; Morales-Sanfrutos, J.; Mann, D.J.; Tate, E.W. N-Myristoyltransferase Inhibition Induces ER-Stress, Cell Cycle Arrest, and Apoptosis in Cancer Cells. *ACS Chem. Biol.* **2016**, *11*, 2165–2176, doi:10.1021/acschembio.6b00371.
188. Schiavone, M.L.; Millucci, L.; Bernardini, G.; Giustarini, D.; Rossi, R.; Marzocchi, B.; Santucci, A. Homogentisic acid affects human osteoblastic functionality by oxidative stress and alteration of the Wnt/β-catenin signaling pathway. *J. Cell. Physiol.* **2020**, *235*, 6808–6816, doi:10.1002/jcp.29575.
189. Fisher, A.L.; Page, K.E.; Lithgow, G.J.; Nash, L. The Caenorhabditis elegans K10C2.4 gene encodes a member of the fumarylacetoacetate hydrolase family: A Caenorhabditis elegans model of type I tyrosinemia. *J. Biol. Chem.* **2008**, *283*, 9127–9135, doi:10.1074/jbc.M708341200.
190. Wang, H.; Chen, H.; Hao, G.; Yang, B.; Feng, Y.; Wang, Y.; Feng, L.; Zhao, J.; Song, Y.; Zhang, H.; et al. Role of the phenylalanine-hydroxylating system in aromatic substance degradation and lipid metabolism in the oleaginous fungus mortierella alpina. *Appl. Environ. Microbiol.* **2013**, *79*, 3225–3233, doi:10.1128/AEM.00238-13.
191. Moseley, K.; Koch, R.; Moser, A.B. Lipid status and long-chain polyunsaturated fatty acid concentrations in adults and adolescents with phenylketonuria on phenylalanine-restricted diet. *J. Inherit. Metab. Dis.* **2002**, *25*, 56–64, doi:10.1023/A:1015142001578.
192. Perkins, R.; Vaida, V. Phenylalanine Increases Membrane Permeability. *J. Am. Chem. Soc.* **2017**, *139*, 14388–14391, doi:10.1021/jacs.7b09219.
193. Entchev, E. V.; Schwudke, D.; Zagoriy, V.; Matyash, V.; Bogdanova, A.; Habermann, B.; Zhu, L.; Shevchenko, A.; Kurzchalia, T. V. LET-767 is required for the production of branched chain and long chain fatty acids in Caenorhabditis elegans. *J. Biol. Chem.* **2008**, *283*, 17550–17560, doi:10.1074/jbc.M800965200.
194. Zhang, H.; Abraham, N.; Khan, L.A.; Hall, D.H.; Fleming, J.T.; Göbel, V. Apicobasal domain identities of expanding tubular membranes depend on glycosphingolipid biosynthesis. *Nat. Cell Biol.* **2011**, *13*, 1189–1201, doi:10.1038/ncb2328.
195. Kuervers, L.M.; Jones, C.L.; O'Neil, N.J.; Baillie, D.L. The sterol modifying enzyme LET-767 is essential for growth, reproduction and development in Caenorhabditis elegans. *Mol. Genet. Genomics* **2003**, *270*, 121–131, doi:10.1007/s00438-003-0900-9.
196. Galles, C.; Prez, G.M.; Penkov, S.; Boland, S.; Porta, E.O.J.; Altabe, S.G.; Labadie, G.R.; Schmidt, U.; Knölker, H.J.; Kurzchalia, T. V.; et al. Endocannabinoids in Caenorhabditis elegans are essential for the mobilization of cholesterol from internal reserves. *Sci. Rep.* **2018**, *8*, 1–12, doi:10.1038/s41598-018-24925-8.
197. Garcia, G. Lipid homeostasis is essential for endoplasmic reticulum protein quality control, Doctoral dissertation, University of California, Berkeley, Berkeley, CA, United States, 2019.
198. Kniazeva, M.; Crawford, Q.T.; Seiber, M.; Wang, C.Y.; Han, M. Monomethyl branched-chain fatty acids play an essential role in Caenorhabditis elegans development. *PLoS Biol.* **2004**, *2*, e257, doi:10.1371/journal.pbio.0020257.
199. Micoogullari, Y.; Basu, S.S.; Ang, J.; Weisshaar, N.; Schmitt, N.D.; Abdelmoula, W.M.; Lopez, B.; Agar, J.N.; Agar, N.; Hanna, J. Dysregulation of very-long-chain fatty acid

metabolism causes membrane saturation and induction of the unfolded protein response. *Mol. Biol. Cell* **2020**, *31*, 7–17, doi:10.1091/mbc.E19-07-0392.
200. Williamson, C.D.; Wong, D.S.; Bozidis, P.; Zhang, A.; Colberg-Poley, A.M. Isolation of Endoplasmic Reticulum, Mitochondria, and Mitochondria-Associated Membrane and Detergent Resistant Membrane Fractions from Transfected Cells and from Human Cytomegalovirus-Infected Primary Fibroblasts. *Curr. Protoc. Cell Biol.* **2015**, *68*, 3.27.1-3.27.33, doi:10.1002/0471143030.cb0327s68.
201. Encalada, S.E.; Martin, P.R.; Phillips, J.B.; Lyczak, R.; Hamill, D.R.; Swan, K.A.; Bowerman, B. DNA replication defects delay cell division and disrupt cell polarity in early Caenorhabditis elegans embryos. *Dev. Biol.* **2000**, *228*, 225–238, doi:10.1006/dbio.2000.9965.
202. Nair, G.; Walton, T.; Murray, J.I.; Raj, A. Gene transcription is coordinated with, but not dependent on, cell divisions during C. elegans embryonic fate specification. *Dev.* **2013**, *140*, 3385–3394, doi:10.1242/dev.098012.
203. Rodrigues, A.J.; Neves-Carvalho, A.; Teixeira-Castro, A.; Rokka, A.; Corthals, G.; Logarinho, E.; Maciel, P. Absence of Ataxin-3 Leads to Enhanced Stress Response in C. elegans. *PLoS One* **2011**, *6*, e18512, doi:10.1371/journal.pone.0018512.
204. Taylor, S.K.B.; Minhas, M.H.; Tong, J.; Selvaganapathy, P.R.; Mishra, R.K.; Gupta, B.P. C. elegans electrotaxis behavior is modulated by heat shock response and unfolded protein response signaling pathways. *Sci. Rep.* **2021**, *11*, 3115, doi:10.1038/s41598-021-82466-z.
205. Bartoszewska, S.; Collawn, J.F. Unfolded protein response (UPR) integrated signaling networks determine cell fate during hypoxia. *Cell. Mol. Biol. Lett.* 2020, *25*, 1–20.
206. Cornaglia, M.; Mouchiroud, L.; Marette, A.; Narasimhan, S.; Lehnert, T.; Jovaisaite, V.; Auwerx, J.; Gijs, M.A.M. An automated microfluidic platform for C. elegans embryo arraying, phenotyping, and long-term live imaging. *Sci. Rep.* **2015**, *5*, 1–13, doi:10.1038/srep10192.
207. Zha, J.; Ying, M.; Alexander-Floyd, J.; Gidalevitz, T. HSP-4/BiP expression in secretory cells is regulated by a developmental program and not by the unfolded protein response. *PLOS Biol.* **2019**, *17*, e3000196, doi:10.1371/journal.pbio.3000196.
208. Levi-Ferber, M.; Salzberg, Y.; Safra, M.; Haviv-Chesner, A.; Bülow, H.E.; Henis-Korenblit, S. It's All in Your Mind: Determining Germ Cell Fate by Neuronal IRE-1 in C. elegans. *PLoS Genet.* **2014**, *10*, 1004747, doi:10.1371/journal.pgen.1004747.
209. Conte, D.; MacNei, L.T.; Walhout, A.J.M.; Mello, C.C. RNA Interference in Caenorhabditis elegans. *Curr. Protoc. Mol. Biol.* **2015**, *2015*, 26.3.1-26.3.30, doi:10.1002/0471142727.mb2603s109.

List of Supplementary Material

Table S1. RNAi screen for metabolic genes whose inactivation induces the IRE-1 branch of the UPR-ER in *C. elegans* (readout: activation of the *hsp-4p::gfp* reporter)

The results are presented as supplementary files. The supplementary files can be accessed as an external excel file

Table S2. RNAi and sequence validation of yeast hit screen orthologues in *C. elegans*

The results are presented as supplementary files. The supplementary files can be accessed as an external excel file

Table S3. A summary of yeast and *C. elegans* screen hit orthologues

The results are presented as supplementary files. The supplementary files can be accessed as an external excel file

Table S4. A summary of the PEK-1 branch activation by RNAi against the 34 hit metabolic genes in *C. elegans* (readout: activation of the *Patf-4(uORF)::gfp* reporter)

The results are presented as supplementary files. The supplementary files can be accessed as an external excel file